AD-A084 239 GENERAL ELECTRIC CO SANTA BARBARA CA TEMPO F/G 17/7
LORAN-C SIGNAL ANALYSIS.(U)
DEC 79 L W NELSON, B GAMBILL DOT-CG-64810A
UNCLASSIFIED GE79TMP-78 USCG -D-4-80 NL

1 OF 2
AD
A084239

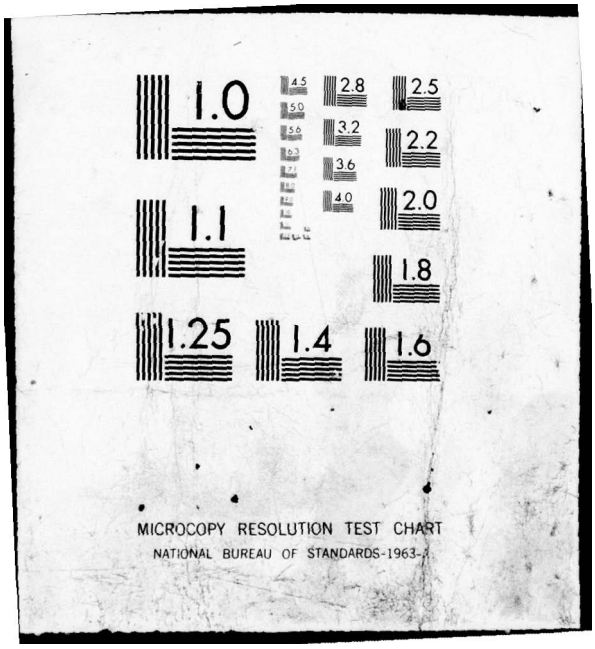
1.0
1.1
1.25
1.4
1.6
1.8
2.0
2.2
2.5
2.8
3.2
3.6
4.0
4.5
5.0
5.6
6.3
7.1
MICROCOPY RESOLUTION TEST CHART
NATIONAL BUREAU OF STANDARDS-1963-A

REPORT NO. GG-D-4-80

LEVEL II

LORAN-C SIGNAL ANALYSIS
FINAL REPORT

Larry W. Nelson
Burt Gambill

General Electric—TEMPO
816 State Street
Santa Barbara, CA 93110

December 1979

FINAL REPORT

PREPARED FOR

U.S. DEPARTMENT OF TRANSPORTATION
UNITED STATES COAST GUARD
OFFICE OF RESEARCH AND DEVELOPMENT
WASHINGTON, D.C. 20590

LORAN-C SIGNAL ANALYSIS FINAL REPORT REPORT NO. GG-D-4-80

NOTICE

This document is disseminated under the sponsorship of the Department of Transportation in the interest of information exchange. The United States Government assumes no liability for its contents or use thereof.

The contents of this report do not necessarilv reflect the official view or policy of the Coast Guard; and they do not constitute a standard, specification, or regulation.

This report, or portions thereof may not be used for advertising or sales promotion purposes. Citation of trade names and manufacturers does not constitute endorsement or approval of such products.

Technical Report Documentation Page

1. Report No.	2. Government Accession No.	3. Recipient's Catalog No.
USGG D-4-80	AD-A084 239	

4. Title and Subtitle
Loran-C Signal Analysis,
Final Report

5. Report Date
Dec[redacted]79

6. Performing Organization Code

7. Author(s)
Larry W. Nelson, Burt Gambill

8. Performing Organization Report No.
GE79TMP-78

9. Performing Organization Name and Address
General Electric-TEMPO
816 State Street
Santa Barbara, CA 93102

10. Work Unit No. (TRAIS)

11. Contract or Grant No.
DOT-CG-64810A

12. Sponsoring Agency Name and Address
U.S. Coast Guard
G-FPC-2/71
Washington, DC 20590

13. Type of Report and Period Covered
Final Report,
Aug[redacted]77 - Dec[redacted]79

14. Sponsoring Agency Code

15. Supplementary Notes
-

16. Abstract

This report summarizes the results of experimental efforts and theoretical analysis conducted on the Loran-C Signal Analysis project. Experiments to test the stability of the U.S. West Coast Chain, to provide a data base for assessing the predictability of Loran-C signal phase, and to provide data for calibrating San Francisco Harbor are described. Estimates of system error budgets and evaluation of the performance of Loran-C in various operational modes are also described.

17. Key Words	18. Distribution Statement
Loran-C System Stability Propagation Prediction Differential Loran	Document is available to the public through the National Technical Information Service, Springfield, VA 22161.

19. Security Classif. (of this report)	20. Security Classif. (of this page)	21. No. of Pages	22. Price
Unclassified	Unclassified	95	

Form DOT F 1700.7 (8-72) Reproduction of completed page authorized

346420

ACKNOWLEDGMENTS

This work was supported by the United States Coast Guard Office of Research and Development. Coast Guard Project Officers have included Commander R. Cassis, Commander James Walker, Captain William Flanders, and Dr. Surendra Nath Samaddar. A project this size has major contributions from several individuals and organizations. These are listed below in alphabetical order.

1. Commander James Alexander (USCG-CCGD-11). Provided logistic and site support.

2. Dr. Donald Chandler (General Electric—TEMPO). Provided numerous technical suggestions during the experiments and analysis phases.

3. Mr. Dallis Copeland (Decca Systems). Operated Trisponder Radar system on board the vessel.

4. Dr. Donald Dahm (USCG, CCGD-12). Provided logistic and site support.

5. Mr. Walter Dean (Magnavox). Provided the TOA receiver, TOA calibrator and in-field maintenance and control support. Mr. Dean provided the TOA receiver operator instructions for the "Experiment Program Plan."

6. Dr. Donald Feldman (USCG G-D). Provided technical guidance for the processing and analysis of the harbor data.

7. Mrs. Edith Feniger (General Electric—TEMPO). Developed, implemented, and tested Loran-C data reduction and processing software. Assisted in the planning phases of the experiments.

8. Mr. Brandon Finney (General Electric—TEMPO). Assisted in debugging system programs and setting up tapes and files as required. Assisted in the development of the Loran-C data reduction and processing software.

9. Mr. Robert Frank (General Electric—TEMPO consultant). Provided inputs to the Experiment Program Plan, Fort Cronkhite data collection, Verification, and Worst Case Path Field Test Coordination Plans.

10. Mr. Burt Gambill (General Electric—TEMPO). Provided numerous technical suggestions during the experiments and analysis phases. Was the key analyst for the propagation path analysis and propagation prediction program evaluation.

11. Mr. Robert Goddard (Internav). Provided in-field maintenance for the LC-204 TD receivers and other equipment. Provided technicians to operate receivers, set up and dismantle sites, calibrate receivers, and kept thorough records of in-field activities.

12. Lt. Richard Harvey (USCG, West Coast Loran-C Chain COCO). Provided continual operational assistance to analyst and field personnel. Provided all pertinent system operational data (LPAs, transmitter outages).

13. Mr. John Illgen (General Electric—TEMPO). Provided overall direction of the planning, execution and control of the experiments, and subsequent data analysis.

14. Dr. Lawrence Nelson (General Electric—TEMPO). Provided numerous technical suggestions throughout the experiments and analysis phases. Was the key analyst for the system analysis activities.

15. Commander Cyrus Potts (USCG-PACAREA). Provided and explained required details to define chain control doctrine).

16. Dr. Kenneth Schwartz (General Electric—TEMPO). Interpreted and corrected the GFE propagation prediction technique (Integral Equation Approach). Key analyst in prediction program evaluation.

17. Mr. Jim Stegall (Del Norte Technology). Assisted in operation of Trisponder Radar System.

18. Commander Ralph Winn (USCG, CCGD-12). Provided logistic and site support. Provided assistance whenever required.

19. CDRS Bill Walker, Bill Schorr, Bill Mohin, D. Haislip, Bill Jones, and Dave Clemments provided useful suggestions throughout the experimental program.

CONTENTS

ILLUSTRATIONS

TABLES

SECTION 1
INTRODUCTION

The Loran-C radio navigation system has long been recognized to be capable of greater accuracy than the official stated accuracy of a quarter nautical mile. It has been conjectured that Loran-C is potentially accurate enough to provide a valuable navigation aid for use in harbors and harbor entrances. To evaluate this conjecture, the Loran-C Signal Analysis Project was undertaken by the U.S. Coast Guard. This project used a combination of experimental measurements and theoretical analyses to determine the limits on accuracy and to identify and quantify fundamental error sources. The measurements were conducted in the southern triad of the U.S. West Coast Loran-C chain from August 1977 to May 1978. This report presents a summary of the experiments conducted, the analyses performed, and the results obtained. It represents the final status of this effort.

The measurement portion of the project encompassed four major data collections or experiments. These experiments and associated objectives are:

1. Fort Cronkhite Experiment - designed to measure long term stability and provide experimental control for the following experiments.
2. Stability Experiment - designed to measure time varying error components of the Loran-C signal due to chain equipment and propagation medium effects.
3. Propagation Experiment - designed to provide data to evaluate the accuracy of groundwave phase delay prediction models.
4. San Francisco Harbor Experiment - designed to provide data to study spatial grid distortion in a harbor environment, harbor calibration techniques, differential Loran-C, and the effects of large steel structures such as bridges.

The analysis of this project focused primarily on identification of error sources and the conversion of Loran-C time differences to geodetic coordinates. To produce the high-accuracy conversion necessary for harbor navigation, precise prediction of signal phase delay is required. Both theoretical and empirical models are considered for this purpose. In addition, errors unaccounted for in these models are investigated, such as signal reflections from large steel bridges.

Finally, an assessment is made of the ability of Loran-C to provide a low-cost, all-weather navigation aid for use in harbors and harbor entrances. This assessment is based on the results of the measurements and analyses performed and shows that Loran-C has the potential for use in this environment.

The report begins by summarizing the major results of the project and the conclusions drawn from the analysis of these results. Recommendations are then made for continued effort in propagation prediction, charting of harbors and harbor entrances, system improvements, user equipment development, and future data collections. These recommendations are based on the experience and results obtained during the project.

Each of the four experiments is then presented in some detail. The summary of each experiment includes the following:

- The experiment rationale and goal planning
- Experimental configuration
- Measurement techniques
- Data processing and results
- Related theoretical predictions
- Comparison of predictions and measured results
- Conclusions.

Finally, a comparative analysis of Loran-C in four modes of system operation is presented. These modes are absolute, differentially augmented absolute, relative, and differentially augmented relative modes. The purpose of this analysis is to determine how well each mode achieves the objective of providing navigation information which can be used to safely navigate in San Francisco Harbor. Navaid accuracy requirements are postulated for San Francisco Harbor in order to evaluate each mode. The $2D_{rms}$ accuracy measure is used as a metric. This analysis is based on an error budget derived from the experimental data obtained during the project.

This final report is largely arranged in an order that follows the performance sequence of the experimental field measurements. This organization not only demonstrates how each experiment relates to its predecessors, but also attests to the project's success in achieving the overall objective.

SECTION 2
SUMMARY OF RESULTS AND CONCLUSIONS

The Loran-C Signal Analysis project consisted of a series of experiments and supporting theoretical analysis. Several significant results were obtained in both the experimental and theoretical phases, especially in the areas of propagation prediction, harbor grid calibration, and differential Loran-C in the harbor and harbor entrance environment. The results of the experiment and associated analyses are summarized below. A general conclusion supported by all the experiments is that the southern triad of the U.S. West Coast chain is very stable and system control and management is excellent.

FORT CRONKHITE EXPERIMENT

The Fort Cronkhite experiment was designed to measure long-term signal fluctuations and to provide experiment control data during the other experiments. The experiment, conducted between August 1977 and May 1978, showed no discernible seasonal changes in the received time differences in the San Francisco Bay area. This observed system stability is the result of a combination of the closeness of the system area monitor (SAM) and the low percentage of the total signal fluctuation caused by propagation media changes. The sample standard deviations of the received signal were in the 20 to 30 ns rms range for receiver averaging times of 55 to 100 seconds. One word of caution is given. The average user should not expect to obtain the excellent results stated above unless his receiver has comparable averaging time, extra notch filters, and either selected attenuation of the X-ray signal or a receiver with a very wide dynamic signal range.

VERIFICATION EXPERIMENT

The Verification experiment was conducted to verify assumptions that are required to process TD data to separate sources of signal fluctuations. The verification procedures required the use of TOA receivers. The data from the verification experiment collected during 3 weeks of October 1977 again reflected the high stability of the southern triad. Although the receivers were quite far from the SAM, the standard deviations of the received TD were still in the 20 to 30 ns range. The standard deviations of the signal fluctuations* due to chain equipment ranged from 15 to 20 ns from 55 to 100 second receiver averaging times.

*The difference between the instantaneous signal value and its long-term average.

Chain fluctuations computed from both TOA and TD data were highly correlated ($\rho > 0.74$), confirming that chain fluctuations could be derived from TD data.

Propagation fluctuations were also computed from both TOA and TD data. Analysis of the correlation between these time series showed that receiver fluctuations exceeded propagation-induced fluctuations during this experiment period. Since there were no significant propagation fluctuations (ie, significant compared to approximately 10 ns rms receiver fluctuations), no conclusions could be drawn about the observability of these phenomena using TD data.

STABILITY EXPERIMENT

The stability experiment was designed to provide data to measure the magnitude of signal fluctuations due to chain equipment and propagation effects. Data for this purpose were collected from 1 December 1977 to 27 January 1978. The data showed the chain to be generally stable. However, one identifiable propagation fluctuation did occur during this time period which produced some interesting effects.

The weekly standard deviations for the collected data ranged from 15 to 40 ns rms with the exception of the second week of December, when a propagation fluctuation occurred on the X-ray baseline raising the standard deviation of TDX to 64 ns rms at Silver Springs, NV (near Master) and 38 ns rms at Arbuckle, CA (near X-ray).

Chain and propagation fluctuations were computed using formulations developed in Section 4. The weekly standard deviations of the chain and propagation-induced fluctuations ranged from 14 to 27 ns rms and 10 to 16 ns rms, respectively, with the exception again of the second week of December. For this week the chain and propagation fluctuations were 33 and 35 ns rms, respectively. Propagation fluctuations on the Jean, NV, to Arbuckle, CA, path were small during the entire experiment, ranging from 15 to 23 ns rms.

The chain-induced fluctuations were well behaved, showing that the chain was being well controlled and operated by Coast Guard personnel. The processed data revealed no large timing jumps as have been described in the past, indicating that the new CALOC control system is performing well and not overreacting in times of stress.

The propagation fluctuations were in general not significant except for one clearly identifiable disturbance which occurred on 16 December. The fluctuation was composed of a transitory rapid change in TDX of about 80 ns, which coincided with a strong weather front passing over the entire X-ray baseline, and a long-term drift in TDX which continued for many days. The drift in TDX is attributed to a change in surface impedance. This event was clearly observed in the processed data,

demonstrating that significant baseline propagation fluctuations can be observed from TD data. The assumption of no significant atmospheric-refractive-index-induced variations on short paths, while reasonable, was neither verified nor refuted by the experimental data. However, phase variations are clearly predictable when surface impedance changes occur on the short path. The propagation disturbances observed, even the unusual one, were much smaller than those previously reported for data collected on the East Coast and the effects of refractive index changes could not be verified. The data were taken under different seasonal and weather conditions than prior data which may explain the discrepancy. Even so, this discrepancy warrants further investigation.

PROPAGATION EXPERIMENT

The purpose of the propagation experiment and associated theoretical analyses was to obtain a better understanding of the predictability of Loran-C signal phase and amplitude. The effort was divided into experiment design, execution, and data analysis, evaluation of prediction models, and comparison of predicted and measured results.

Experiment Design, Execution, and Data Analysis

A propagation path was selected between the Yankee transmitter site at Searchlight, NV, and a measurement site near Ft. Cronkhite, CA. This long ($\approx$ 750 km) overland path was selected because of the extreme variation in terrain and impedance along the path. Eight sites were selected approximately on the geodesic connecting path termini, and incremental time of arrival measurements (difference in time of arrival of the Loran-C signal at adjacent sites) were obtained. Special measurement techniques requiring a TOA calibrator were used to minimize the effect of cesium clock frequency offsets. When closures were properly completed, this technique produced estimated measurement accuracy of $\approx \pm$ 50 ns, based on the closure errors. These data were subsequently used to test the validity of time of arrival predictions.

Evaluation of Prediction Models

Four prediction models were evaluated. They are

1. Classical, Homogeneous Spherical Earth - a well researched technique documented by comprehensive published literature.
2. Pressey's or Millington's - a semi-empirical technique that accounts for inhomogeneous impedance, and is currently used for Loran-C chart preparation.
3. Multisegment Spherical Earch (MULSEG) - an extension of the classical theory to account for inhomogeneous impedance.
4. Integral Equation Solution - a GFE computer program (HUFLOC) provided by the U.S. Coast Guard to calculate signals over irregular, inhomogeneous terrain.

More complete definitions and references are provided in Section 6.

The classical technique was not expected to produce useful results for the very inhomogeneous path selected for this experiment. Numerical procedures and approximations were validated and efficient computation procedures defined because the classical approach is imbedded in the other techniques.

A comparison was made between Millington's technique and MULSEG for several hypothetical cases. The results were nearly identical in all cases, and Millington's method was chosen for subsequent comparisons with the experimental data because computations are easier than those for the more rigorous MULSEG.

Predictions from Millington's and from the integral equation techniques were compared for a path with highly inhomogeneous surface impedance, but with no terrain variation. Here again the results agreed well, verifying the usefulness of Millington's technique when terrain variations are not important.

Comparison of Predicted and Measured Results

A detailed data base was prepared defining the terrain and impedance along the propagation path for input to the integral equation calculation. Terrain data were obtained from detailed topographic maps because digitized terrain data tapes were unavailable for the experiment area. Surface impedance data were estimated using data on geophysical and electrical properties of surface and subsurface layers along the path. The data sources were USGS and the California and Nevada Bureaus of Mines. This data preparation was a formidible task (1 man-month) and would not be practical for many paths unless it is highly automated.

Predictions of incremental time of arrival between the measurement sites were computed using the data base just described. The predictions were compared with the experimental data, and differences varied from a few tens of nanoseconds to approximately one-half microsecond.

Several difficulties arose during the computations which required some special calculations to select calculation step-size and terrain data smoothing interval. These difficulties were resolved, and we believe the largest source of error in the predictions is in the a priori estimate of surface impedance. One additional set of sensitivity calculations indicated that the surface impedance needs to be specified with an error much less than a factor of 2 to allow predictions accurate to less than 100 ns.

Predictions made with Millington's technique showed poorer agreement with the measured data than the integral equation results using the a priori impedance estimates. This comparison illustrated the importance of terrain on signal phase, which was, for this path, significantly increased (greater phase delay) by the terrain variation.

One sample of weather-induced phase variations was computed. The computation was made using a simplified theory that accounts for refractive index modification by varying the effective earth curvature. The refractive index calculations were based on some very sparse surface weather data. The predicted variations were a few nanoseconds, which is generally in agreement with observations during most of the experiments. We conclude that an improved theory to account for refractive index changes is required to obtain a better understanding of weather-induced effects.

HARBOR EXPERIMENT

The purpose of this experiment was to provide data for evaluating the potential of Loran-C for accurate all-weather navigation in the harbor and harbor entrance environment. The experiment was divided into a planning phase, a land-site measurement phase, and a vessel measurement phase in San Francisco Harbor.

Planning Phase

To aid the planning phase, we first defined an idealized grid. This grid is based on using average phase propagation velocities between the transmitters and positions in the harbor to relate TDs to absolute position. Six parameters (two emission delays and four propagation velocities) define the grid. TD measurements at three or more locations can be used to define the parameters experimentally. In the planning phase, the parameters were estimated using a combination of theoretical predictions, USCG calibration data, and TD measurements at Ft. Cronkhite.

Next, estimates of spatial distortion—difference between actual TDs and grid TDs—were generated assuming the primary source of distortion to be the phase recovery at the land-sea interface. The approximate magnitude and spatial extent of distortions produced by the Golden Gate and Oakland Bay bridges were also estimated by using a crude scattering model.

The estimates of spatial distortion were then used to select fixed land sites and vessel tracks to sample the areas of high expected spatial distortion and to confirm or refute the hypothesis that spatial distortion results primarily from the land-sea interface phase recovery.

Land Site Measurement Phase

The purpose of the land site measurements was to provide data for an accurate harbor grid, evaluate spatial anomalies, and assess the performance of normal and differentially augmented Loran-C.

Data were collected at 13 sites around the periphery and on islands inside San Francisco Harbor. Data collection periods were typically 7 to 9 days and observed standard deviations in TDX and TDY were approximately 20 nanoseconds.

Parameters for the idealized grid were estimated using various combinations of the measurement sites. Errors were computed by differencing the measured TD values and values predicted by the idealized grid. A summary of the error results from various sets of grid parameters is shown in Table 2-1. Error values are in nanoseconds.

Note the improvement in the grid as the method of estimating the grid parameter changes. The parameters used in the planning phase were poor, and in general it was found that estimating phase spatial anomalies using only land-sea interface phase recovery is inadequate. The nonlinear phase versus distance relationship, particularly near the land-sea interface and/or close to the transmitter, requires a careful choice of calibration sites both on the periphery and in the interior of the harbor.

The grid fit error is estimated to be 250 ns for the area bounded by the measurement site and about 100 ns for the area best sampled by the measurements.

Multiple idealized grids could be used to improve the grid accuracy. The required number of grids and their boundaries was not determined.

Table 2-1. Summary of linearized grid results from fixed site data.

	Planning Phase Grid Parameter	Four Sites With All Over-land Paths	Three Sites On Shore and Mid-Harbor	All Thirteen Sites Least Squares Fit
Mean TDX Error	505	544	-39	1.0
STD Dev (TDX)	307	302	155	111
Mean TDY Error	207	-97	10	0
Std Dev (TDY)	127	173	93	81
Max Error TDX	995	1027	426	211
Max Error TDY	512	380	124	141

Evaluation of Differential Loran-C

Five fixed sites were selected to simulate two differential Loran-C system configurations. Sears Point was selected as differential monitor to correct Point Molate, Angel Island, and Hunters Point measurements, and Angel Island was selected as Monitor to correct Treasure Island measurements. Improvement ratios, defined as the ratio of the standard deviations of the uncorrected to corrected TDs, were computed using two procedures. In one procedure, the full differential correction—the difference between the monitor site's current TD and its long term average—was applied at the corrected site. In the other, a fraction of the full correction, based on the estimated covariance of monitor and corrected site time difference fluctuation, was applied at the correction interval—the averaging interval for monitor and site current TD estimate—and as a function of distance between monitor and corrected site.

The results of the evaluation are summarized below:

- Improvement ratios of 1.3 to 2.5 were observed. The ratios were in general lower than reported in previous demonstrations. The reason for the small improvement is the close proximity of the SAM to the harbor; ie, Loran-C in the harbor already approximates differential Loran.
- Improvements for TDX exceed those for TDY. This is attributed to the higher signal-to-noise ratio for the X-ray signal.
- Improvements using the modified differential correction slightly exceeded those using the full correction. The signal fluctuations are primarily chain induced and are thus highly correlated. Improvements from using the differential gain calculation are expected to be greater at sites farther from the monitor or when propagation-induced fluctuations are more important.
- Best correction intervals were 100 seconds (shortest available for test) for TDX corrections and 15 minutes for TDY corrections. The improvement with averaging for TDY is attributed to the lower signal-to-noise ratio for the Yankee signal.
- No consistent pattern was noted for improvement ratio as a function of separation distance between monitor and corrected site.

Vessel Measurements

Loran-C TDs were measured along various tracks in the inner and outer San Francisco Harbor. The vessel location was accurately determined using a Trisponder microwave location system.

The Loran-C TDs were converted to absolute position using the idealized grid developed from the land site data. Loran-C position error was then computed as the difference between the converted location and the corresponding location from the Trisponder data.

Significant data processing other than the conversions were required to correct for the vessel motion during the 100-second averaging interval. Also, a Kalman filter processor was required to edit the Trisponder data for bad data and to fill in data gaps that occurred when one of the Trisponder transponders was temporarily obscured by another vessel.

More details on the coordinate conversions and the data processing techniques are provided in Section 7.

In the inner harbor, the mean and standard deviations of the difference between measured time difference and time difference obtained from the idealized grid were

means	$\Delta TDX \approx 34$ ns	$\sigma_{TDX} \approx 65$ ns	standard deviations
	$\Delta TDY \approx 1$ ns	$\sigma_{TDY} \approx 65$ ns	

In San Pablo Bay and seaward from the Golden Gate Bridge, the errors were larger, which was expected because the calibration sites were not appropriately located for these areas.

When the vessel approached Golden Gate Bridge from the inner harbor, the error in TDX began to increase 1000 to 1200 meters from the bridge and became too unstable for navigation purposes 400 to 600 meters from the bridge. After the vessel passed under the bridge, the signal recovered about 400 to 600 meters on the seaward side.

The results obtained during this experiment show that harbors should be calibrated by a carefully designed set of measurements. Results obtained in the inner harbor suggest that the idealized grid approach is a useful technique. Estimated achievable operational results for various modes of operation are discussed in the next subsection.

System Analysis Results

The system analysis study sought to establish an experimental error budget and to evaluate the performance of Loran-C in the harbor. For the experiment area and time frame, the error budget estimates were

Chain equipment	15 ns
Propagation effects	10 ns
Receiver fluctuations	10 ns
User prediction	100 ns

The latter figure is of course a function of the number and location of calibration sites.

System performance estimates for the various modes of operation were prepared for the inner harbor, excluding areas within about 1000 meters of the Golden Gate and Oakland Bay bridges. The $2D_{rms}$ error estimates are:

Mode	$2D_{rms}$ Error (m)
Absolute mode	75
Differentially augmented absolute mode	69
Repeatable mode	38
Differentially augmented repeatable mode	25

The absolute mode error could be reduced slightly by removing a bias from the idealized grid.

We conclude then that Loran-C can be used in San Francisco Harbor in the repeatable or differentially augmented repeatable modes, provided a high-quality receiver is used. Loran-C could be used in the absolute or differentially augmented absolute modes with better coordinate conversion. We feel the required coordinate conversion accuracy could be obtained by using multiple idealized grids.

SECTION 3
RECOMMENDATIONS

During the execution of the Loran-C signal project measurements, a number of problems were encountered and resolved with varying degrees of success. The experience gained in coping with these problems leads to many recommendations that should enhance the success of measurement programs which may follow. Additionally, areas that require more theoretical development as well as means to improve system performance, utilization, and acceptance have been identified. These recommendations are presented in this section.

It is important to recognize that the results for differential Loran-C and the vessel measurements were obtained by post-experiment data processing. However, the results obtained by this project on the use of Loran-C in the harbor and harbor entrance environment (HHE) are promising enough to warrant further action. Thus, like most projects, this project will end by recommending that additional experiments or demonstrations be performed. This project has shown that Loran-C has the potential accuracy for use in the HHE. An operational demonstration now is needed.

The enormous quantity of data collected during this project produced significant logistical and data handling problems. During the field experiments, raw data was recorded on cassettes, mailed to the data processing facility, and transferred from cassettes to half-inch magnetic tape prior to data reduction. This technique is a cumbersome and expensive process. Further, it does not always provide the timely reduction of data which is so important for experiment control. A much more efficient approach would be to perform some of the data processing and reduction in the field while still recording the raw data on cassette. This would provide much better experiment control and would allow the analyst to choose appropriate portions of the data for detailed processing at the central computer facility. The field data processing probably could be performed by either a microcomputer or a desk top calculator such as the HP-9825A. The computer could be coupled to a plotter or strip chart recorder to provide graphical output to aid the analyst and experiment director.

Despite numerous hardware and operational improvements to the Loran-C system in the last few years, we believe that one area still in need of research effort is chain control. The study should consider

the placement and number of system area monitors as well as the optimal use of SAM data for chain control. An improved chain control concept might include use of data from monitoring receivers near the transmitters, since it has been shown in this project that such data can be processed to identify signal fluctuations due to transmitting equipment. Furthermore, the concept of multiple SAM's should be investigated in response to providing highly stable signals in several coverage areas. The need for an improved chain control policy becomes very important in light of new and expanded roles for Loran-C such as harbor and river navigation and terrestrial uses. In fact, the lifetime of the Loran-C system may be shortened considerably unless the user community can be expanded by offering improved and expanded navigation capabilities.

To improve the current accuracy available in the absolute mode of operation, more accurate conversion of Loran-C time differences to geodetic position is required. This conversion is highly dependent upon information supplied to the user usually in the form of charts. Several methods of improving the coordinate conversion process for high-accuracy HHE and restricted waterway navigation are possible. They are:

- Multiple Linear Grids* fit to calibration data. It has been demonstrated in other projects that the calibration process can be automated and the data processed in real time.
- Multiple Idealized Grids* fit to calibration data. Again, the calibration can be automated and data processed in real time.
- Improved Idealized Grid* which uses model calibration data and also the major error sources.

The various conversion techniques mentioned above need to be analyzed and compared to determine their accuracy limits, ease of implementation, and areas of optimum application.

While the idealized grid and the associated calibration techniques developed in Section 7 have been shown to be accurate and practical for use in high-accuracy HHE applications, it should be noted that they can also be applied to the generation of enhanced accuracy charts for navigation in open waters. The Coast Guard appears to be heading in this direction in their proposed chart verification program. Before recommending any change to current chart development procedures, we believe that the proper balance between calibration data acquisition and use of prediction techniques needs to be evaluated.

Several recommendations concerning propagation prediction models spring from the analysis and results of this project. First, a more complete examination of the theory for weather-induced signal fluctuations

*See Section 7 for the definitions of "linear grid" and "idealized grid."

is needed since such fluctuations are in general noticeably absent from the data collected during this project. This is in contradiction to earlier projects. A recent paper by Samaddar (Reference 3-1) may be a step in the right direction. Secondly, a sensitivity analysis of integral equation techniques* is required to better define accuracy requirements of the necessary input data, a necessary step in evaluating the utility and practical usefulness of the method.

We recommend the continued use of Millington's method and the adjustment of conductivities to make phase predictions match calibration data, since this appears to be adequate to provide quarter-mile accuracy. However, the program and algorithms used should be improved. Finally, we recommend the development of an empirical propagation prediction model similar to Millington's technique which would also incorporate the effects of terrain. This model would be based on predicted and measured effects of large terrain features and would allow better extrapolation to areas between calibration points, while offering decreased computation time and data preparation compared to the current integral equation approach.

The manual plotting of time differences on a chart is too time-consuming and inaccurate to be useful for harbor navigation. Thus, new equipment and means of data display are necessary. Equipment manufacturers now offer latitude-longitude converters. However, the accuracy of such equipment is not in general good enough for restricted waterway navigation. A standard high-accuracy grid should be selected. Then standard high-accuracy conversions should be developed and users could obtain the necessary parameters for a particular area from standard government publications such as *Aids to Navigation*.

3-1. Samaddar, Dr. S.N., *Weather Effects on Loran-C Propagation*, U.S. Coast Guard (G-DOE-4/TP54), Washington, D.C. 20590 (to be published).

*See Section 7 for a description of the propagation prediction technique.

SECTION 4
THE FORT CRONKHITE DATA COLLECTION

The Fort Cronkhite data collection began in August 1977 and ended in May 1978. The purpose of this data collection was to provide data on long-term signal fluctuations (seasonal effects) since the other experiment periods were of limited duration. During the 9-month duration of the experiment, one DCU* and one PLDCS† collected data at Fort Cronkhite, except for one period when the PLDCS was used in the verification experiment. Because at least one receiver was located at Fort Cronkhite during the execution of all of the experiments, the data collected there provides a control point which is useful for evaluating the results of experiments conducted at different time periods. Since this experiment began first, the initial portion of the experiment was intended to provide operator training and to identify any unforeseen operational problems.

The initial receiver setup revealed several problems. One was due to very strong spectral interference from a Navy transmitter of 119.6 kHz. It was necessary to use an additional notch filter to sufficiently attenuate the signal. The strong X-ray signal also caused some problems for the DCU, which is based on a commercial hard-limiting receiver. A switched attenuator which attenuated only the X-ray signal was used to correct the severe differential signal imbalance. The PLDCS operated satisfactorily with the large signal imbalance due to its wide dynamic range. In addition, a 10 dB attenuator was used on all signals (M, X, and Y) to obtain optimum performance from the DCU.

Figures 4-1 and 4-2 show a plot of the weekly means for the PLDCS which covers a 41-week period. The data collected show no discernible long-term effects. For the X-ray signal there was an 80 ns difference between the minimum and maximum values, with a sample standard deviation of 20 ns about the mean value of 27192.444 μs. The Y signal showed similar behavior with a 43 ns difference between minimum and maximum

*Consists of an Internav LC204 TD receiver, interface, and Texas Instruments Silent 733 ASR data terminal.

†Consists of Magnavox BRN-5 sensor, HP-2108 minicomputer, cesium beam frequency standard, and Texas Instruments data terminal.

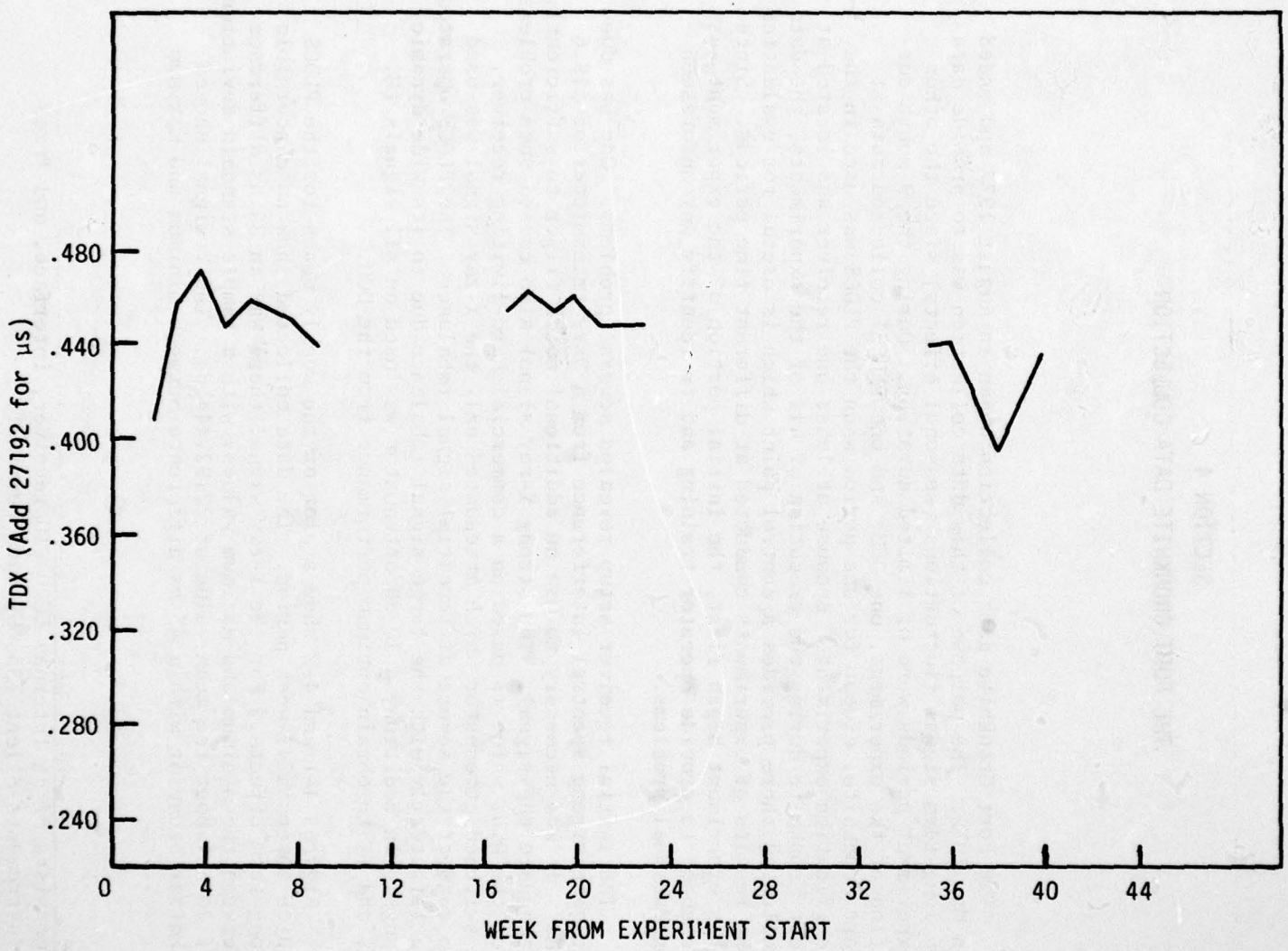

Figure 4-1. Weekly TDX mean data at Fort Cronkhite collected using the PLDCS.

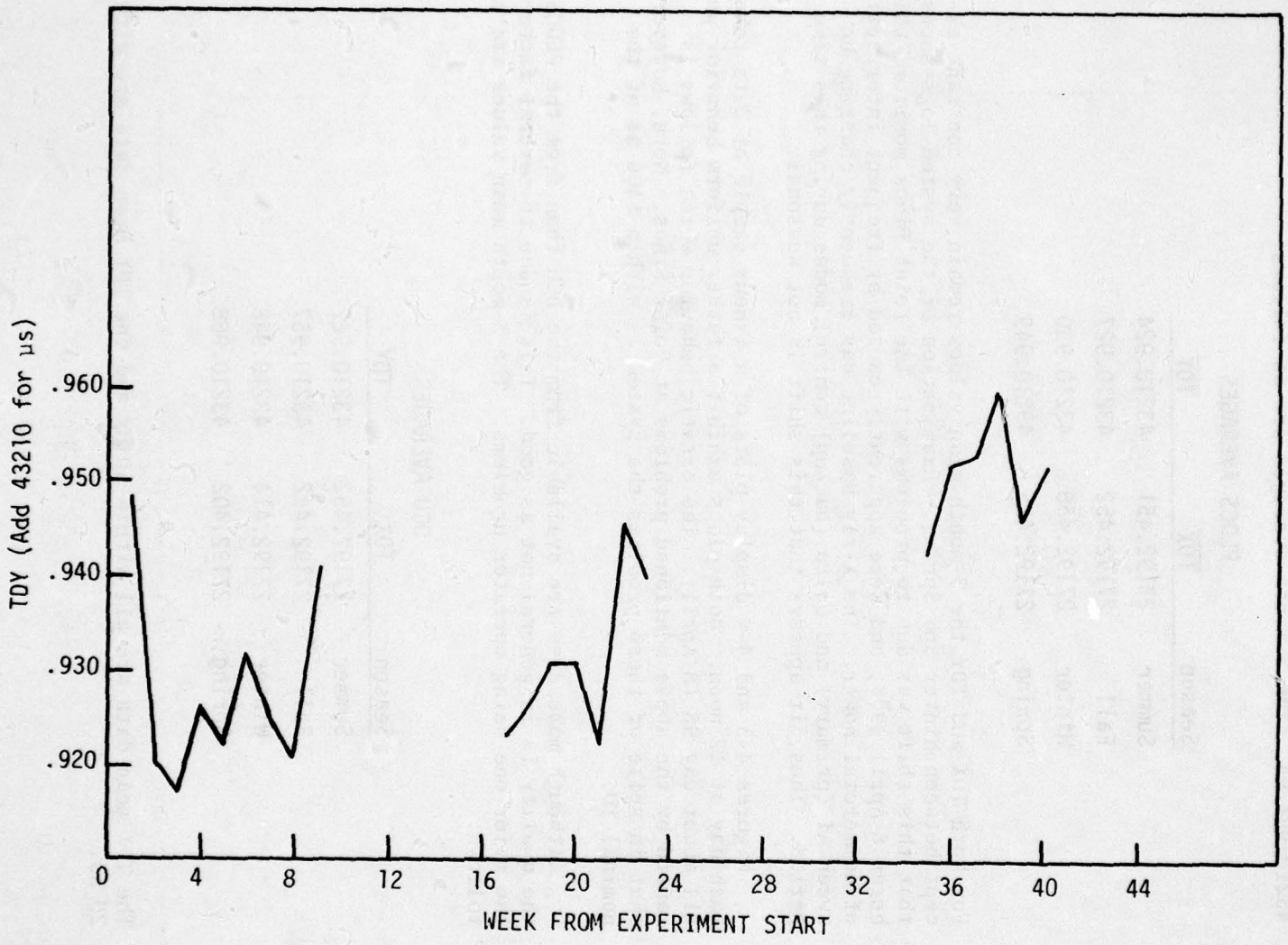

Figure 4-2. Weekly TDY mean data at Fort Cronkhite collected using the PLDCS.

values and sample standard deviation of 13 ns about the mean value of 43210.934 μs. The 3-month averages are as follows:

PLDCS AVERAGES

Season	$\overline{TDX}$	$\overline{TDY}$
Summer	27192.451	43210.924
Fall	27192.452	43210.927
Winter	27192.456	43210.930
Spring	27192.425	43210.949

For both TDX and TDY the 3-month mean values remain very constant except between Winter and Spring. Examination of the system logs shows that this shift was due to problems with the Point Piños monitor, which began 8 April 1978, and were apparently caused by frequent interruption of commercial power. The X-ray baseline was frequently changing between A1 (primary) and Delta (backup) control modes during this time period. Thus, it appears that this shift is not seasonal.

Figures 4-3 and 4-4 display plots of a 1-hour sample of data taken each day at 12 noon. Both plots exhibit a rather uniform behavior until about day 98 (8 April). The erratic behavior which follows is caused by the above mentioned problems at Point Piños. Note, however, that in spite of these problems the system is within ±100 ns of the nominal TD.

Although more data are available from the DCU than from the PLDCS, the quality is in general not as good. This is due to several factors, the major one being operator problems. The 3-month mean values are as follows:

DCU AVERAGES

Season	TDX	TDY
Summer	27192.452	43210.962
Fall	27192.442	43210.957
Winter	27192.414	43210.948
Spring	27192.402	43210.968

The TDX mean data are all within 50 ns and the TDY mean data are within 20 ns.

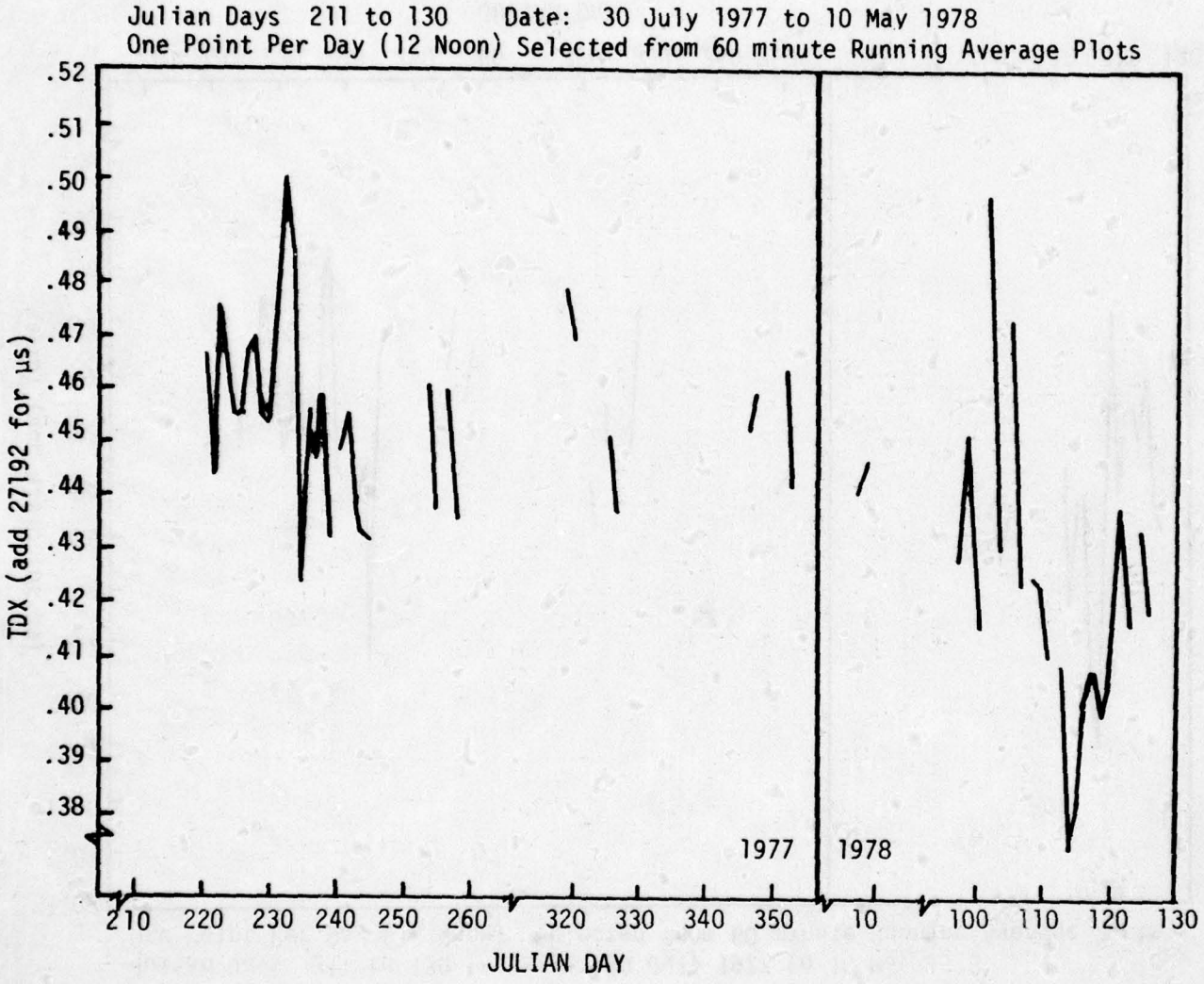

Figure 4-3. Daily sample of TDX from PLDCS at Fort Cronkhite.

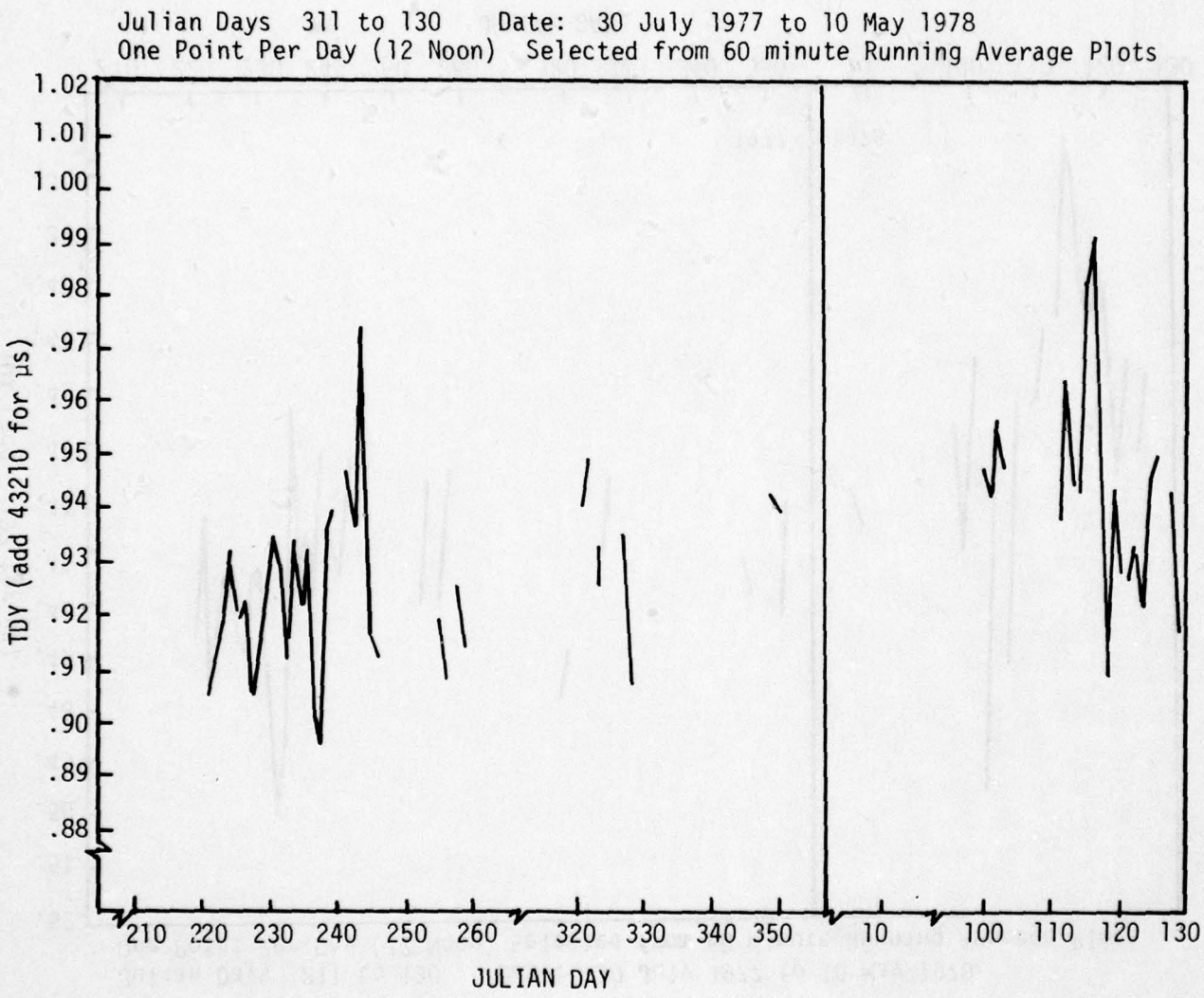

Figure 4-4. Daily sample of TDY from PLDCS at Fort Cronkhite.

Examination of the Fort Cronkhite data reveals no discernible seasonal effects. In fact the data show the Loran-C grid to be very stable in the San Francisco area. This was expected and in fact is one of the reasons San Francisco Harbor was chosen as a test area. The sample standard deviations for both TDX and TDY remained in the 20 to 30 ns range during the entire experiment for receiver averaging times of 55 to 100 seconds. The typical Loran-C user, however, should not expect to obtain the excellent results shown here unless his receiver has comparable signal averaging time, extra notch filters, and attenuation of the X-ray signal.

SECTION 5

THE STABILITY AND VERIFICATION EXPERIMENTS

To assess Loran-C's potential for high-accuracy navigation, a combination of theoretical analysis and experimental results has been used to separate and quantify error sources. The three categories of error sources considered are receiver-induced fluctuations (which includes noise and spectral interference), transmitting equipment fluctuations, and propagation fluctuations. The stability experiment was designed to yield the magnitude, source, and frequency of occurrence of errors produced by the transmitting equipment and propagation sources. The experiment design called for three DCUs (data collection units) to be placed near X-ray (Arbuckle, CA), Master (Silver Springs, NV), and Yankee (Jean, NV) as shown in Figure 5-1. DCUs (ie, TD receivers) were used instead of TOA receivers due to the high cost of obtaining additional TOA receivers.

Because several assumptions and special processing are required to separate chain and propagation fluctuations, a preliminary experiment, the verification experiment, was designed to test the stability experiment assumptions and procedures. The data processing procedures and the two experiments are described below.

EXPERIMENT ANALYSIS MODEL

The empirical model to be used for data analysis is briefly described here. A detailed derivation can be found in Reference 5-1. We shall denote receiver fluctuations by a subscript Γ, transmitting equipment fluctuations by a subscript Ω, and propagation fluctuations by a subscript θ. Nomenclature used will be as follows:

For TOA (time of arrival) measurements,

TOAKM(t) = Time of arrival of master signal received at site K at time t

$\widehat{\text{TOAKM}}(t)$ = Linear least squares fit to TOAKM data over some time interval that includes t

5-1. Nelson, L.W., *Loran-C System Analysis Interim Report No. 1*, GE77TMP-54, General Electric-TEMPO, September 1977.

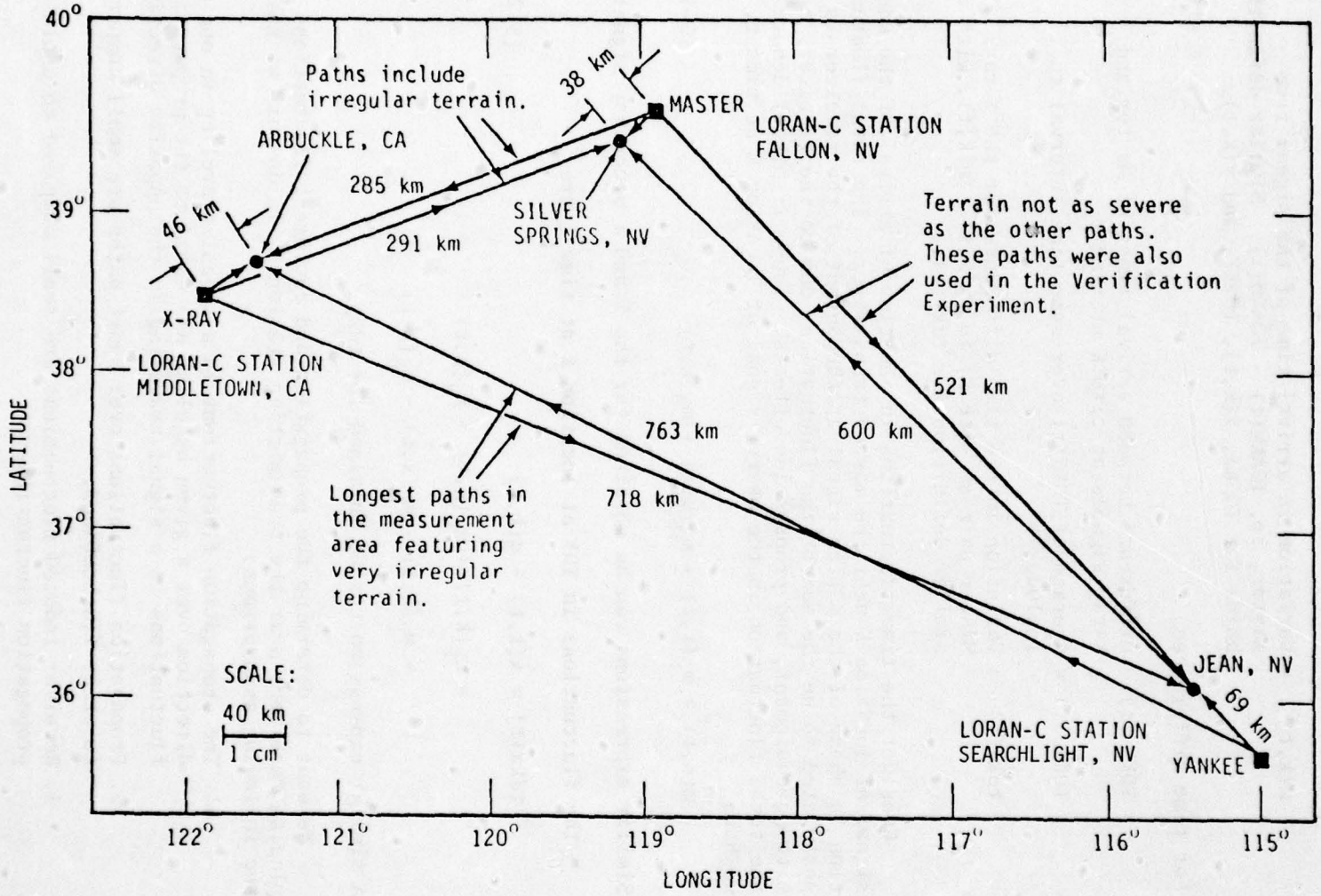

Figure 5-1. Verification experiment and stability experiment measurement sites, transmitter locations, and signal paths.

m(k,t) = Variation in arrival time of the signal from master, ie, TOAKM(t) - $\widehat{\text{TOAKM}}$(t). Similar definition holds for TOAKX, x(k,t), TOAKY, and y(k,t).

For time differences,

TDKX (t) = Difference between arrival times of Master and X-ray signals at site K at time t

TDKX = Average of TDKX(t) over some time interval that includes t

tdkx(t) = Variation in the time difference for the X-ray/Master pair at site K, ie, x(k,t) - m(k,t), with a similar definition for tdky(t).

Consider the time fluctuations in the time of arrival of the master signal at location K near the master transmitter. The total fluctuation in phase of the master signal at the output of the receiver is postulated to be the sum of the fluctuations due to the receiver, transmitting equipment, and propagation effects. Thus, if m(k,t) denotes the total fluctuation in the master signal at location K at time t, we have

$$m(k,t) = m_{\Gamma}(k,t) + m_{\Omega}(k,t) + m_{\theta}(k,t) \quad . \tag{5-1}$$

Similar expressions can be obtained for the X and Y secondary signals.

The fluctuations in TDX at location K at time t are

$$\begin{aligned} tdkx(t) &= x(k,t) - m(k,t) \qquad (5\text{-}2) \\ &= x_{\Gamma}(k,t) + x_{\Omega}(k,t) + x_{\theta}(k,t) \\ &\quad - m_{\Gamma}(k,t) - m_{\Omega}(k,t) - m_{\theta}(k,t) \quad . \end{aligned}$$

A similar expression can be obtained for tdky.

We want to determine the propagation and equipment fluctuations by placing receivers near the transmitting stations. To do this we make the following assumptions:

1. The propagation fluctuations in a signal traveling in one direction over a given baseline are equal to the propagation fluctuations in a signal traveling in the opposite direction.
2. Propagation fluctuations over short paths are small compared to other fluctuations.
3. Receiver-induced fluctuations are small compared to chain and propagation fluctuations.

4. Chain fluctuations are the same for all receivers in the coverage area; ie, chain fluctuations are not spatially dependent.

It is postulated that by placing TD receivers at site H near X-ray, site K near Master, and site L near Yankee, chain and propagation fluctuation could be deduced (see Reference 5-1) if the above listed assumptions hold. The chain fluctuations for the X-ray/Master pair are computed as follows:

$$x_{\Omega}(t) - m_{\Omega}(t) = [tdkx(t) + tdhx(t)]/2 \quad . \tag{5-3}$$

The Yankee-Master pair chain fluctuations are given by

$$y_{\Omega}(t) - m_{\Omega}(t) = [tdky(t) + td\ell y(t)]/2 \quad . \tag{5-4}$$

The propagation fluctuations on the X baseline are given by

$$x_{\theta}(k,t) = m_{\theta}(h,t) = [tdkx(t) - tdhx(t)]/2 \quad , \tag{5-5}$$

while the propagation fluctuations on the Y baseline are given by

$$y_{\theta}(k,t) = m_{\theta}(\ell,t) = [tdky(t) - td\ell y(t)]/2 \quad . \tag{5-6}$$

Additionally, the propagation fluctuations on the path from X-ray to Yankee are given by

$$y_{\theta}(h,t) = x_{\theta}(\ell,t) = \frac{[tdhy(t) - tdhx(t) + td\ x(t) - td\ y(t)]}{2} \tag{5-7}$$

The model postulates the existence of a given fluctuation but does not define a specific physical cause for the fluctuation.

VERIFICATION EXPERIMENT

The verification experiment was conducted prior to the stability experiment to show that the data from the three TD receivers could be processed (ie, using TD receivers instead of TOA receivers) to yield chain and baseline propagation fluctuations. Measurements were conducted by collocating DCUs (TD receiver) and PLDCSs (TOA receivers) at both Jean, NV, near the Yankee transmitter and Silver Springs, NV, near the Master transmitter (see Figure 5-1). Data were collected for 3 weeks from 6 October 1977 until 27 October 1977. The purpose of this experiment was to verify that the data from TD receivers placed near chain transmitters can be manipulated under a reasonable set of assumptions to yield chain equipment fluctuations and baseline propagation fluctuations. Using the above model, the Master and Yankee TOAs at Silver Springs should be composed of the following fluctuations:

$$m(k,t) = m_{\theta}(k,t) + m_{\Omega}(k,t) + m_{\Gamma}(k,t) \qquad (5\text{-}8)$$

and

$$y(k,t) = y_{\theta}(k,t) + y_{\Omega}(k,t) + y_{\Gamma}(k,t) \quad . \qquad (5\text{-}9)$$

Due to the short length of the path to site K from Master, we have $m_{\theta}(k,t) \approx 0$; thus

$$m(k,t) = m_{\Omega}(k,t) + m_{\Gamma}(k,t) \quad . \qquad (5\text{-}10)$$

If we neglect receiver error for the moment, we see from Equation 5-10 that the fluctuations in Master TOA at site K are primarily due to the transmitting equipment at Master. Similarly, the Y secondary TOA fluctuations at site K are primarily due to the transmitting equipment at Yankee and the propagation path from Yankee to site K.

A TOA receiver at Jean will measure the following TOA fluctuations:

$$m(\ell,t) = m_{\theta}(\ell,t) + m_{\Omega}(\ell,t) + m_{\Gamma}(\ell,t) \qquad (5\text{-}11)$$

and

$$y(\ell,t) = y_{\theta}(\ell,t) + y_{\Omega}(\ell,t) + m_{\Gamma}(\ell,t) \quad . \qquad (5\text{-}12)$$

Again noting the short path from Yankee to site L, we obtain

$$y(\ell,t) = y_{\Omega}(\ell,t) + y_{\Gamma}(\ell,t) \quad . \qquad (5\text{-}13)$$

Neglecting the receiver fluctuations leads to the conclusion that the Master TOA fluctuations at site L are primarily due to the transmitting equipment at Master and the propagation path from Master to site L, while the Y secondary TOA fluctuations at site L are primarily due only to the transmitting equipment at Yankee.

Recall that the Y TDs measured at sites K and L could be manipulated (applying the above assumptions) to give

$$(tdky(t) + td\ell y(t))/2 = y_{\Omega}(t) - m_{\Omega}(t), \qquad (5\text{-}14)$$

where equipment fluctuations are assumed spatially independent. To determine the validity of Equation 5-14, we can use TOA data to determine $y_{\Omega}(t) - m_{\Omega}(t)$ by subtracting Equations 5-10 from Equation 5-13 and neglecting receiver fluctuations. This yields

$$y(\ell,t) - m(k,t) \approx y_{\Omega}(t) - m_{\Omega}(t) \quad . \qquad (5\text{-}15)$$

Experimental Results

The results of using the left-hand side of Equation 5-15 are called the TOA chain fluctuations, and the results of using the left-hand side of Equation 5-14 are called TD chain fluctuations. Table 5-1 shows the sample standard deviations of the TD and TOA chain fluctuations and their correlation coefficient (computed from PLDCS data). The data show that TD and TOA chain fluctuations are highly correlated. Thus, chain fluctuations are indeed large compared to receiver fluctuations. We conclude that the data from TD receivers placed near transmitters can be manipulated to yield fluctuations due to transmitting equipment.

It is interesting to note that the standard deviations of the TOA chain fluctuations are consistently higher than the TD chain fluctuations. This is attributed to the fact that receiver-induced errors are common to the master and secondary TOAs and cancel when the TD is computed. TD data are thus inherently more stable than TOA data. The BRN-5 receiver used in the PLDCS has a maximum error of about 15 nanoseconds due to delay changes in the RF filter, AGC (automatic gain control), and notch filters. Based on the data in Table 5-1, it is estimated that about a 10 ns rms error occurs which is common to both the Master and Y secondary signals.

Propagation fluctuations on the Yankee baseline can be computed from TDs by

$$(tdky(t) - td\ell y(t))/2 = m_\theta(\ell,t) = y_\theta(k,t) \quad . \tag{5-16}$$

To verify this using TOA measurements, we use Equations 5-11 and 5-10 to get

$$m(\ell,t) - m(k,t) = m_\theta(\ell,t) + m_\Gamma(\ell,t) - m_\Gamma(k,t) \quad . \tag{5-17}$$

Table 5-1. Standard deviations of the instantaneous fluctuations from the mean time differences for TD and TOA (and correlation coefficient) (BRN-5 data only).

	TD Chain Fluctuations Sigma (ns rms)	TOA Chain Fluctuations Sigma (ns rms)	Correlation Coefficient
Week 1	17.7	21.5	0.82
Week 2	17.5	20.6	0.76
Week 3	15.0	16.4	0.74

Neglecting receiver error yields

$$m(\ell,t) - m(k,t) = m_\theta(\ell,t) \quad . \tag{5-18}$$

A similar manipulation using Equations 5-9 and 5-13 gives

$$y(k,t) - y(\ell,t) = y_\theta(k,t) \quad . \tag{5-19}$$

The results of using the right-hand side of Equation 5-16 are called TD propagation fluctuations. The results of applying the right-hand side of Equation 5-18 to the TOA data are called K to L propagation fluctuations, while the application of the right-hand side of Equation 5-19 yields L to K propagation fluctuations. The average of the L to K and K to L fluctuations is called the TOA propagation fluctuation and in fact is identical to the TD propagation fluctuations.

Table 5-2 gives the sample standard deviation for the TD propagation fluctuations and the K to L and L to K TOA propagation fluctuations. The standard deviation for the TD propagation fluctuations is on the order of the receiver standard deviation as measured in receiver simulator tests. Further, we notice that the correlation coefficient of the L to K versus the K to L TOA fluctuation is negative. This implies that the receiver error dominates. To see this, let us express the numerator of the correlation coefficient in terms of signal fluctuations. If we assume independence of propagation and receiver fluctuations and independence of receiver fluctuations at the two sites, we obtain

$$\begin{aligned} &E\{[m_\theta(\ell,t) + m_\Gamma(\ell,t) - m_\Gamma(k,t)][y_\theta(k,t) + y_\Gamma(k,t) - y_\Gamma(\ell,t)]\} \\ &= E\{ m_\theta(\ell,t)y_\theta(k,t)\} - E\{m_\Gamma(k,t)y_\Gamma(k,t)\} - E\{m_\Gamma(\ell,t)y_\Gamma(\ell,t)\} \end{aligned} \tag{5-20}$$

where $E\{\cdot\}$ is the expectation operator.

Table 5-2. Standard deviation of the instantaneous fluctuations from the mean time difference for TD propagation fluctuations and TOA L to K and K to L propagation fluctuations and their correlation coefficients (BRN-5 data only).

Time	Standard Deviation rms (ns))			Correlation Coefficient of TOA Fluctuations
	TD Propagation Fluctuations Silver Springs and Jean	TOA K (Silver Springs to L (Jean) Propagation Fluctuations	TOA L (Jean) to K (Silver Springs) Propagation Fluctuations	
Week 1	6.9	12.7	15.6	-0.54
Week 2	7.7	13.8	17.0	-0.52
Week 3	7.5	12.0	15.2	-0.41

Since E $\{m_\theta(\ell,t)y_\theta(k,t)\}$ is positive, the only way Equation 5-20 can be negative is for the last two terms to be large compared to the first. The data in Table 5-2 are quite consistent for the 3 weeks. Analysis of the processed and reduced data leads to the conclusion that there were no measurable propagation fluctuations during the 3 week time period of sufficient magnitude to be significant compared to receiver-induced fluctuations.

Weather data show that at least four strong cold fronts passed over the Y baseline. However, these fronts did not affect a major portion of the baseline as they passed; thus weather-induced fluctuations were expected to be small. No conclusion could be reached concerning the observability of propagation fluctuations from this data due to the absence of any significant propagation fluctuations.

Data were also taken using DCUs during the Verification experiment. It is possible to compare fluctuations computed from PLDCS data with those computed from DCU data. Although the two receivers are quite different in their signal processing, it was felt that the two would correlate quite well. This conjecture was based on data collected in August 1977 for a collocated PLDCS and DCU at Fort Cronkhite, California. The Fort Cronkhite data showed the TDs of the two receivers tracked quite well over a data collection period of 4 continuous weeks. Table 5-3 shows the sample standard deviation of the TD chain fluctuations as computed from PLDCS and DCU data and the correlation coefficient.

For Week 1, the correlation is quite good, implying the receivers measured the same phenomena, while for Weeks 2 and 3 it is decreased but is still significant. The decrease in correlation during Weeks 2 and 3 has been traced to nighttime skywave interference from a Canadian transmitter at about 76 kHz. This spectral interference caused a significant diurnal fluctuation in the DCU data. The PLDCS was unaffected because its autonotch filter effectively eliminated the interfering signal.

Table 5-3. Comparison of PLDCS and DCU TD chain fluctuations (standard deviations) during the verification experiment.

Time	Chain Fluctuations (ns) rms		Correlation Coefficient
	PLDCS	DCU	
Week 1	17.7	15.0	0.81
Week 2	17.5	24.7	0.51
Week 3	15.0	17.9	0.58

Table 5-4 presents a comparison of propagation fluctuations computed from PLDCS and DCU data. One might expect the agreement between DCU and PLDCS to be worse for propagation fluctuations since the previous data showed that the receiver error dominates. This in fact is the case as witnessed by the small correlation coefficient.

Conclusions for the Verification Experiment

The results and conclusions for the verification experiment can be summarized as follows. First, the experiment proved that variations due to the Loran-C transmitting equipment can be observed by manipulating the data from TD receivers placed near the transmitters. Second, due to the absence of significant propagation-media-induced variations, no definite conclusion could be reached about the observability of propagation fluctuations using TD receivers. However, whatever is measured is the average of the one-way propagation fluctuations. Finally, during the month of October 1977 the southern triad as measured at Silver Springs, NV, and Jean, NV (several hundred kilometers from the system area monitor) was very stable.

THE STABILITY EXPERIMENT

The stability experiment (see Figure 5-1) started on 1 December 1977 and continued through 23 January 1978. Continuous data collected in October 1977, December 1977, and January 1978 have shown the system to be remarkably stable (ie, the fluctuation is less than 25 nanoseconds). Table 5-5 shows a summary of these data for December 1977, while Table 5-6 shows a summary for January 1978. The data from the three receivers were processed using Equations 5-3, 5-4, 5-5 and 5-6 to yield the chain and baseline propagation fluctuations shown in Tables 5-5 and 5-6.

In addition, the propagation fluctuations on the Jean-Arbuckle path (the longest path in the southern triad) can be computed by

$$y(h,t) = x(\ell,t) = [tdhy(t) - tdhx(t) + td\ell x(t) - td\ell y(t)]/2 \quad (5\text{-}21)$$

Table 5-4. Comparison of PLDCS and DCU propagation fluctuations (standard deviations) during the verification experiment.

Time	Propagation Fluctuations (ns) rms		Correlation Coefficient
	PLDCS	DCU	
Week 1	6.9	10.1	0.28
Week 2	7.7	21.8	0.05
Week 3	7.5	14.0	0.10

Table 5-5. Loran-C stability experiment data summary for December 1977.

Location	Week	Mean TDX	Mean TDY	Std. Dev. TDX (rms)	Std. Dev. TDY (rms)	Data Sample (days)
Silver Springs	1	28933.9232	43842.2094	0.0338	0.0367	7
	2	28933.8840	43842.2022	0.0637	0.0384	7
	3	28933.7997	43842.1858	0.0293	0.0210	3
Arbuckle	1	27296.2207	43565.3130	0.0233	0.0363	7
	2	27296.2305	43565.3215	0.0223	0.0409	7
	3	27296.2650	43565.3509	0.0135	0.0316	3
Jean	1	28752.2519	40455.9560	0.0381	0.0172	7
	2	28752.2484	40455.9334	0.0336	0.0219	7
	3	28752.2181	40455.9261	0.0303	0.0158	3

Standard deviations (data from Silver Springs, Arbuckle, and Jean) of the instantaneous fluctuations (rms)

Week 1

X - Chain fluctuations 0.0270 X - Propagation fluctuations 0.0164

Y - Chain fluctuations 0.0208 Y - Propagation fluctuations 0.0146

Week 2

X - Chain fluctuations 0.0330 X - Propagation fluctuations 0.0352

Y - Chain fluctuations 0.0274 Y - Propagation fluctuations 0.0119

Week 3

X - Chain fluctuations 0.0186 X - Propagation fluctuations 0.0135

Y - Chain fluctuations 0.0173 Y - Propagation fluctuations 0.0112

Table 5-6. Stability experiment data summary for January 1978.

Location	Week	Mean TDX	Mean TDY	Std. Dev. TDX (rms)	Std. Dev. TDY (rms)	Data Sample (days)
Silver Springs	2	28933.7898	43842.2219	0.0276	0.0204	4
	3	28933.7179	43842.211	0.030	0.013	1
Arbuckle	2	27296.202	43565.470	0.020	0.015	4
	3	27296.179	43565.489	0.014	0.021	1
Jean	2	28752.1946	40455.9711	0.024	0.0232	4
	3	28752.157	40456.026	0.024	0.008	1

Standard deviations (data from Silver Springs, Arbuckle, and Jean) of the instantaneous fluctuations (rms)

Week 1

X - Chain fluctuations 0.0223 X - Propagation fluctuations 0.0114

Y - Chain fluctuations 0.0160 Y - Propagation fluctuations 0.0104

Week 2

X - Chain fluctuations 0.0178 X - Propagation fluctuations 0.0148

Y - Chain fluctuations 0.0137 Y - Propagation fluctuations 0.0094

It was not originally planned to process data using Equation 5-21, because it was felt that receiver error may be too large as a result of the four TDs in Equation 5-21 instead of two. The unexpected absence of the operator at Silver Springs caused a loss of about 10 days of expected stability data. Since good data are available from Arbuckle and Jean for this time period, they were processed using Equation 5-21. These data are shown in Table 5-7.

The results given in Tables 5-5 and 5-6 are consistent with those obtained from the verification experiment with the exception of Week 2. During this time period the TDX standard deviation for Silver Springs, NV jumped to 64 ns and the propagation fluctuation standard deviation more than doubled. These large changes appear to be caused by passage of a weather front across the entire X-ray baseline on December 14 and subsequent rain storms which lasted for the next 3 or 4 days. Examination of the raw data from Arbuckle and Silver Springs reveals a transitory fluctuation of about 80 ns in magnitude that was coincident with the passage of the frontal system. While TDX at Arbuckle partially recovered, TDX at Silver Springs remained below the earlier mean value for the duration of the experiment.

Figures 5-2 and 5-3 show TDX at Silver Springs and Arbuckle for the time period of interest. The data at both sites (worst at Silver Springs) have significant diurnal fluctuations believed to be caused by nighttime spectral interference. These fluctuations make precise interpretation of the data difficult; however, crude estimates are that the mean TDX decreased 120 to 160 ns at Silver Springs and increased 40 to 60 ns at Arbuckle. The data manipulated using Equations 5-3 and 5-5, which assume negligible propagation fluctuations over the short paths, produced an estimate of about 50 ns decrease in TDX due to chain equipment fluctuations and about 80 ns decrease in propagation phase delay on the baseline. The assumption of negligible fluctuation on the short paths may be approximately satisfied for propagation fluctuations induced by atmospheric refractive index changes but is not satisfied for fluctuations induced by surface impedance changes. The long duration of the shift in TDX also indicates that its cause was due to surface impedance changes, not refractive index changes.

In a subsequent analysis, Samaddar (Reference 5-2) used supporting TINO (time interval number or pseudo time difference) data taken at the transmitter sites to further explain the observations. This data is free from propagation fluctuations on the short paths since the receiver is located at the transmitter. His analysis of the TINO data for the same time period indicates that

---

5-2. Samaddar, Dr. S.N., *Weather Effects on Loran-C Propagation*, U.S. Coast Guard (G-DOE-4/TP54) Washington, DC 20590 (to be published).

Table 5-7. Stability experiment results of means, standard deviations, and propagation fluctuations* on Arbuckle to Jean paths.

Receiver Site	Code	Time Frames of Data Samples (days/hours) From	To	TDX Mean (μs)	TDY Mean (μs)	TDX Std. Dev. (ns rms)	TDY Std. Dev. (ns rms)
Jean	I	340 12	346 09	52.2561	55.9545	38.1	17.2
TDX = 28752 ...		346 09	353 09	52.2489	55.9339	33.6	21.0
		353 12	364 09	52.2225	55.9372	35.9	20.8
TDY = 40455 ...		364 16	001 11	52.1810	55.9550	26.0	13.6
		002 17	011 10	52.1856	55.9506	22.5	17.3
		011 15	013 11	52.1990	55.9664	18.4	17.2
		013 12	021 16	52.1763	56.0001	24.1	25.6
Arbuckle	H	340 12	364 09	96.2208	65.3131	23.3	36.3
TDX = 27296 ...		346 09	353 09	96.2306	65.3221	22.3	40.9
		353 12	364 09	96.2648	65.3509	18.6	40.2
TDY = 43565 ...		364 16	001 11	96.2199	65.4009	11.1	29.9
		002 17	011 10	96.2050	65.4673	22.0	23.1
		011 15	013 11	96.1992	65.4700	14.3	21.6
		013 12	021 16	96.1868	65.4795	14.0	24.4

Propagation fluctuations on the Yankee to Arbuckle and X-ray to Jean paths in nanoseconds.

From	To	ns rms
340 12	346 09	20.9
346 09	353 09	22.6
353 12	364 09	23.1
364 16	001 11	19.0
002 17	011 10	15.2
011 15	013 11	14.8
013 12	021 16	18.1

*Standard deviations of the instantaneous fluctuations from the mean time differences.

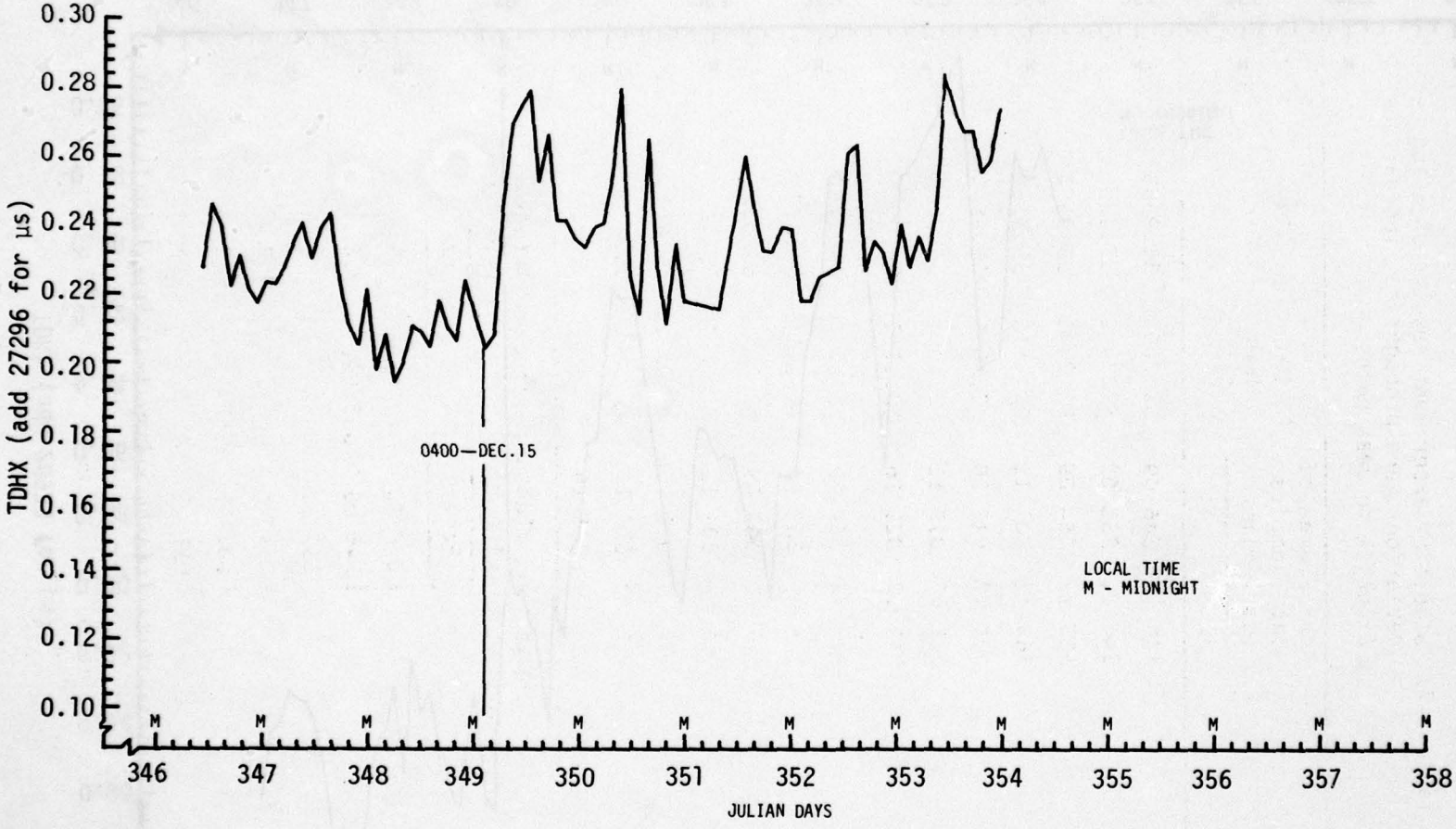

Figure 5-2. TDX at Arbuckle.

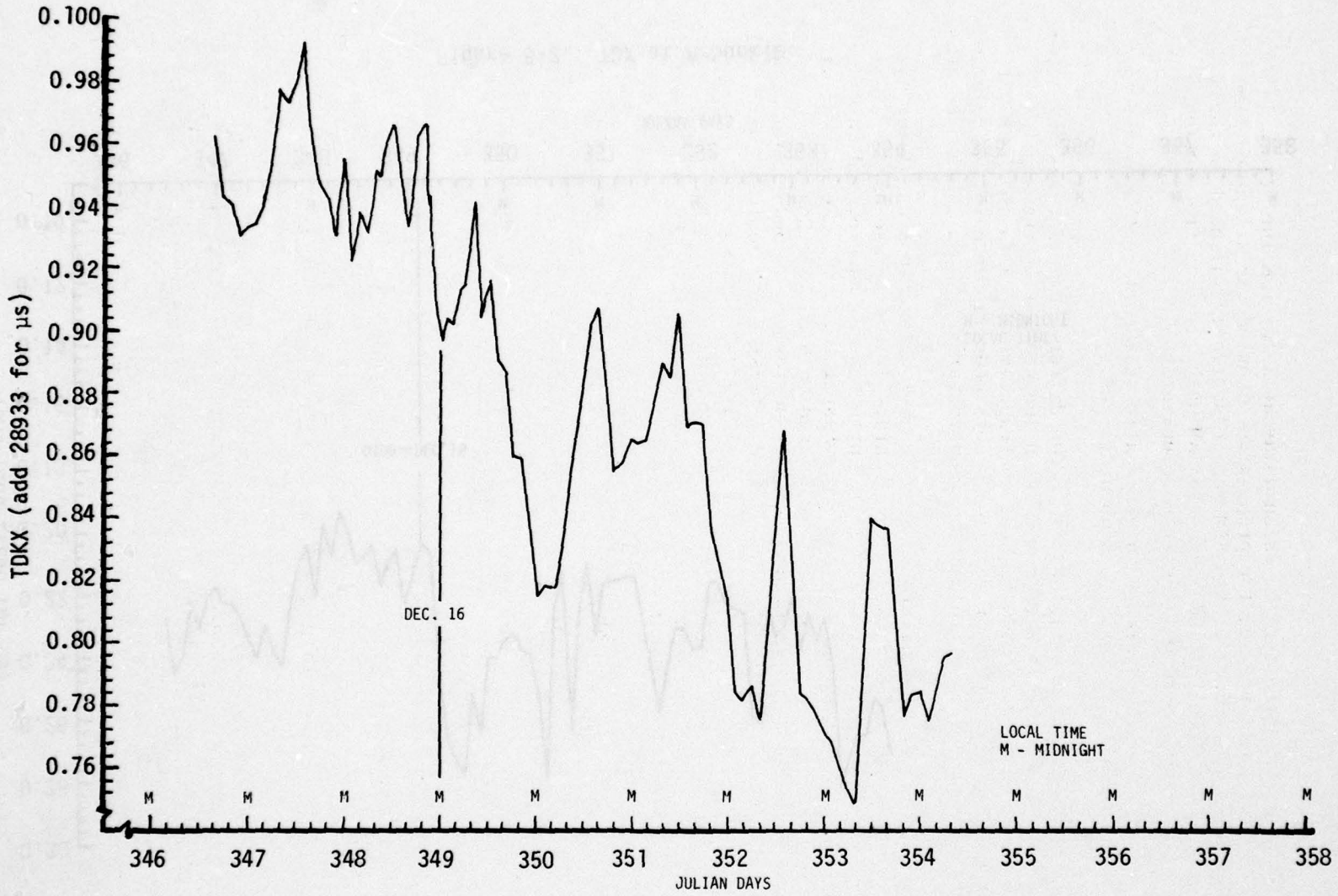

Figure 5-3. TDX at Silver Springs.

1. The effective emission delay at X-ray remained essentially constant; ie, the propagation-induced variations on time difference at the SAM were essentially balanced on the X-ray to SAM and Master to SAM paths, and control action corrected only relative clock drift.
2. The net decrease in propagation delay along the path from X-ray to Master was about 116 ns.

Based on (1) above, the total time difference variations at Silver Springs and Arbuckle were propagation induced. Thus the apparent chain variations we deduced from the experimental data should be attributed to violation of the assumptions made in the data manipulations, primarily neglecting propagation induced variations on the short paths.

The following analysis suggests two of a countless number of possible explanations of the observed data. In one we use our original estimates of TDX changes at Silver Springs and Arbuckle, and Samaddar's results for TDX changes on the X-ray-Master baseline. We use nominal conductivity boundaries and values based on USCG West Coast calibration data as illustrated in Figure 5-4. By performing secondary phase calculations using Millington's technique, first using nominal conductivity value for the segments shown in Figure 5-4 and then values slightly above the nominal values, and by assuming that phase versus conductivity variations are linear over a small range in conductivity, we can obtain the following equations:

$$\Delta TD_{SS} = -86\Delta\sigma_A - 5\Delta\sigma_B - 31\Delta\sigma_C - 977\Delta\sigma_D + 176\Delta\sigma_E \approx -120 \text{ to } -160 \text{ ns}$$

$$\Delta TD_A = -116\Delta\sigma_A + 11\Delta\sigma_B + 36\Delta\sigma_C + 307\Delta\sigma_D + 103\Delta\sigma_E \approx 40 \text{ to } 60 \text{ ns}$$

$$\Delta T_{XM} = -85\Delta\sigma_A - 8\Delta\sigma_B - 29\Delta\sigma_C - 420\Delta\sigma_D - 101\Delta\sigma_E \approx -116 \text{ ns}$$

where

$\Delta\sigma_i$ = change in conductivity for the ith segment (mhos/m)

ΔTD_{SS} = change in X-ray TD at Silver Spring (ns)

ΔTD_A = change in X-ray TD at Arbuckle (ns)

ΔT_{XM} = change in phase delay along the Master/X-ray path (ns)

A trial and error solution produced the results in Table 5-8. Since there are more unknowns than equations, an infinite number of solutions may be obtained.

An alternate interpretation can be obtained by estimating that the time difference decrease at Silver Springs is slightly less than the time difference decrease on the X-ray-Master baseline. This would result in time difference changes approximately proportional to path length and could be explained by a general but small increase in conductivity on the baseline.

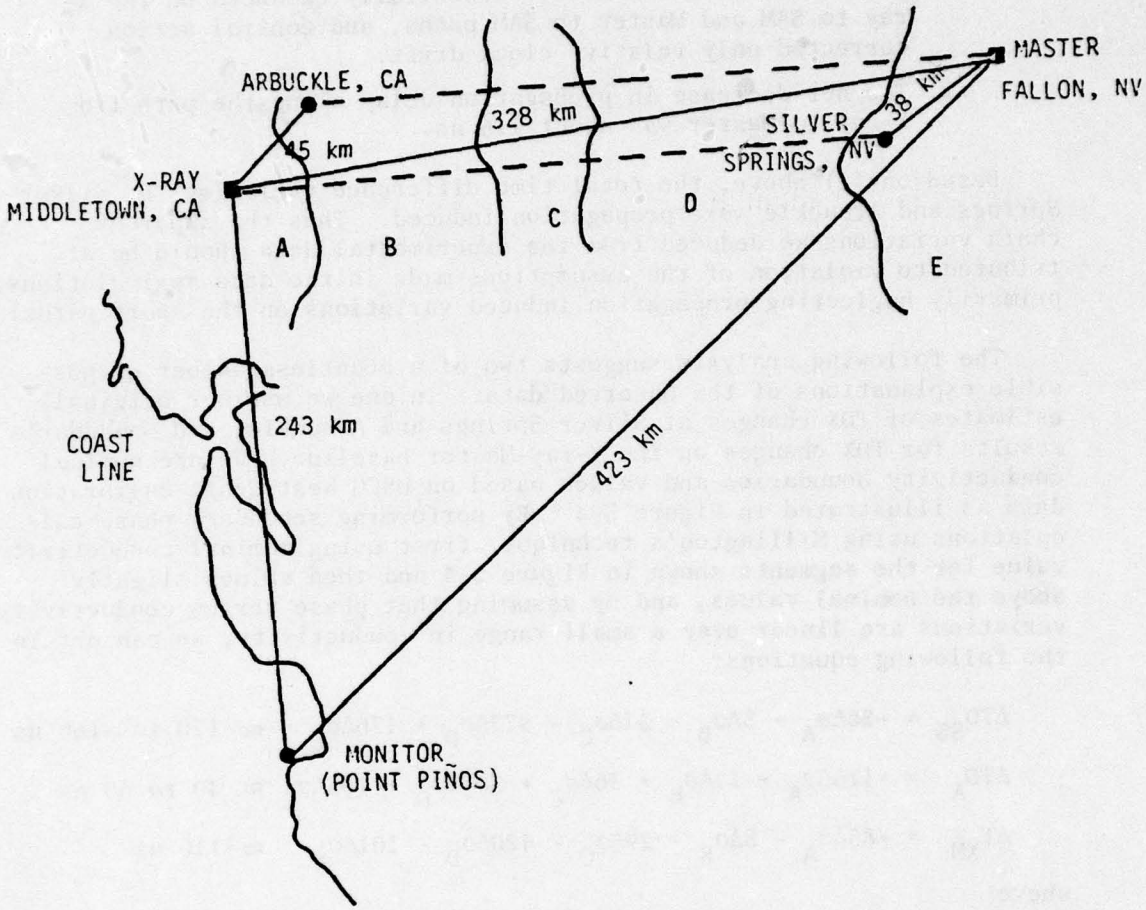

Other distances:
Arbuckle to Master - 284 km
Silver Springs to Middletown - 290 km

Figure 5-4. Measurement sites and conductivity area boundaries for the stability experiment.

Table 5-8. Conductivity variations (mmhos/m), and predicted time difference changes.

Segment	Nominal	New	Time Difference	Predicted Change
A	2	2.3	ΔTD_{SS}	-136.9 ns
B	8	8	ΔTD_{A}	+ 42.2 ns
C	2	3	ΔT_{XM}	-107.1 ns
D	0.5	0.53		
E	2	2.1		

Other interpretations of the data, so long as the variations are in the one hundreds of ns range, may also be explained by reasonable choices of conductivity.

Instrumentation errors in the measurement of the data were minimal (other than spectral interference effects) as indicated by the following:

- Portable simulator tests of the receiver at Silver Springs performed during the verification and stability experiments showed highly correlated results and no drift in TDs.
- The computed equipment fluctuations for TDY were consistent (ie, in the 20 ns rms range) for the verification and stability experiments.
- Post-experiment receiver simulator tests conducted at the U.S. Coast Guard Electronic Engineering Center verified the results of the portable simulator test.

We also rule out chain control problems due to the SAM at Point Piños, because the mean TD's at Fort Cronkhite varied less than 20 ns for the same time frame.

Although not proven in the verification experiment, it appears, based on the above results, that propagation fluctuations can be observed by manipulating the data from TD receivers placed near (or better yet at) the transmitter. However, we cannot conclusively make the statement since we have only one sample. It is also very interesting that the Y baseline and the Arbuckle-Jean paths showed no discernible propagation fluctuations. This seems to be due to orientation of these paths relative to the weather fronts, such that only a small portion of the paths is affected by the fronts. Thus, the fluctuations would be small since the magnitude is proportional to the length of the affected portion. However, even the largest propagation

fluctuation observed during the stability experiment is much smaller than the 0.5 μs or larger fluctuations reported in earlier measurements conducted on the East Coast chain. Recent analysis by Samaddar (Reference 5-2) offers a possible explanation for this apparently contradictory behavior.

SECTION 6
PROPAGATION PATH EXPERIMENT

The objective of the propagation path experiment was to obtain an accurate data base to evaluate propagation prediction capabilities and to provide a better understanding of the effects of terrain and impedance variations on received signal phase. The experiment procedures, results, and associated data analysis and theoretical studies are described in Reference 6-1.

Incremental time-of-arrival (ΔTOA)—difference in measured signal arrival time at two sites—and time difference (TD) data were collected at eight sites approximately on the geodesic from the Yankee secondary at Searchlight, NV, to a control site near Fort Cronkhite, CA. Emphasis was directed toward the ΔTOA data, and these data were compared to predictions made using a semiempirical technique and the most sophisticated available technique, referred to as the integral equation program.

The experiment configuration, procedures, and summarized results, the intercomparison of prediction techniques, the comparison of measured and predicted time-of-arrival values, and the conclusions and recommendations are discussed in the following subsections.

EXPERIMENT CONFIGURATION AND PROCEDURES

The propagation path chosen for this experiment is between the Yankee transmitter at Searchlight, NV, and Fort Cronkhite, CA. The path was chosen because of the large variations in terrain and the history of short-term weather fluctuations along the propagation path. The variations along the path, particularly the terrain, were expected to provide a data base that would rigorously test propagation prediction models.

Figure 6-1 illustrates the location of measurement sites relative to the geodesic. Sites are named after the closest town. The figure is not to scale, but it shows approximately correct relative spacing between measurement sites. The offset of the measurement sites from the geodesic can be estimated using the scale factor on the figure.

6-1. Gambill, B., and K. Schwartz, *Loran-C Signal Analysis—Propagation Model Evaluation*, DOT (TBD), GE78TMP-51, General Electric-TEMPO, Santa Barbara, CA, July 1979.

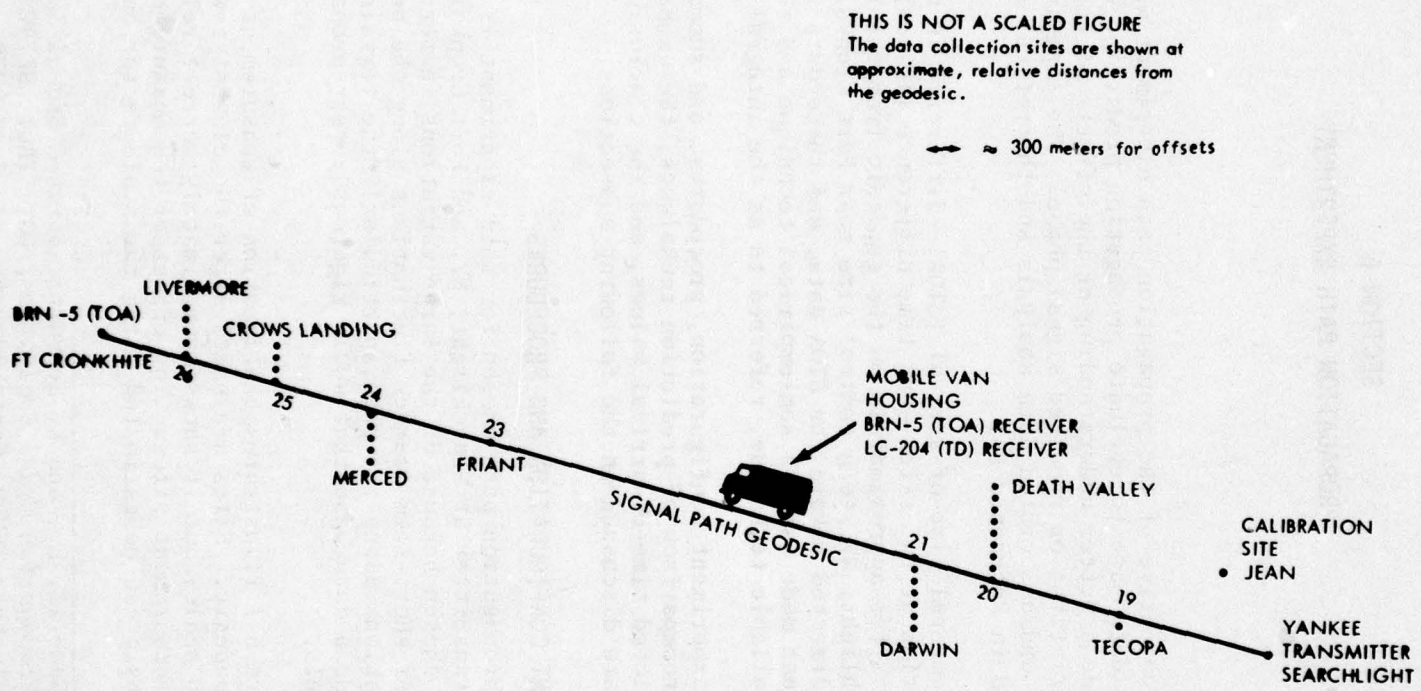

Figure 6-1. Data collection sites relative to the geodesic.

In the original site selection, an attempt was made to locate sites on the geodesic. The offsets resulted because of access limitations and initial location accuracy limitations using simple surveying techniques and existing geodetic markers. The sites were subsequently surveyed by a DMA field team and located to an accuracy of approximately 1 meter (one sigma). An additional site was surveyed between Darwin and Friant, but was inaccessible during the experiment. Actual distances from the Yankee transmitter to the accurately surveyed sites are tabulated later in this section.

MEASURED DATA

Time-of-arrival data from Master (TOAM), Yankee (TOAY), and X-ray (TOAX) and time difference data for Yankee (TDY) and X-ray (TDX) were recorded for approximately 3 days at each measurement site. The data were taken using the PLDCS TOA receiver. Emphasis was placed on the TOAY data since it could be processed to estimate incremental time-of-arrival between measurement sites.

Because of the length of the experiment, the difficult terrain, and equipment transfer difficulties, it was not possible to maintain continuous power and signal lock on the PLDCS. Therefore, a TOA calibrator was designed and used to reference the cesium standard in the PLDCS to the cesium standard at Searchlight.

The TOA calibrator consisted of a cesium standard and a Loran-C signal generator. The calibration technique used the measurement site at Jean, NV, as the reference site, which required the assumption that propagation variations over the short path from Searchlight to Jean (65 km) were negligible. The calibration procedure was as follows:

1. At the beginning of a measurement period at each site, the TOA calibrator signal replaced the X-ray signal in a time difference receiver at Jean. The Master-calibrator time difference (TDC) and the Master-Yankee time difference (TDY) both depend on the common Master signal and can be processed to provide TOAY-TOAC at Jean.
2. The calibrator was then driven to the measurement site and its Loran-C signal replaced the Master signal in the PLDCS. This produced simultaneous measurements of calibrator time-of-arrivel (TOAC) and TOAY at the measurement sites. Data taken at the beginning and end of the measurement period allowed definition of the frequency offset between the calibrator and PLDCS cesium standards. Knowing this drift rate allowed the TOAC-TOAY data taken at the field sites to be extrapolated to other times.
3. The calibrator returned to Jean and step 1 above was repeated. The two measurements at Jean allowed an estimate of the relative drift rate (frequency offset) between the calibrator

and Yankee transmitter cesium standards. Knowing this drift rate allowed the TOAY-TOAC measured data at the reference site to be extrapolated to other times.

4. The difference in TOAY-TOAC at the measurement site and TOAY-TOAC at Jean provided an estimate of TOAY at the site referenced to TOAY at Jean.

Steps 1, 2, 3, and 4 were then repeated at another site, farther from the transmitter along the geodesic. The difference between TOAY's (referenced to the value at Jean) at the two sites then provided an estimate of the change in TOAY (ΔTOAY) between the two sites.

Because there was a frequency offset between the PLDCS and Yankee cesium standards, the TOAY-TOAC data measured at the two sites must be referenced to a common time point. This was done by using the measured estimates of drift rate to extrapolate TOAY-TOAC to a point in time midway between the measurement periods. The difference in the TOAY-TOAC data so extrapolated is reported as the time-of-arrival increment.

Because the frequency offset between the calibrator and PLDCS cesium standards did not remain constant, an error was introduced in the ΔTOA estimates; ie, the estimates are dependent on the time chosen to compare the extrapolated values. To provide an estimate of the measurement error, we extrapolated the earlier measurement forward in time to the center of the later measurement period and the later measurement back in time to the center of the earlier measurement period. The difference in the ΔTOA values at these two times was assumed to bound the error. The error was $\pm$50 ns or less except at Crows Landing and Livermore, where it was $\pm$150 ns.

The results obtained from the measurement and data reduction procedures described above are shown in Table 6-1. The data are compared to predicted values later in this section.

Table 6-1. Summary of experimental incremental time-of-arrival measurements.

Site	ΔTOA(μs)	CUM ΔTOA	Distance from Searchlight(km)	Site-to-Site Increment (km)	Site-to-Site Increment (μs)*
Tecopa	Reference		136.678		
Death Valley	216.732	216.732	201.449	64.771	216.052
Darwin	268.536	485.268	281.737	80.288	267.812
Delilah	No Data	No Data	422.010	140.273	467.900
Friant	657.282	1142.550	478.270	196.533†	655.563†
Merced	204.753	1347.303	539.778	61.508	205.168
Crows Landing	239.227	1586.530	611.493	71.715	239.215
Livermore	209.521	1796.051	674.053	62.560	208.677
Ft. Cronkhite	242.298	2038.348	746.697	72.644	242.314

*Computed using free-space propagation velocity (2.997925×10^5 km/s).
†Measured from Darwin.

EVALUATION OF PREDICTION TECHNIQUES

Prediction techniques in this report refer to numerical models used to predict the amplitude and/or phase of a signal propagated via the groundwave. Required inputs are the effective earth radius (earth radius modified to account for the effects of atmospheric refraction), surface impedance, and in some cases variations in the terrain relative to a smooth sphere. Computed outputs are the amplitude and phase of the groundwave signal relative to the amplitude and phase of a signal that propagates the same distance in free space.

The evaluation was performed in two phases. In the first phase, results from different models were compared for accuracy and consistency. In the second, results from two selected models were compared with experimental results. The models considered were:

1. Classical, homogeneous spherical earth - a well researched technique documented by comprehensive published literature. (Reference 6-2).
2. Pressey's or Millington's - a semiempirical technique that accounts for inhomogeneous impedance, and is currently used for Loran-C chart preparation (References 6-3 and 6-4).
3. Wait's multisegment spherical earth (MULSEG) - an extension of the classical theory to account for inhomogeneous impedance. (Reference 6-2).
4. Integral equation solution - a GFE computer program (HUFLOC) provided by the U.S. Coast Guard to calculate signals over irregular, inhomogeneous terrain (References 6-5 and 6-6).

Note that only in the last model can terrain variations be included.

6-2. Wait, J.R., "Electromagnetic Surface Waves," *Advances in Radio Research* (Ed. by J.A. Saxton), vol 1, pp 157-217, Academic Press, London 1964.

6-3. Millington, G., "Groundwave Propagation Over Inhomogeneous Smooth Earch," *Proceedings IEE*, Parts I, II (1949, vol 96, p 53) and Part III (1959, vol 97, p 200).

6-4. Pressey, G.F., "The Measurement of the Phase Velocity of Groundwave Propagation at Low Frequencies over a Land Path," Paper 1438, Radio Section, *Proceedings IEE*, October 1952.

6-5. Hufford, G.A., "An Integral Equation Approach to the Problem of Wave Propagation over an Irregular Surface," *Quart. Appl. Math.*, 9, p 391, 1952.

6-6. Johler, J.R., and L.A. Berry, *Loran-C Phase Corrections over Inhomogeneous, Irregular Terrain*, ESSA Tech. Report IER59-ITSA-56,1967.

Model Intercomparison

CLASSICAL TECHNIQUES. There was no expectation that this idealized technique would produce phase delay estimates with useful accuracy for the path considered in this experiment. However, because the classical technique is imbedded in some of the other techniques, the numerical procedures were evaluated.

The general classical theory solution results in an infinite series representation for the complex groundwave loss function. The series converges rapidly for long paths but requires many terms for paths less than 100 kilometers in length. Two short-path approximations are available, one for high surface impedance and the other for low surface impedance.

The evaluation of the classical theory determined the required number of terms in the series for a specified path length and level of accuracy, and also defined appropriate distances to switch from the accurate series solution to the short-distance approximations.

MILLINGTON"S TECHNIQUE COMPARED TO WAIT'S MULTIPLE SEGMENT TECHNIQUE (MULSEG). Both these techniques account for inhomogeneous impedance along the path. The results produced by these two techniques were compared for several hypothetical cases. One example is shown in Figure 6-2 for a five-segment path. The results are typical of results obtained for a number of other cases. As a result of this comparison, we concluded that the prediction differences were small compared to errors caused by the neglect of terrain variations. Thus, we chose Millington's technique for subsequent comparisons with experimental data, because it requires fewer computations than MULSEG.

MILLINGTON'S TECHNIQUE COMPARED TO THE INTEGRAL EQUATION SOLUTION. Results from Millington's technique and the integral equation technique were compared for two cases: one where terrain effects are important, and one where terrain effects are suppressed. These comparisons were made during the process of comparing experimental and predicted results and are discussed later.

DATA PREPARATION

All methods considered require an accurate definition of geodetic path length as input. Also, all methods currently use a single value for the effective earth radius along the path. The classical approach requires a single value of surface impedance for the entire path. Millington's technique and MULSEG require surface impedance data for as many segments as are required to account for inhomogeneity along the path. The integral equation requires inhomogeneous impedance data for segments along the path and terrain variations relative to a smooth spherical reference.

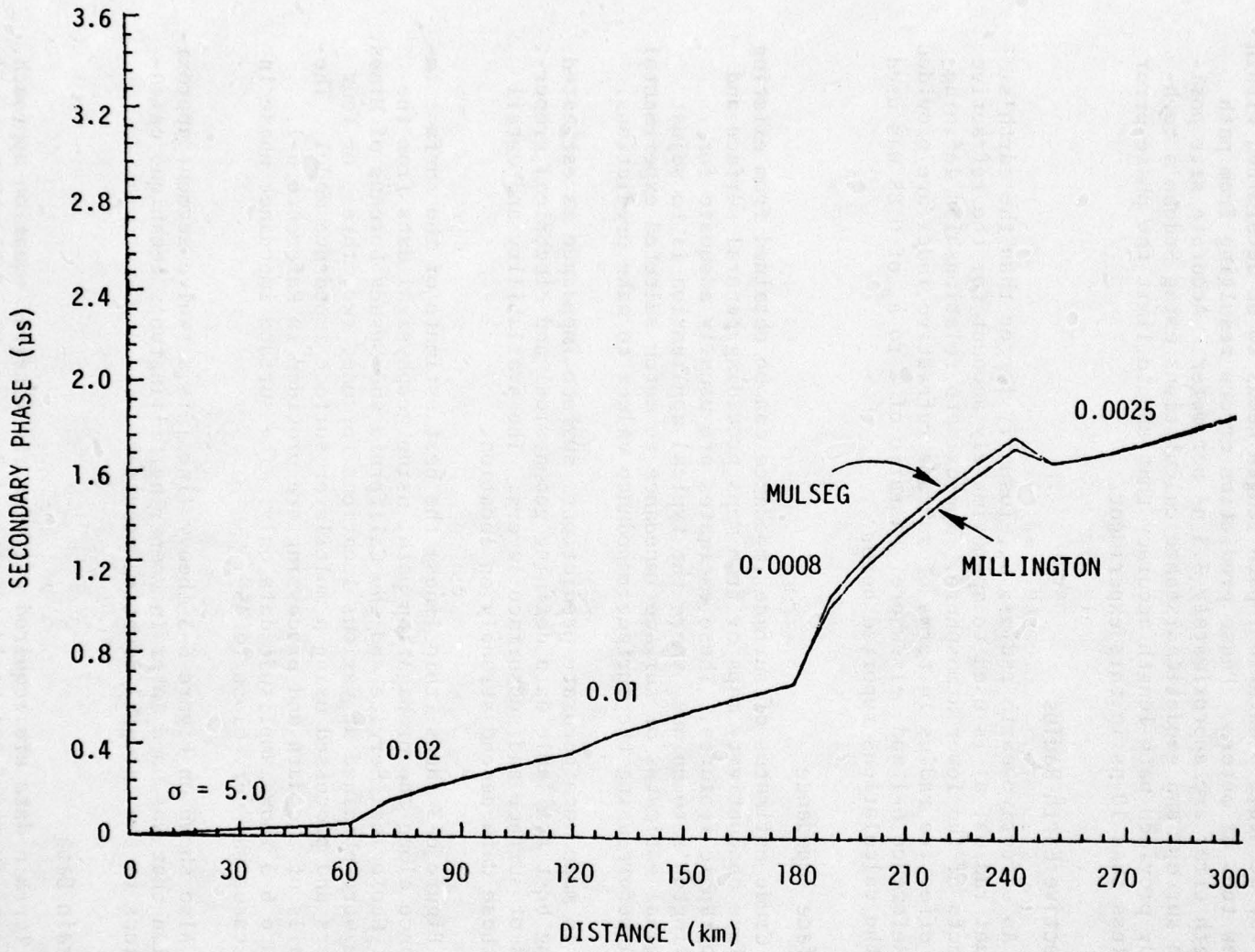

Figure 6-2. Comparison of MULSEG and Millington for a five-segment path (sea to land).

Path Length

For accurate prediction, path length needs to be determined within a few tens of meters. Phase prediction errors resulting from path length error are approximately 3.3 ns per meter. Accurate site position surveys and geodetic distance calculations using Sodano's technique provided path length accuracy that should limit the phase error to less than 10 ns in this experiment.

Effective Earth Radius

An effective earth radius, a_e, (usually larger than the earth's actual radius, a) is used to approximately account for the refractive effects of the lower atmosphere. Approximate relationships defining the effective radius in terms of surface refractive index are provided in Reference 6-1 and elsewhere. A ratio of a to a_e of 0.85 was used in the calculations reported here.

Surface Impedance

Crude estimates of surface impedance can be obtained from existing surface conductivity maps or from maps providing general surface and topographic features. These estimates are usually adequate for Millington's technique, where the typical application is to adjust original estimates of surface impedance to match selected experimental data before using the surface impedance values to make predictions.

To make more accurate predictions, surface impedance is estimated using best available data defining geophysical and electrical properties of surface and subsurface layers. The availability and detail of these data depend strongly on location.

Figure 6-3 shows (thin lines) the best estimate of the surface impedance along the propagation path, using geophysical data from the U.S. Geological Service and the California and Nevada Bureaus of Mines. Data were obtained at various locations for one, two, three, or four layers and processed using a multilayer surface impedance model. The details of the data and processing are provided in Reference 6-1. Figure 6-3 shows amplitude data only. The surface impedance phase in all cases was very close to 45°.

Also shown on Figure 6-3 (heavy lines) is a twelve-segment approximation that was used later in comparing Millington's technique calculations to the integral equation results.

Terrain Data

Terrain data are required only for the integral equation approach. For many areas of the world, digitized data are available that provide

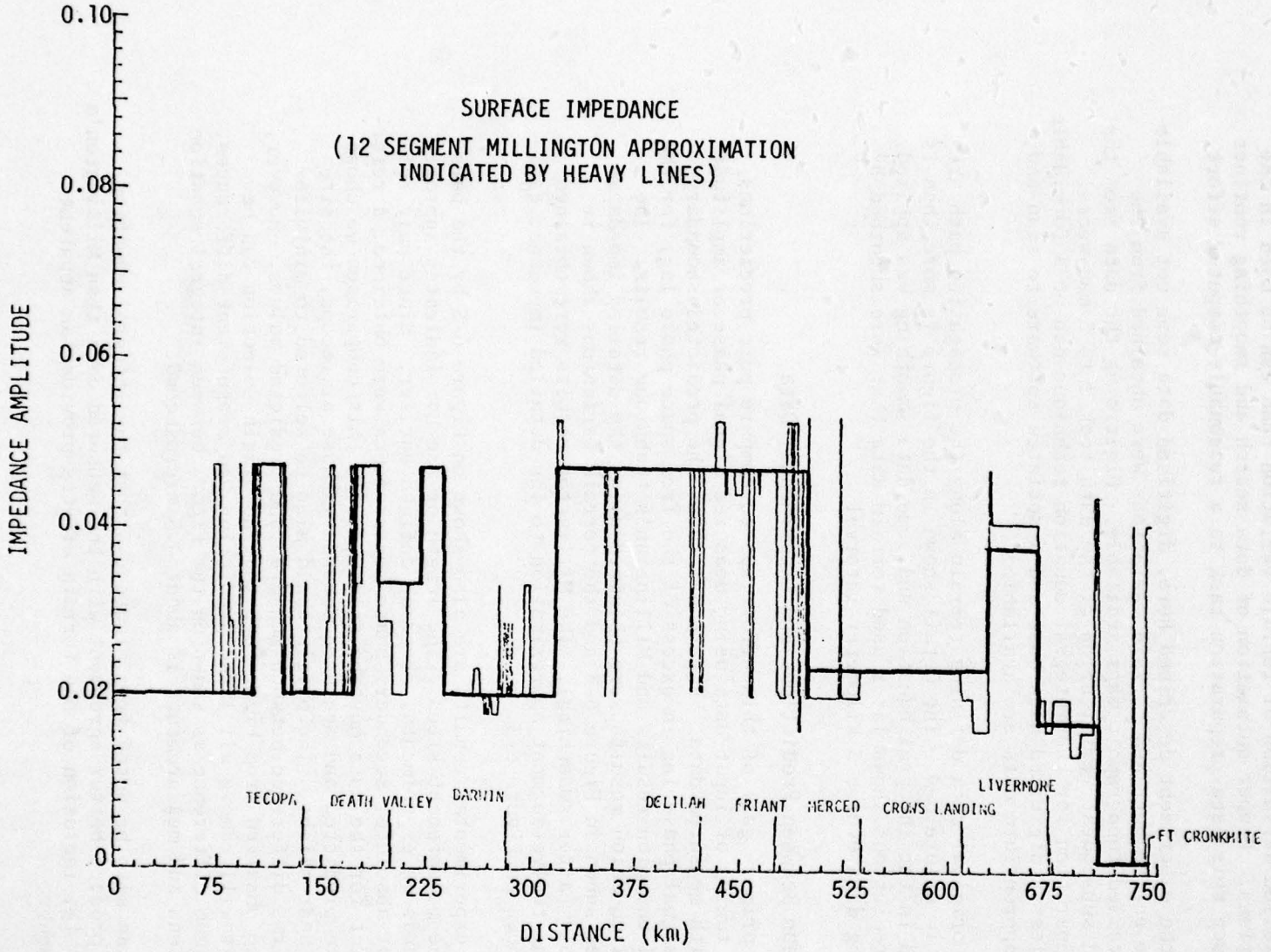

Figure 6-3. Approximation to the surface impedance for a Millington calculation.

more detailed definition of terrain variation than can be used in the computations. Proper automation of data search and smoothing routines can reduce this data preparation task to a reasonable computer effort.

In the experiment described here, digitized data were not available over the entire path and terrain variations were obtained from the most detailed topographic maps available. Digitizing the data from the maps and subsequent verification of the data took 2 to 3 man-weeks. Data preparation for the integral equation technique can be a formidable task unless a digitized data base and associated software to scan and select appropriate data are available.

The original data defining terrain along the propagation path are plotted in Figure 6-4. The detail shown in the figure is more than is required in the integral equation and some data smoothing was applied. Phase predictions shown later used terrain data that were smoothed by averaging data over a 3 kilometer interval.

Comparison Between Predictions and Experimental Data

One primary goal of this effort was to compare pure predictions (ie, no tuning of input data using measured signal phase or amplitude data) with measured data. Figure 6-5 shows the predicted secondary phase (signal phase lag in excess of the free space phase lag) for the integral equation results and Millington's technique results. The integral equation results were obtained using the detailed impedance estimates shown in Figure 6-3 and the terrain variations shown in Figure 6-4 (after smoothing). The Millington results were obtained using the twelve-segment approximation to the detailed impedance estimates shown on Figure 6-3.

The experimental results are also shown on Figure 6-5 by the bars above the measurement sites. The length of the bar indicates approximate bounds on experimental error as defined earlier. Since only relative (not absolute) secondary phase measurements were obtained, a reference point for the data must be selected. In this comparison we chose to equate predicted and measured secondary phase at Tecopa, the site nearest Searchlight. The origin could also be selected to minimize mean or rms difference between measured and predicted values. However, it can be observed from Figure 6-5 that no origin selection can be made that will remove all large prediction and measurement differences. The maximum difference as shown on the figure between integral equation predictions and measurements is about 0.5 microsecond.

It can also be noted from Figure 6-5 that the integral equation results produce better agreement with the measured data than Millington's results; ie, inclusion of the terrain effects provides an apparent improvement.

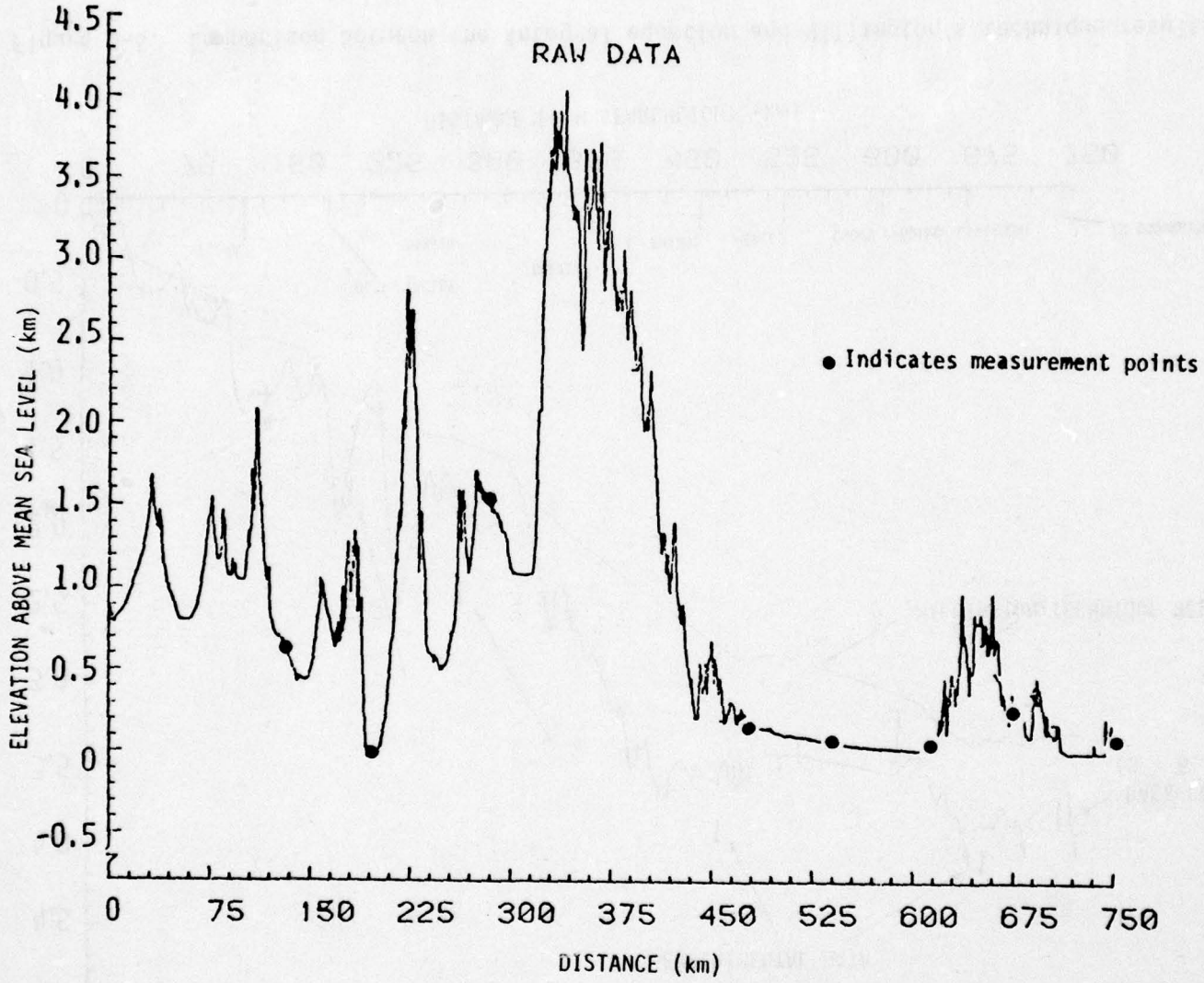

Figure 6-4. Original worst case path terrain data.

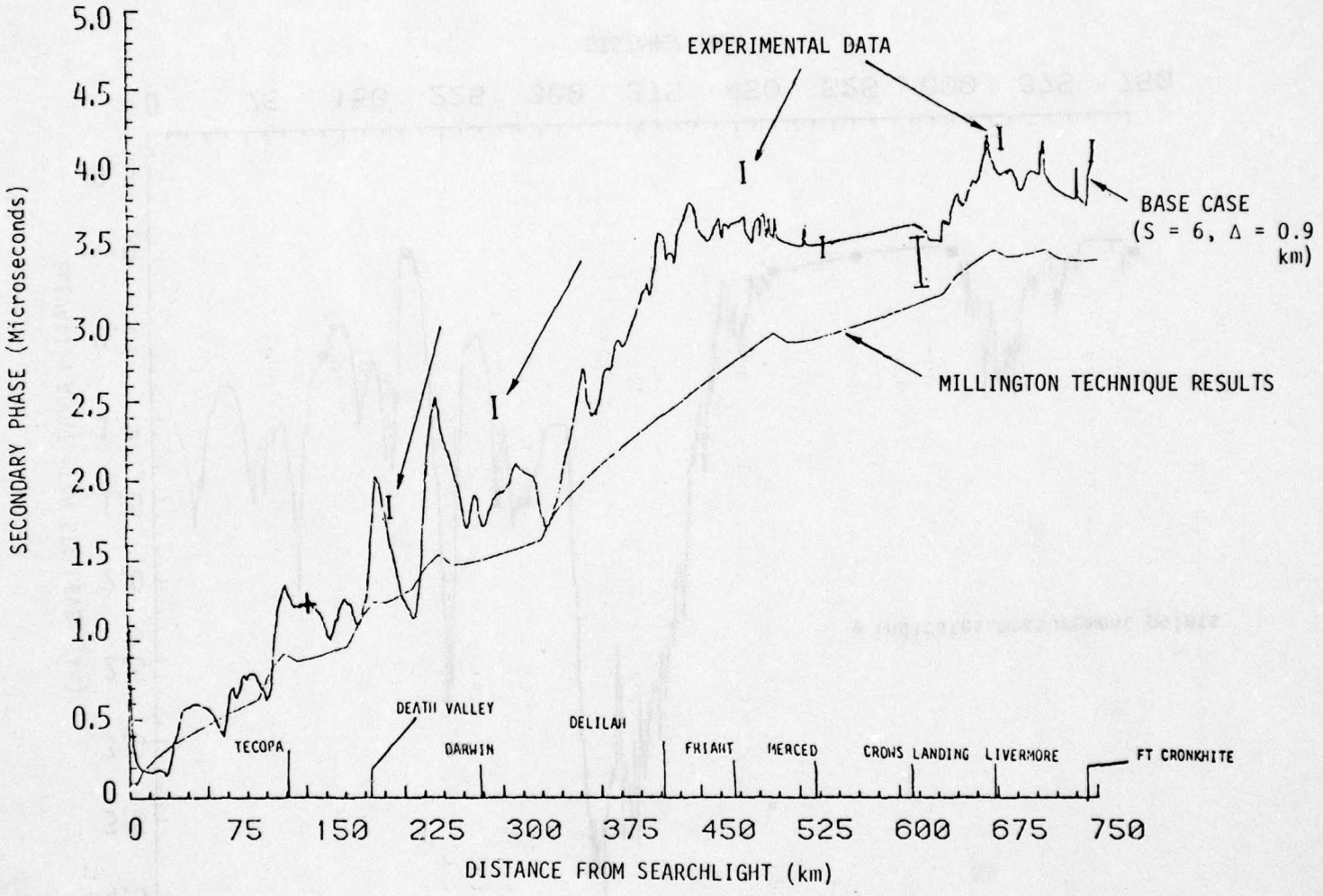

Figure 6-5. Comparison between the integral equation and Millington's technique results.

To verify that the differences between the Millington and integral equation predictions are due to terrain effects, a second calculation was performed with the integral equation, but with terrain effects suppressed. These results, with Millington's technique results repeated, are shown in Figure 6-6. The agreement between predictions is very good and provides confidence in the computational models. The results provide further verification that Millington's technique is useful when terrain effects are minimal.

Additional Comparison

Two additional sets of calculations were performed to provide a crude measure of sensitivity of predicted versus measurement differences to input parameters. We believe that terrain data is adequately defined and input value errors would most likely be the surface impedance definition. Figure 6-7 shows the original integral equation predictions, the measurements, and a new integral equation prediction made with the conductivity of all segments along the path decreased by a factor of 2 (this increases the surface impedance by approximately a factor of $\sqrt{2}$). Note that the two predictions now almost bracket the measured data. It is clear that selective adjustment of the conductivity of different segments by a factor of approximately 2 could produce good agreement between measured and predicted values. These adjustments were not performed because of the computer costs for repetitive calculations with the integral equation program.

Also shown on Figure 6-7 are results obtained with Millington's technique with the impedance of the twelve-segment approximation adjusted to approximately minimize the rms difference between Millington's predictions and measurements. Figure 6-8 shows the impedance values that were required to produce the results shown in Figure 6-7. Impedance values had to be generally increased to compensate for terrain effects and/or errors in the original impedance values. The results obtained by varying the impedance values indicate:

1. Variation of impedance values by about a factor of 2 can produce good agreement between predictions and measurements for this particular path
2. The impedance values need to be known much better than a factor of 2 for accurate (<100 ns) predictions over long overland paths.

PREDICTED WEATHER EFFECTS

Except for one isolated incident, no significant weather-produced fluctuations were observed during the experiments. As a result, little emphasis was placed on prediction of weather effects. One example of predicted weather-produced fluctuations was produced using surface weather data from a station (Reno, NV) near the Master transmitter.

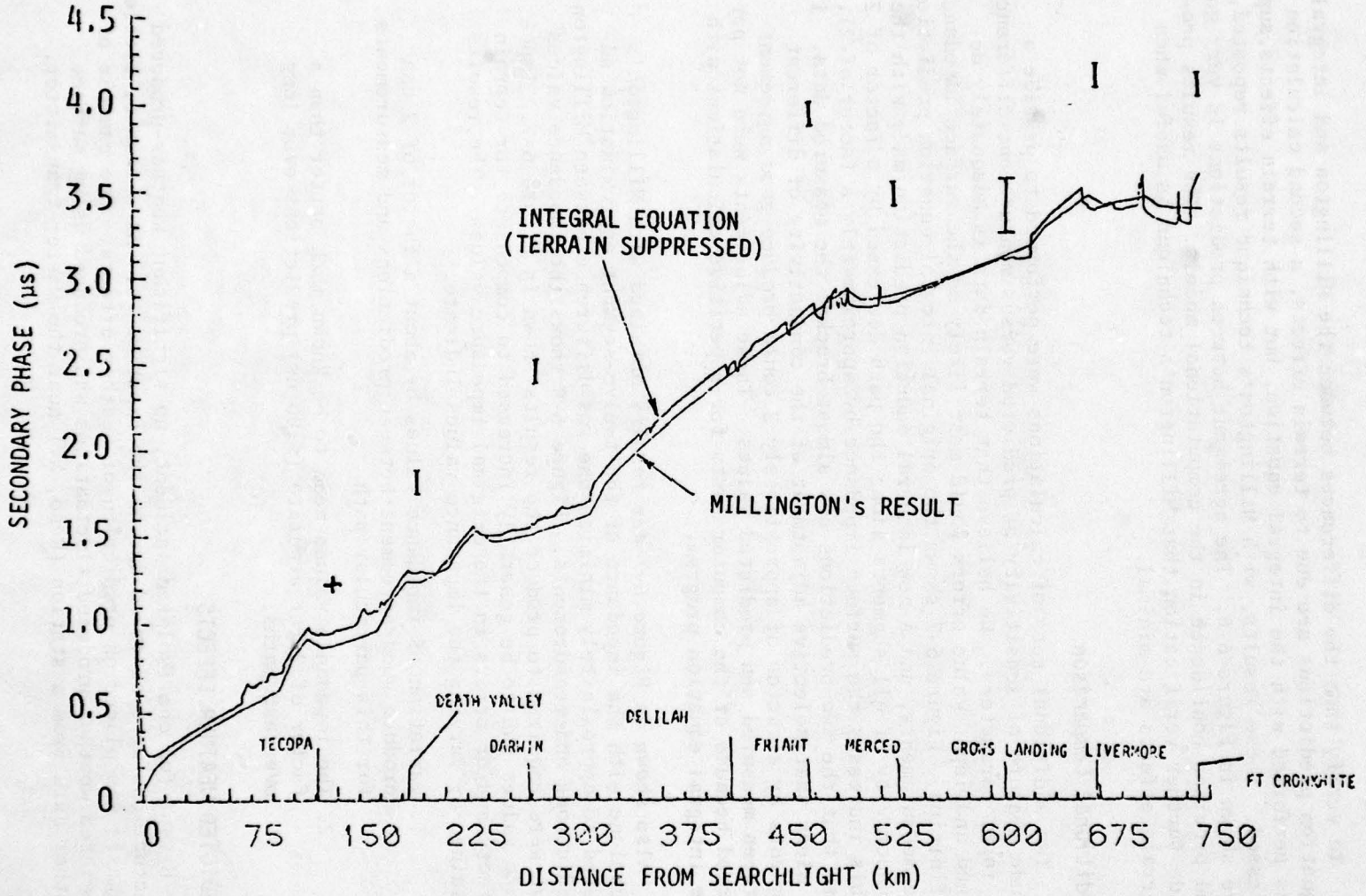

Figure 6-6. Comparison of Millington's technique with the integral equation technique (with terrain variations suppressed).

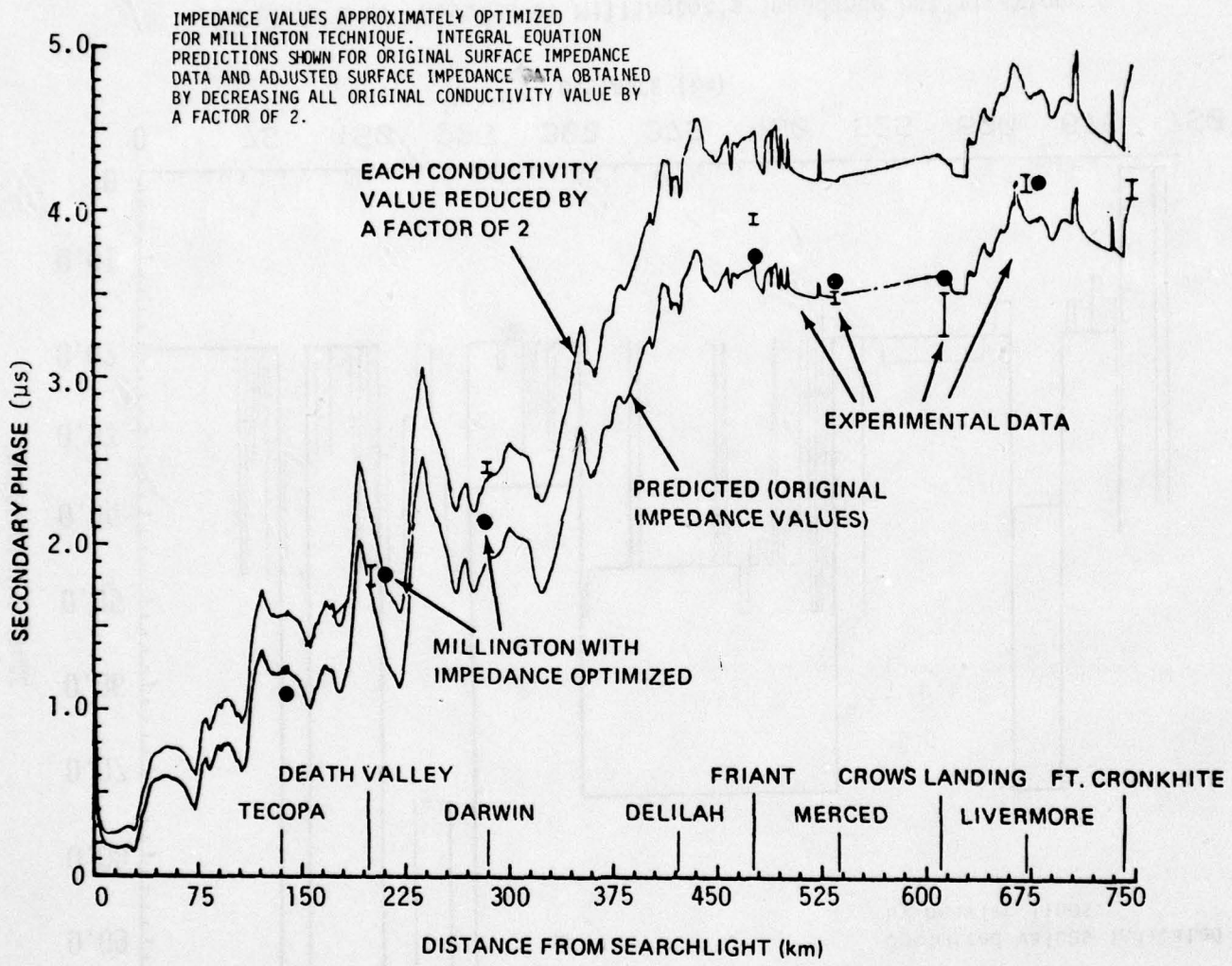

Figure 6-7. Comparison of measurement with Millington and integral equation predictions after surface impedance adjustment.

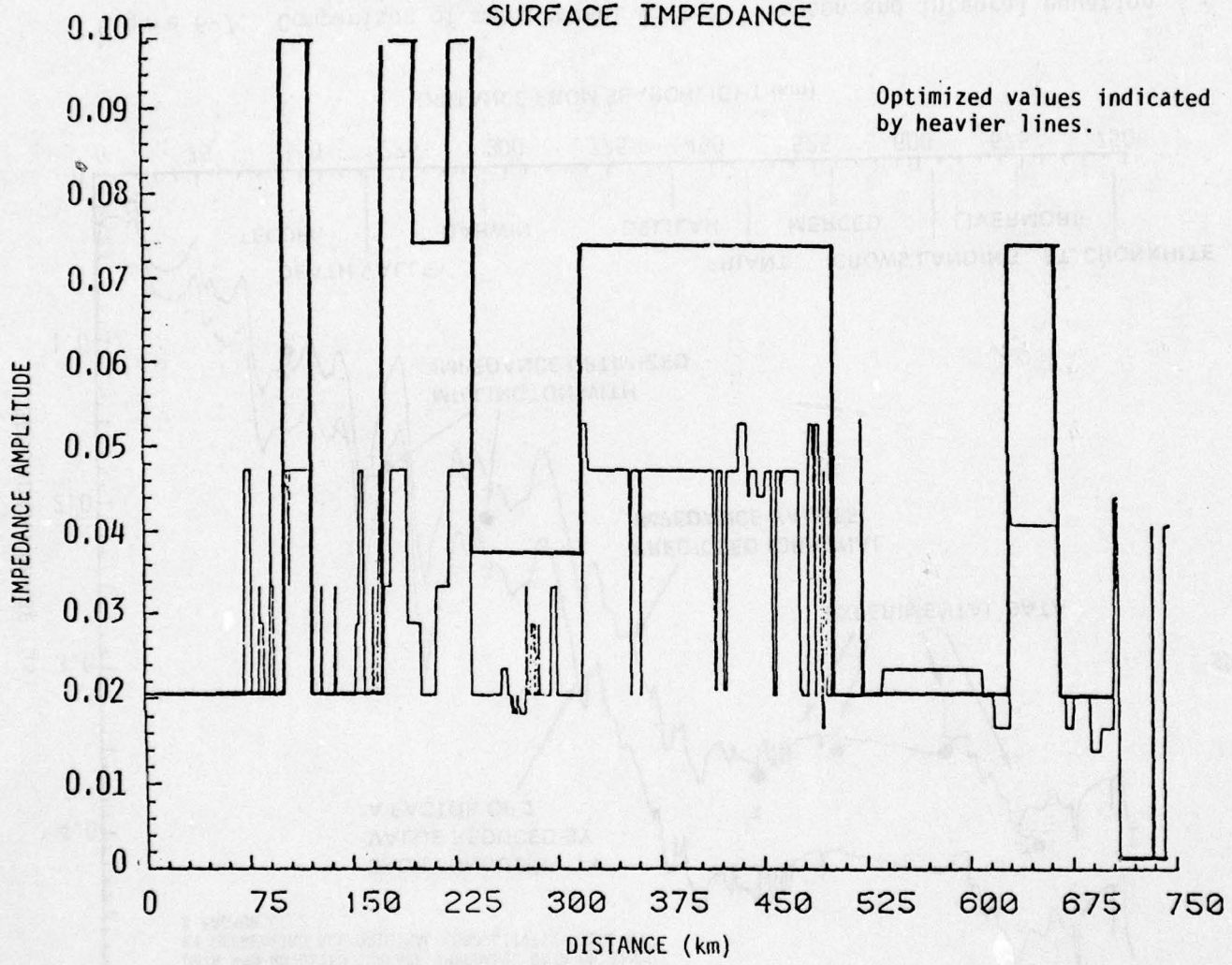

Figure 6-8. Results of Millington's impedance optimization.

The atmospheric pressure in millibars, the temperature, and dew point temperature were taken at Reno. These values were used to compute the surface refractive index and a corresponding value of effective earth radius. Phase fluctuations, which are the sum of the primary and secondary phase fluctuations, were computed for path lengths of 100, 300, 500, and 700 kilometers. The predicted phase fluctuations were small, showing a maximum value of 15 nanoseconds. These values agree in order of magnitude with the experimental observations during the Loran-C Signal Analysis West Coast Experiment with one exception, where it is postulated that a larger change was produced as a result of precipitation-induced surface impedance changes. A discussion of this exceptional case was provided in the Stability Experiment Section.

CONCLUSIONS AND RECOMMENDATIONS

Detailed conclusions and recommendations are provided in Reference 6-1. A summary of the discussion in Reference 6-1 is provided below.

Conclusions

1. For a smooth, inhomogeneous earth, Millington's technique and Wait's multiple segment technique produce nearly identical results. Therefore, Millington's technique should be used in preference to Wait's because of its greater simplicity and shorter running time.
2. Millington's technique and the integral equation technique give nearly identical results for a path with highly inhomogeneous impedance when the terrain variations are suppressed for the integral equation calculations.
3. The integral equation calculations show that both terrain and surface impedance variations are important in predicting secondary phase. Our numerical computations indicated that the terrain can be defined with sufficient accuracy with data points spaced at approximately 1 kilometer. Our experimental observations and predictions indicate that to obtain prediction accuracy on the order of 100 nanoseconds or better, the surface impedance uncertainty must be much less than a factor of 2 for overland paths.
4. The effect of terrain variations (in this case elevations greater than one wavelength above the mean geoid) was to increase the secondary phase. Thus, matching calibration data with impedance variations alone requires higher than actual impedance values to compensate for the terrain effects.
5. Data preparation for the integral equation method is a formidable task. The hand preparation of the data for the worst-case path required an effort of about 1 man-month. Digital terrain data tapes for the path were not available. Hand preparation of data for a coverage area would not be practical.

6. Computation time for the integral equation method is very long. For computational accuracy, an integration step size of approximately 1 kilometer is required.

7. Results from the propagation path experiment show that good experimental data can be acquired using the techniques described and that the uncertainty associated with the experimental data is of the order of ±50 ns.

8. The highly variable terrain and surface impedance along the worst-case path and the differences between predicted and measured values indicate the need for more closely spaced measurement points to adequately calibrate phase change along the overland portion of the path. On the other hand, measurements made beyond the region of major terrain variations can be used to compensate for the cumulative effect of terrain-induced fluctuations.

Recommendations

The following recommendations are made for additional effort related to predictions:

1. Procedures more efficient than scaling and reading quantities from maps by hand must be developed for generating both the terrain and surface impedance data bases that are required for the proper employment of numerical predictive techniques. The surface impedance data base is a requirement not only for the integral equation technique but also for the Millington technique or Wait multisegment theory.

2. The test calculations on the integral equation technique indicate that a systematic sensitivity study is required. This study should begin with the numerical analysis techniques used to obtain the solution and should include variation of the computation step size and the terrain and surface impedance specification. The study should determine the detail of data input for both the terrain and impedance profiles consistent with the accuracy of the available data.

3. Until a better understanding of the limitations and data requirements for the integral equation technique are established, the current combination of calibration and the utilization of Millington's technique should be continued. The impedance description which results from currently used optimization techniques is not unique. The optimization procedures should be improved. Some of the more efficient optimization techniques which might be applied include Rosenbock's direct search method, Powell's method or any

of the gradient techniques. (See Reference 6-7 for a discussion of optimization). Another potential improvement could result from using the integral equation technique to develop empirical techniques for evaluating the effects of significant terrain features. A combined semiempirical impedance/terrain model would have a better physical basis than an impedance-only model and should allow better extrapolation to areas between calibration points.

4. Future experiments to obtain data for comparison with prediction techniques should use control procedures similar to those described in this section but with the emphasis on more frequent closures with calibration equipment. Data should be acquired at more sites (less data collection per site). The choice of measurement sites should be based on prior detailed predictions. Measurements should be made at sites slightly offset from originally established sites (both along and transverse to the geodesic) when in-field data analysis and comparison with predictions indicate large differences between experimental and predicted results.

6-7. Luenberger, D.G., *Introduction to Linear and Nonlinear Programming*, Addison-Wesley, Reading, Massachusettes, 1973.

SECTION 7

THE HARBOR EXPERIMENT

The final experiment conducted during the Signal Analysis project was the harbor experiment. Its purpose was to provide necessary data for the evaluation of the potential use of Loran-C for high accuracy all-weather navigation in a harbor, harbor entrance (HHE) environment. Four modes of system operation were considered:

1. Absolute location
2. Relative location
3. Differentially augmented absolute location
4. Differentially augmented relative location.

To provide an assessment of the absolute mode, a means of converting TDs to absolute geodetic position is necessary. The mariner normally performs this conversion with the aid of nautical charts which have Loran-C grid lines drawn on them. However, there are no such published charts for the San Francisco harbor, and an intermediate step to provide a calibrated grid for the harbor is necessary.

The specific objectives of this experiment were thus to provide a calibrated grid for the San Francisco harbor and estimates of the spatial distortion, and obtain the data required to assess the performance of Loran-C in the above mentioned modes.

To accomplish these objectives, a series of measurement deployments were planned which included both land site and vessel measurements. The measurements began April 8 and were terminated May 9, 1978.

The harbor experiment was divided into three phases: (1) a planning phase, (2) a land site measurement phase at sites around the periphery of the harbor and on Treasure, Angel, and Alcatraz Islands, and (3) a vessel measurement phase conducted aboard the USGS research vessel Polaris. Figure 7-1 shows the location of the 13 land sites and an outline of the areas covered by the Polaris.

Planning Phase

The specific objectives of the planning phase were to (1) select the land measurement sites, (2) select vessel tracks, and (3) estimate spatial grid anomalies. To aid in the planning phase, data analyzed from Fort Cronkhite, USCG calibration data collected at Treasure Island, and data from the propagation path experiment were used.

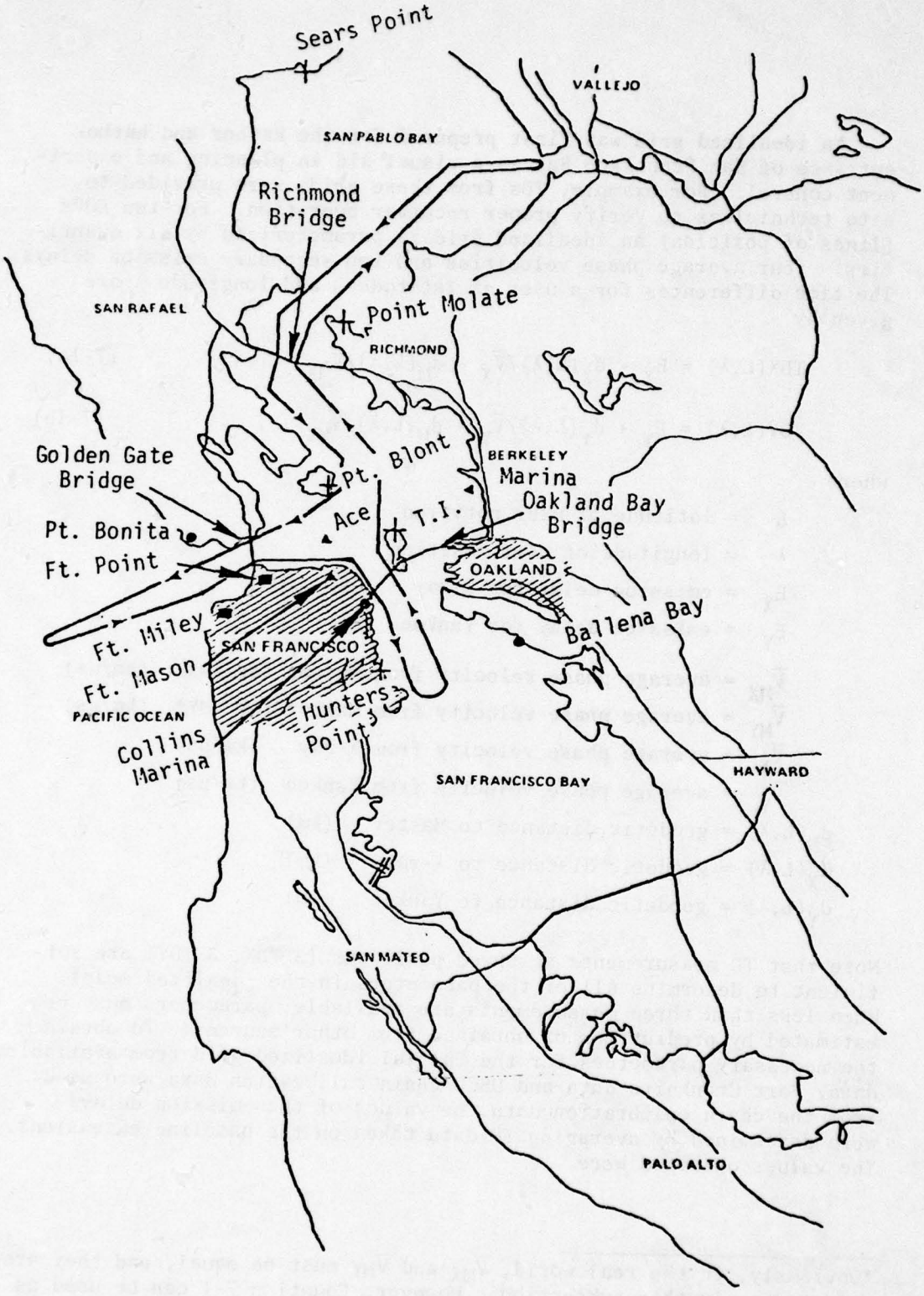

Figure 7-1. San Francisco Harbor test area.

An idealized grid was first prepared for the harbor and harbor entrance of San Francisco Bay as a visual aid in planning and experiment control. For example, TDs from these grids were provided to site technicians to verify proper receiver operation. For two LOPs (lines of position) an idealized grid is parameterized by six quantities: four average phase velocities and two secondary emission delays. The time differences for a user at latitude L and longitude λ are given by

$$TDX(L,\lambda) = E_X + d_X(L,\lambda)/\bar{V}_X - d_M(L,\lambda)/\bar{V}_{MX} \qquad (7\text{-}1a)$$

$$TDY(L,\lambda) = E_Y + d_Y(L,\lambda)/\bar{V}_Y - d_M(L,\lambda)/\bar{V}_{MY} \quad , \qquad (7\text{-}1b)$$

where

L = latitude of user potition

λ = longitude of user position

E_X = emission delay for X-ray (μs)

E_Y = emission delay for Yankee (μs)

$\bar{V}_{MX}$ = average phase velocity from Master for TDX (km/μs)

$\bar{V}_{MY}$ = average phase velocity from Master for TDY* (km/μs)

$\bar{V}_X$ = average phase velocity from X-ray (km/μs)

$\bar{V}_Y$ = average phase velocity from Yankee (km/μs)

$d_M(L,\lambda)$ = geodetic distance to Master (km)

$d_X(L,\lambda)$ = geodetic distance to X-ray (km)

$d_Y(L,\lambda)$ = geodetic distance to Yankee (km) .

Note that TD measurements at three positions (3 TDX, 3 TDY) are sufficient to determine all of the parameters in the idealized model. When less than three measurements are available, parameters must be estimated by predictions or obtained from other sources. To obtain the necessary parameters for the initial idealized grid from available data, Fort Cronkhite data and USCG chain calibration data were used. From the chain calibration data the values of the emission delays were determined by averaging TD data taken on the baseline extensions. The values obtained were

*Obviously, in the real world, $\bar{V}_{MX}$ and $\bar{V}_{MY}$ must be equal, and they are treated so in this subsection. However, Equation 7-1 can be used as a numerical fit to data, as it is in later sections, and a better fit can be obtained by allowing $\bar{V}_{MX} \neq \bar{V}_{MY}$.

$$E_X = 28094.467 \quad \mu s$$

$$E_Y = 41967.620 \quad \mu s \quad .$$

The phase velocity $\overline{V}_Y$ was estimated using the phase predicted from the integral equation program for the Yankee path to Fort Cronkhite. Then values were assigned to $\overline{V}_X$, $\overline{V}_{MX}$, and $\overline{V}_{MY}$ which, when adjusted for the land-to-sea interface effects, matched the Fort Cronkhite data for TDX and TDY reasonably well. The phase velocities determined were

$$\overline{V}_{MX} = \overline{V}_{MY} = \overline{V}_M = 0.299061 \quad km/\mu s$$

$$\overline{V}_X = 0.298304 \quad km/\mu s$$

$$\overline{V}_Y = 0.299150 \quad km/\mu s \quad .$$

As a first approximation, we assumed that spatial grid distortions were primarily the result of phase recovery at land-sea interfaces and the scattering of signals from large metallic bridges. At land-sea interfaces the secondary phase of the Loran-C signal undergoes a rapid decrease (see Figure 7-2, which is typical for all lower to higher conductivity changes). When the interface is far from the transmitter, the phase recovery is primarily determined by the overwater distance after the transition, as illustrated in Figure 7-3. This effect was

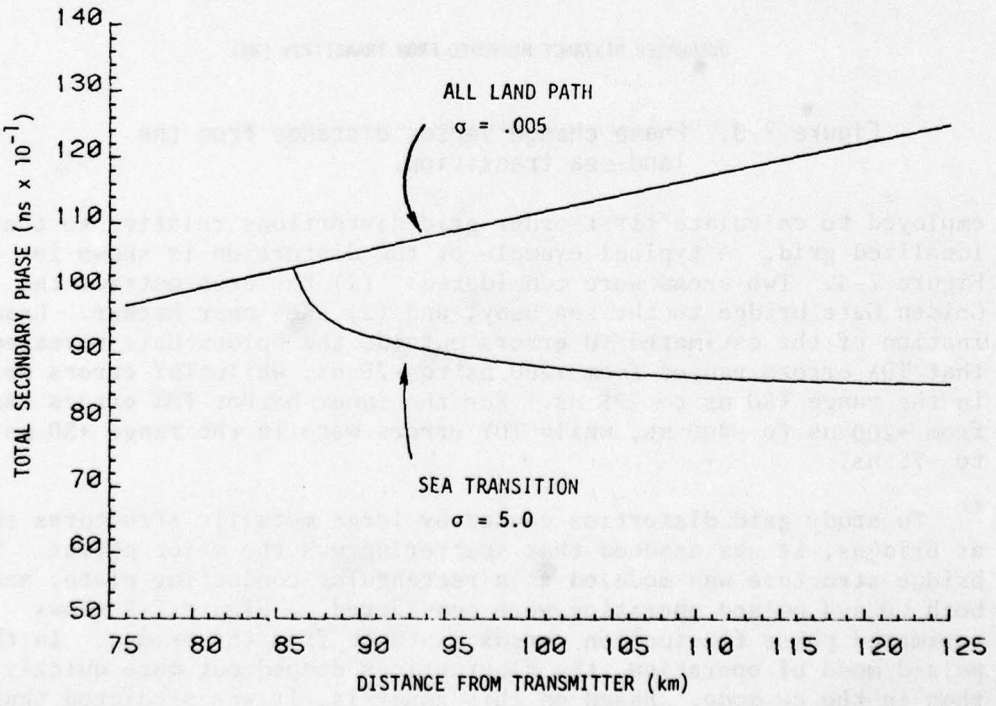

Figure 7-2. Effect of a land-sea interface on the secondary phase.

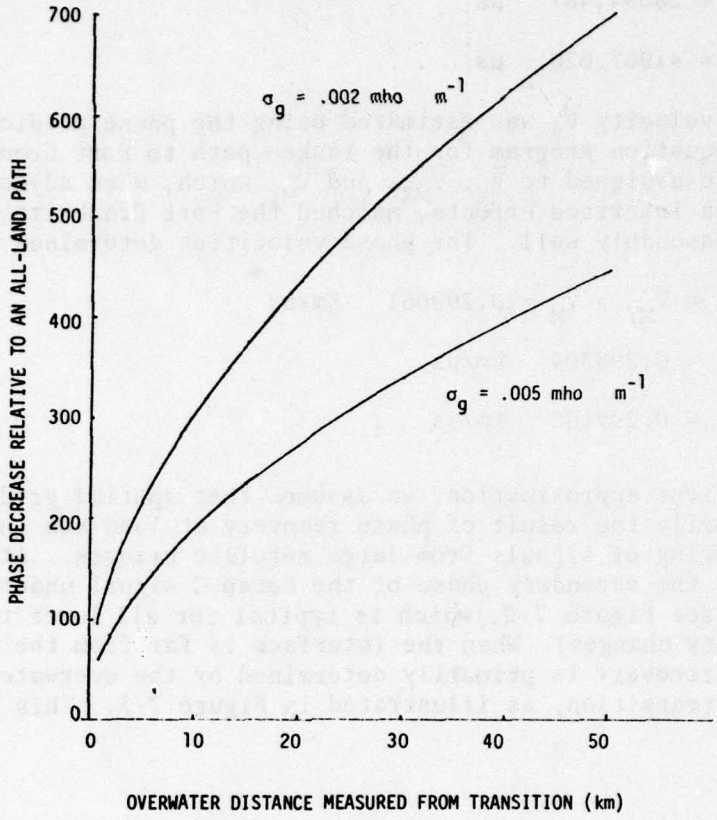

Figure 7-3. Phase change versus distance from the land-sea transition.

employed to calculate first-order grid distortions relative to the idealized grid. A typical example of the distortion is shown in Figure 7-4. Two areas were considered: (1) the area outside the Golden Gate bridge to the sea buoy, and (2) the inner harbor. Examination of the estimated TD errors outside the Golden Gate revealed that TDX errors ranged from +200 ns to -25 ns, while TDY errors were in the range +50 ns to -75 ns. For the inner harbor TDX errors ranged from +200 ns to -400 ns, while TDY errors were in the range +50 ns to -75 ns.

To study grid distortion caused by large metallic structures such as bridges, it was assumed that scattering was the major effect. The bridge structure was modeled as a rectangular conducting plate, and both cw and pulsed operation were considered. Figure 7-5 shows estimated phase fluctuation versus distance from the bridge. In the pulsed mode of operation, the fluctuations damped out more quickly than in the cw mode. Based on this analysis, it was predicted that the largest distortion would occur on the harbor side of the Golden

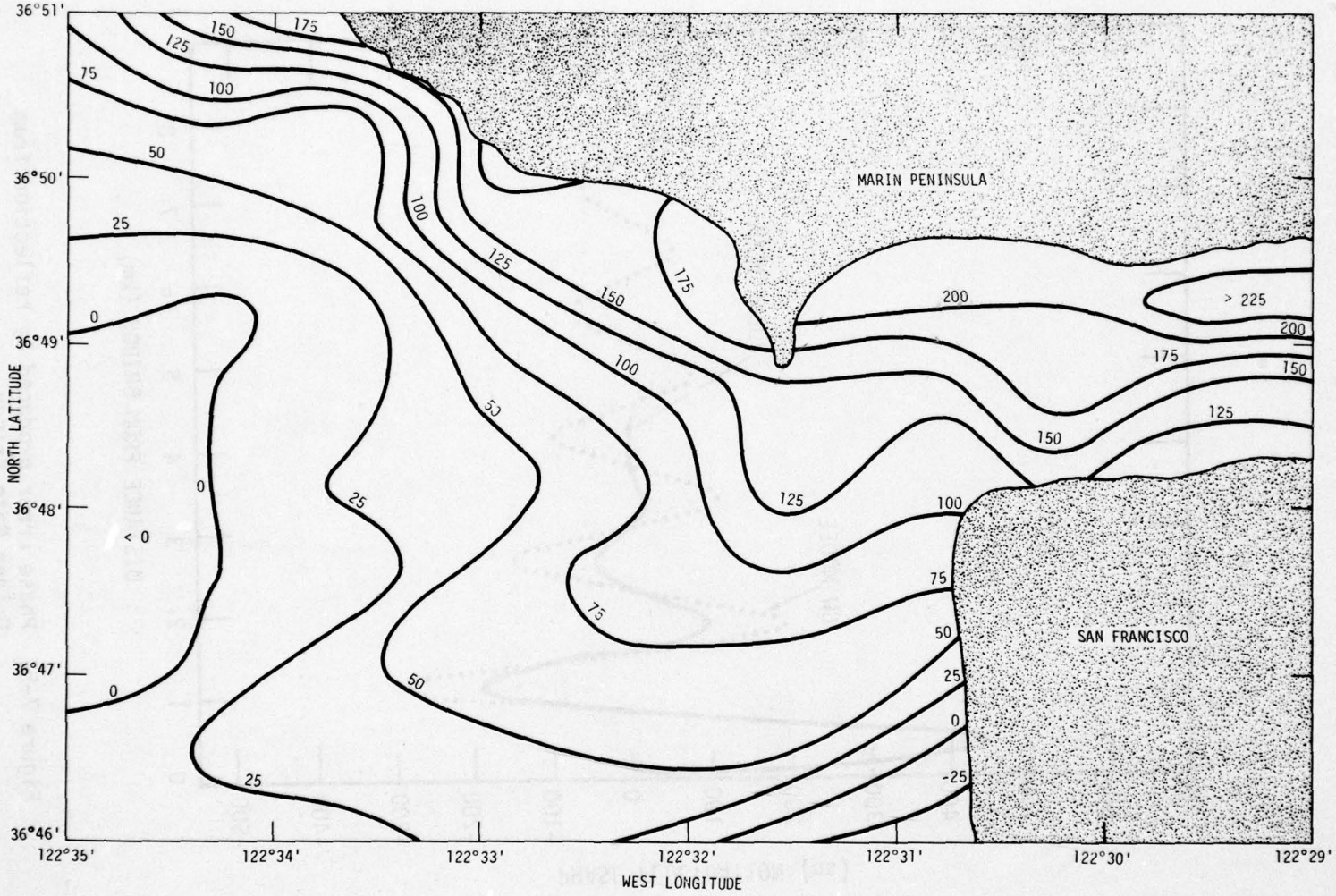

Figure 7-4. First-order TDX variations (ns) produced by the land-sea boundary effect in the outer harbor.

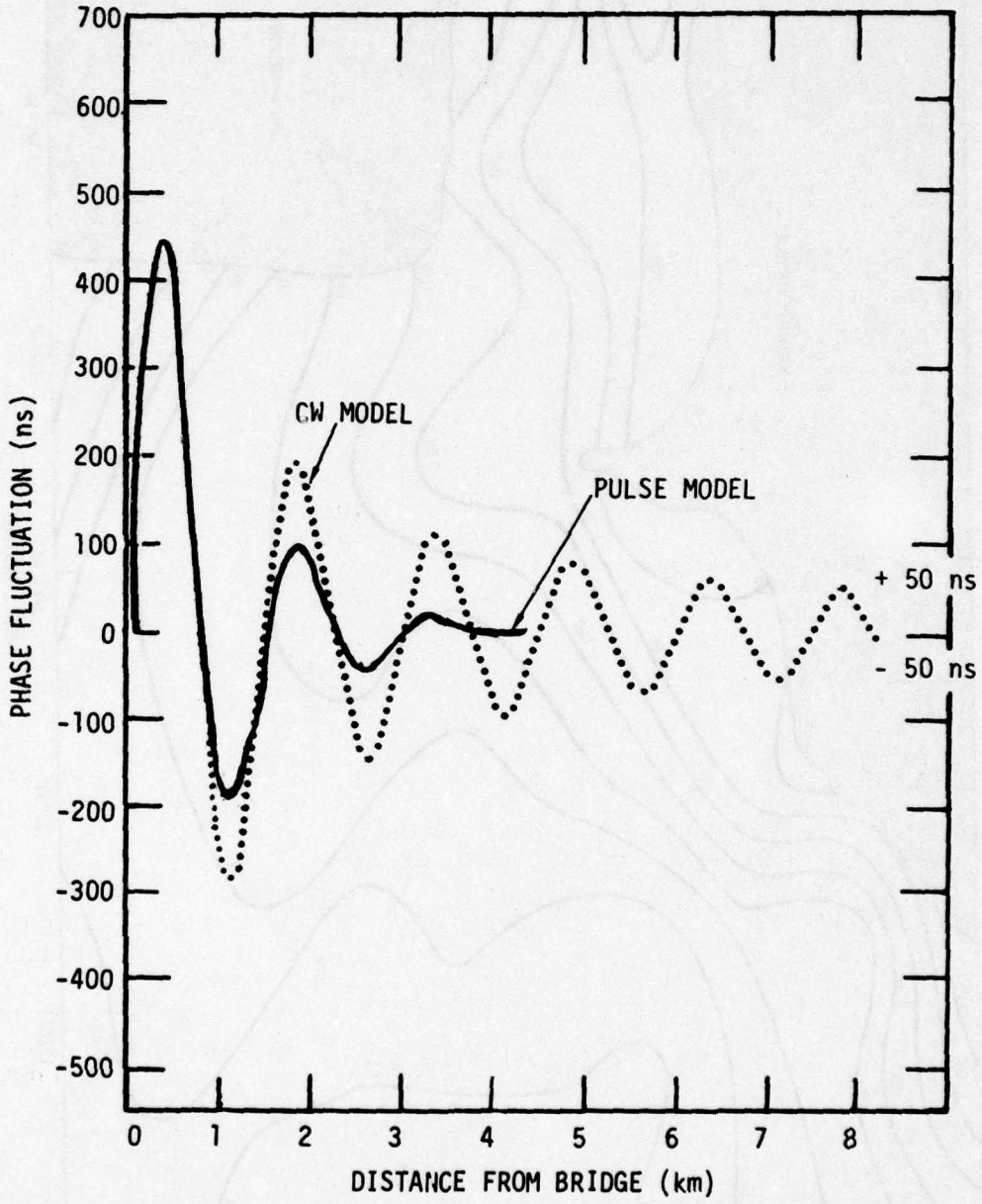

Figure 7-5. Phase error produced by reflection from Golden Gate Bridge.

Gate bridge. This results because the X-ray signal is parallel to the bridge, producing little interfering reflection and the Master signal arrives perpendicular to the bridge, producing maximum reflection. For the Bay bridge the distortion was predicted to be less severe than for the Golden Gate bridge, with TDY being most affected. No significant distortion was expected near the Richmond bridge since its height is only a small fraction of a wavelength at 100 kHz.

The land harbor sites and the vessel tracks were selected on the basis of the analysis described above. For details of the selection process, see Reference 7-1. As an example, a closely spaced series of parallel vessel tracks in the vicinity of the Golden Gate bridge was selected to map the scattering effects predicted.

FIXED LAND SITE PHASE

The purpose of the land site measurements was to provide data necessary to obtain: (1) a calibrated, accurate harbor grid, (2) an evaluation of grid accuracy and anomalies, (3) an evaluation of relative (repeatable) mode Loran-C, and (4) an evaluation of differentially augmented relative mode Loran-C. The land harbor site measurements were made using five receivers in three deployments of approximately 1 week each. Since two sites were visited twice, data were collected at a total of 13 sites. Figure 7-1 showed the location of the sites. The crosses represent deployment 1 sites, the circles represent deployment 2 sites, the triangles represent deployment 3 sites, and the squares represent sites which were common to deployments 2 and 3.

Data Collection and Analysis

The data collected are summarized in Table 7-1. The values in Table 7-1 were computed using 7 to 9 days of data (data sampling interval of 100 seconds) for each site (the actual number of days of data for each site is indicated in the data sample column of Table 7-1). All standard deviations are small (ie, below 30 nanoseconds). Week 2 showed the largest standard deviations. As already mentioned in Section 4, this is attributed to problems at the Point Piños SAM. Note the shift in mean TDX and mean TDY at Fort Point and Fort Mason between weeks 2 and 3. Fort Cronkhite data also exhibited similar behavior.

7-1. Illgen, J.D., B. Gambill, and L.W. Nelson, *Harbor Experiment Analysis Plan*, February 14, 1978. General Electric—TEMPO, (Unpublished Draft).

Table 7-1. Harbor experiment data summary (values in microseconds).

Deployment	Measurement Site	Data Sample (days)	Mean TDX	Mean TDY	Std. Dev. TDX	Std. Dev. TDY
1	1. Sears Point	7	27159.2852	43306.6406	0.0218	0.0195
	2. Point Molate	7	27203.0703	43241.7578	0.0181	0.0185
	3. Angel Island	7	27221.6641	43211.2812	0.0222	0.0177
	4. Hunters Point	7	27256.0820	43167.8594	0.0278	0.0217
	5. Treasure Island	7	27238.0508	43201.4687	0.0243	0.0203
2	6. Ballena Bay	7	27272.6992	43178.0156	0.0249	0.0205
	7. Collins Marine	7	27241.4961	43188.1641	0.0210	0.0255
	8. Fort Mason	9	27226.5898	43196.8047	0.0271	0.0220
	9. Fort Point	7	27217.5937	43197.5937	0.0250	0.0230
	10. Point Bonita	8	27199.4922	43204.2031	0.0292	0.0276
3	11. VA Hospital Ft. Miley	7	27211.7305	43191.1250	0.0227	0.0227
	12. Fort Point	9	27217.5781	43197.5625	0.0189	0.0223
	13. Fort Mason	9	27226.5820	43196.7969	0.0175	0.0193
	14. Alcatraz Island	9	27225.4258	43202.5547	0.0174	0.0196
	15. Berkeley Marina	8	27248.7695	43211.9375	0.0218	0.0276

To evaluate the accuracy of the idealized grid and calibration techniques, a series of grids were prepared based on the data from selected land sites. The accuracy of the resulting grids was estimated by comparing the predicted TD for the measurement sites with the actual measured values. A thorough discussion of these procedures can be found in Reference 7-2. The idealized grids were derived from the following data: (1) the original grid parameters estimated in the planning phase, (2) fixed sites with all over-land paths (Fort Cronkhite, Sears Point, Ballena Bay, and Berkeley Marina), (3) fixed site data with both on-shore and mid-harbor locations (Sears Point, Alcatraz, and Fort Miley), and (4) data from all sites using a least squares fit. The accuracy of the grids fit to the data progressively improved from (1) to (4). This comparison is summarized in Table 7-2.

Conclusions From Fixed Site Data

The error contours from the planning phase did not explain the difference between measured values and the initial idealized grid. It was discovered that an additional major error source was due to the nonlinear phase distance relationship; ie, phase is not really a linear function of

7-2. Nelson, L.W., *Loran-C Signal Analysis: Final System Analysis Report*, GE78TMP-108, General Electric-TEMPO, June 1979.

Table 7-2. Summary of harbor fixed site data reduction and grid preparation.

Site	Distances to Master, X-ray, and Yankee			Measured	Predicted Using	Estimated Parameters Used in Experiment Plan		Overland Path Data		On Shore and Mid Harbor Data		Least Square Fit to 13 Sites	
	D_M(km)	D_X(km)	D_Y(km)	TDX (μs)	TDY(μs)	TDX(μs)	TDY(μs)	TDX(μs)	TDY (μs)	TDX(μs)	TDY(μs)	TDX(μs)	TDY(μs)
Fort Cronkhite	374.588	104.539	746.697	192.402*	210.969*	192.363	211.134	192.402	210.796	191.975	211.100	192.191	211.027
Fort Miley	375.085	110.973	741.214	211.731	191.125	212.271	191.143	212.307	190.780	211.731	191.125	211.908	191.052
Point Bonita	374.455	106.654	744.558	199.492	204.203	199.899	204.427	199.937	204.082	199.456	204.392	199.653	204.321
Fort Point	370.808	108.400	738.861	217.586	197.579	217.947	197.581	217.984	197.242	217.398	197.482	217.511	197.438
Point Blunt	364.550	103.375	736.769	221.664	211.281	222.026	211.511	222.065	211.213	221.496	211.293	221.526	211.290
Alcatraz Island	366.363	106.368	735.957	225.426	202.555	226.000	202.736	226.037	202.420	225.426	202.554	225.468	202.540
Fort Mason	368.020	108.381	735.873	226.586	196.801	227.207	196.916	227.243	196.587	226.611	196.767	226.670	196.742
Hunter's Point	368.596	117.796	727.833	256.082	167.859	256.842	168.113	256.873	167.749	256.019	167.983	256.020	167.960
Ballena Bay	360.146	114.395	722.439	272.699	178.016	273.694	178.335	273.726	178.016	272.812	178.049	272.674	178.082
Collins Marina	366.266	111.073	731.574	241.496	188.164	242.097	188.410	242.131	188.078	241.403	188.231	241.408	188.220
Treasure Island	362.770	106.589	732.047	238.051	201.469	238.754	201.678	238.790	201.375	238.112	201.431	238.084	201.441
Berkeley Marina	356.070	103.164	728.493	248.770	211.938	249.675	212.202	249.713	211.938	249.005	211.830	248.873	211.884
Point Molate	359.703	92.988	741.023	203.070	241.758	203.415	241.942	203.459	241.698	203.063	241.626	203.077	241.650
Sears Point	350.111	70.240	750.937	159.285	306.640	159.229	307.152	159.285	307.021	159.285	306.639	159.283	306.716

*Add 27000 to TDX
Add 43000 to TDY

	Original Estimated Parameters	Overland Paths	On Shore + Harbor	Least Squares
Mean TDX Error	505	544	-39	0.5
Std Dev. (TDX)	307	302	154.5	111
Mean TDY Error	207	-97	10.4	0.3
Std Dev. (TDY)	127	173	93.4	81
Max Error (TDX)	995	1027	426	211
Max Error (TDY)	512	380.5	124	141

Measured Minus Predictions →

Site	TDX(ns)	TDY(ns)	TDX(ns)	TDY(ns)	TDX(ns)	TDY(ns)	TDX(ns)	TDY(ns)
Fort Cronkhite	+39	-165	-0.1	+172.6	+426.7	-130.6	+210.8	-57.9
Fort Miley	-540	-18	-575.6	+344.7	+0.3	+0.5	-176.7	+73.2
Point Bonita	-407	-224	-444.5	+121.5	+36.2	-189.1	-161.1	-118.3
Fort Point	-353	+13	-397.6	+336.8	+188.1	+97.1	+74.5	+141.5
Point Blunt	-362	-230	-400.7	+68.1	+167.9	-12.5	+137.9	-8.6
Alcatraz Island	-574	-181	-600.1	+134.6	+0.5	+0.8	-42.3	+15.4
Fort Mason	-617	-111	-657.2	+213.6	-24.6	+34.4	-84.2	+59.3
Hunter's Point	-760	-254	-791.3	+110.5	+63.0	-124.4	+62.5	-101.0
Ballena Bay	-995	-319	-1027.1	+0.4	-112.8	-32.8	+24.9	-65.5
Collins Marina	-601	-246	-635.1	+86.4	+93.4	-67.0	+87.8	-55.7
Treasure Island	-703	-209	-739.3	+94.0	-61.3	+37.8	-32.7	+27.6
Berkeley Marina	-905	-264	-942.9	+0.0	-235.1	+107.9	-102.6	+53.7
Point Molate	-345	-184	389.0	+59.8	+7.0	+131.5	-7.1	+108.1
Sears Point	+56	-512	+0.1	-380.5	+0.3	+0.8	+1.6	-76.3

of distance even for a short homogeneous path segment as assumed in Equation 7-1. Additionally, it was determined that the land-sea recovery was not as large as predicted when the parameters of Equation 7-1 are estimated from data taken at a carefully selected set of calibration sites. The effects of the nonlinear phase-distance effect are worst at moderately close distances to the transmitter, where the phase versus distance function has significant curvature. Thus, grid fits may have larger errors for short baseline systems than for long baseline systems (given equal accuracy in the calibration data). One reason is that the operational area is close to the transmitters in a region of high phase-distance nonlinearity. Secondly, the sensitivity to conductivity changes is greater. Thus temporal changes in the ground conductivity due to precipitation or freezing can cause significant grid instabilities.

The use of grids which consider phase velocity as a polynomial function of range and bearing from each transmitter was not considered. It was reasoned that the additional complexity of these grid models would only yield slight accuracy improvement, since the required smoothness in the spatial derivatives of the phase is clearly not attained in the complex signal path impedance structure found in harbors.

The analysis of grid calibration techniques found in Reference 7-2 provides an upper bound for grid fit error of 250 ns for the area bounded by the calibration sites. This error analysis also predicted larger grid errors for TDX than TDY, which was confirmed by the measurements. The final idealized grid had about 100 ns accuracy for the harbor area best sampled by the calibration sites. An obvious means of improving grid accuracy would be to use multiple grids. The number of grids and their boundaries could be selected based on an error analysis which bounds the error of each subgrid.

An alternative grid parameterization considered was the linear grid, which is a linearization of Equation 7-1 about some fixed location. Obviously a linear grid is less accurate over a large area, but errors near the linearization point may be quite small. Thus, one might consider the use of multiple linear grids to achieve the same accuracy as the idealized grid. This essentially trades increased parameter storage needed for the simpler coordinate conversion algorithm (ie, one only needs to solve a set of linear instead of nonlinear equations). The linear grid is of interest from the standpoint that it is simple, easily implemented, and need not provide absolute position (see Reference 7-3). Both the idealized grid and the linear grid have the very desirable property that the grid calibration can be completely automated and performed in real time. This is currently being implemented for the linear grid by the USCG.

7-3. Ligon, J.M., and C.R. Edwards, *PILOT, Precision Intercoastal Loran Translocation-Exploiting Loran-C in the Harbor and River Environment*, Presented at the 8th Annual Wild Goose Association, October 1979.

EVALUATION OF DIFFERENTIALLY AUGMENTED RELATIVE MODE (DIFFERENTIAL LORAN-C)

The fixed site data from the first deployment were processed to simulate a differential Loran-C system. The concept of differential Loran-C was tested in the Differential Loran-C Time Stability study (Reference 7-4). In this study, conducted in 1973, it was shown that the differential mode of operation resulted in improvement factors of 1.5 to 3 over the repeatable mode. In the differential mode a monitor receiver at a known, fixed location is used to compute a correction which is provided to users in the area. The user then adds this correction to his receivers's TDs to obtain more accurate TDs. The basic formula for computing the correction for X-ray from data at site G is

$$DC(t_i) = \overline{TDGX} - TDGX(t_i) \quad , \tag{7-2}$$

where $DC(t_i)$ denotes the differential correction at time t_i, $\overline{TDGX}$ is the average monitor or control TD, and $TDGX(t_i)$ is the monitor TD at t_i. The error in the differential correction, or the differential error DE, is the sum of the signal variation at the mobile location and the DC, namely

$$DE(t_i) = (TDSX(t_i) - \overline{TDSX}) - (TDGX(t_i) - \overline{TDGX}) \quad , \tag{7-3}$$

where S is the mobile user site. If the time differences are highly correlated and the two receivers measure without error, then the DE would be quite small.

Consider the problem of finding the optimal estimate of the user TD given the TD at the monitor. It is well known that the linear minimum variance unbiased estimate is given by

$$\widehat{TDSX}(t_i) = K(TDGX(t_i) - \overline{TDGX}) + \overline{TDSX} \quad , \tag{7-4}$$

where $\widehat{TDSX}(t_i)$ denotes the minimum variance estimate of $TDSX(t_i)$ and the gain K is given by

$$K = \frac{E\{(TDSX(t_i) - \overline{TDSX})(TDGX(t_i) - \overline{TDGX})\}}{E\{(TDGX(t_i) - \overline{TDGX})^2\}} \tag{7-5}$$

where $E\{\cdot\}$ is the expectation operator. If we multiply Equation 7-4 by -1 and add $TDSX(t_i)$ to both sides we get

$$(TDSX(t_i) - \overline{TDSX}) - K(TDGX(t_i) - \overline{TDGX}) = TDSX(t_i) - \widehat{TDSX}(t_i) \tag{7-6}$$

7-4. Goddard, R.B., *Differential Loran-C Time Stability Study*, DOT, USCG Final Report, November 1973.

We see that this represents a general expression for the differential error. Since $\hat{TDSX}(t_i)$ minimizes the variance of Equation 7-6, we conclude that

$$DC^*(t_i) = -K(TDGX(t_i) - \overline{TDGX}) \tag{7-7}$$

is the optimum differential correction. It is clear that Equation 7-2 is a special case of Equation 7-7 where K = 1.

If K = 1 as computed by (7-5), then we conclude that

$$COV(TDSX, TDGX) = COV(TDGX, TDGX) \quad , \tag{7-8}$$

or TDSX and TDGX are perfectly correlated. It is obvious that using Equation 7-7 as a correction rather than Equation 7-2 should reduce the variance of the differential error. The form of Equation 7-5 has a nice intuitive explanation. Since we are dividing by the variance of the monitor TD, we see that as the variance goes up, the gain goes down. However, since the numerator of Equation 7-5 is the covariance of the mobile and monitor TDs, we see that for highly correlated TDs the gain will approach unity no matter how large the variance of the monitor becomes. This is a very satisfying and logical result.

The terms in Equation 7-5 can be estimated from experimental data. To do this we can estimate the covariance and variance by computing the sample covariance and the sample variance. The formulas are given by

$$COV(TDSX, TDGX) = \frac{1}{N} \sum_{i=1}^{N} [TDSX(t_i) - \overline{TDSX}][TDGX(t_i) - \overline{TDGX}] \tag{7-9}$$

and

$$COV(TDGX, TDGX) = \frac{1}{N} \sum_{i=1}^{N} [TDGX(t_i) - \overline{TDGX}]^2 \quad , \tag{7-10}$$

where N is the number of data samples. Thus Equation 7-5 becomes

$$K = \frac{\sum_{i=1}^{N} [TDSX(t_i) - \overline{TDSX}][TDGX(t_i) - \overline{TDGX}]}{\sum_{i=1}^{N} [TDGX(t_i) - \overline{TDGX}]^2} \quad . \tag{7-11}$$

Equation 7-11 is fine for investigating the differential concept. However, it is not very useful for real-world use. There are several immediate reasons for this. Among them is the fact that although the sample variance can be computed for the monitor receiver, it may be difficult to compute for the covariance of the mobile receiver against the monitor unless a large sample of data is available from the mobile receiver. For the real-world use of differential Loran-C, we need an expression for COV(TDSX, TDGX) which can be precomputed without the need of experimental data from the mobile receiver.

We can use the fluctuations model described in Section 5 to compute the desired covariance, if we make the following assumptions: (1) that chain, propagation, and receiver variations are mutually independent, (2) the monitor and mobile receiver are close enough so that the propagation fluctuations are identical at both receivers for each signal, (3) the signals from each transmitter are mutually independent, and (4) the receiver fluctuations at each receiver are independent. If these assumptions are satisfied, then

$$E\{tdsx \cdot tdgx\} = E\{x_\theta(t_i)^2\} + E\{m_\theta(t_i)^2\} + E\{[x_\Omega(t_i) - m_\Omega(t_i)]^2\} \quad . \tag{7-12}$$

Using data from the stability experiment, we can estimate the value of K for TDX to be 0.98 and for TDY to be 0.88.

Data Collection and Analysis

One week of data collected at Sears Point, Point Molate, Angel Island, Treasure Island, and Hunters Point was used to simulate differential Loran-C. Sears Point was arbitrarily designated as the monitor receiver to correct Point Molate, Angel Island, and Hunters Point, while Angel Island was designated monitor to correct Treasure Island. The differential error was computed for five different averaging intervals: 100s, 15 min, 2 hours, 6 hours, and 24 hours. For each averaging interval, the differential error was computed for two differential gains, 1.0 and the value computed by Equation 7-11. Histograms of each of these differential error sequences, sample standard deviations, and improvement ratios were produced. Improvement ratio is defined as the ratio of the standard deviations of the uncorrected mobile TD to the corrected mobile TD.

Figures 7-6 and 7-7 show the improvement ratio versus correction averaging interval for TDX and TDY, respectively. Each plot has two curves, one for the standard differential gain (ie, K=1) and the other for the optimal differential gain as computed using Equation 7-11. For TDX the curve exhibits the expected behavior of an exponentially decaying improvement ratio with a maximum for no averaging. Of course

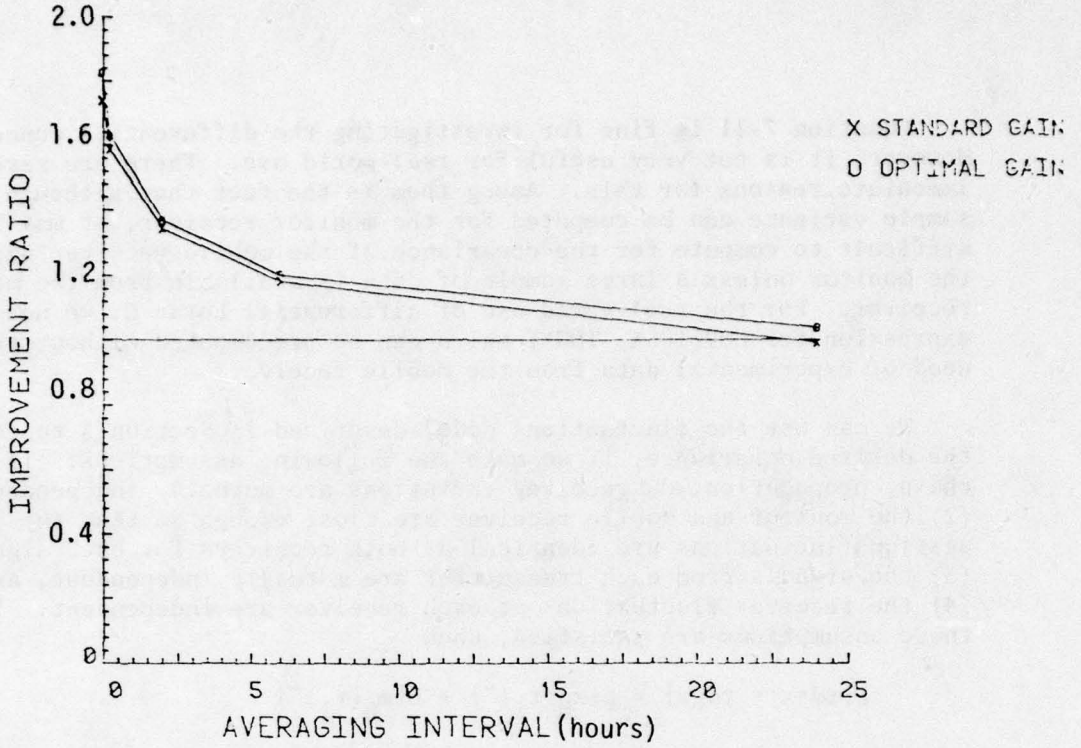

Figure 7-6. Improvement ratio versus correction interval for TDX.

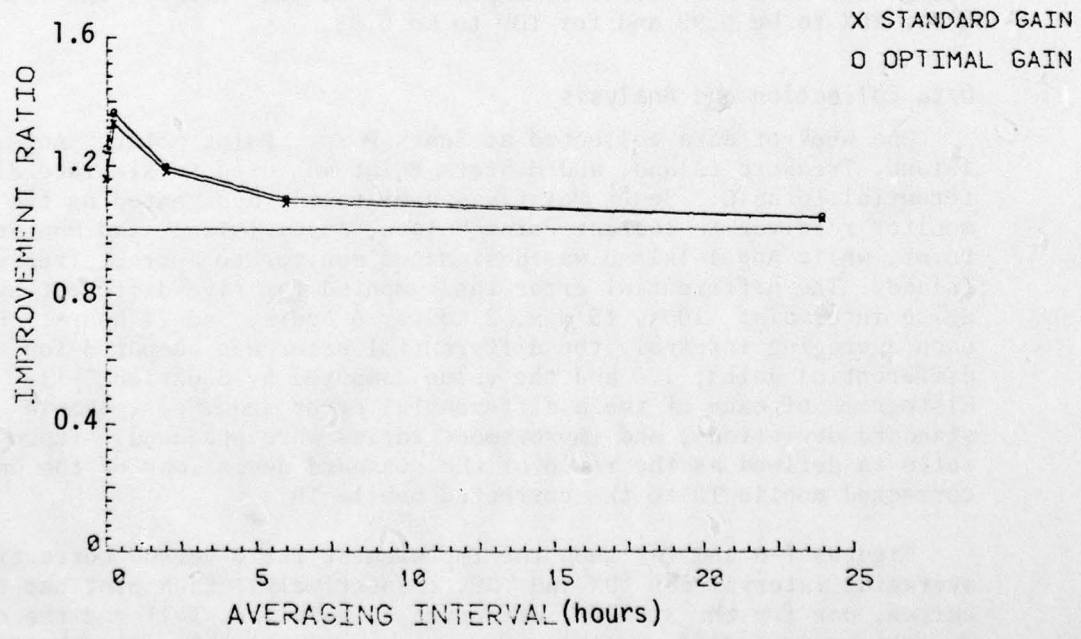

Figure 7-7. Improvement ratio versus correction interval for TDY.

the curve for the optimal gain remains above the curve for standard gain, but the improvement is not dramatic. Figure 7-7 for TDY is much more interesting. Notice that the improvement ratio is a maximum for 15-minute averaging of the correction. Since the Yankee signal has a lower signal-to-noise ratio than X-ray, the variation in TDY at the two sites has a larger independent component, which is reduced by averaging. However, averaging the correction also reduces the components which are correlated with the user TD. Apparently there is sufficient time correlation in TDY to yield improved results even though the correction is averaged longer.

While the standard gain yields degraded performance for 24-hour averaging of the correction on TDX, it yields improvement for this long averaging interval on TDY. This is further proof that TDY has significant long-term correlation. In general, though, the improvement ratios for TDX are higher than those for TDY, as one would expect due to the higher signal-to-noise ratio on the X-ray signal.

In Figures 7-8 and 7-9 the improvement ratio versus distance from the monitor are plotted. There does not appear to be any consistent pattern. In fact, for TDX this curve peaks at 33 km, with the general trend of increasing improvement with distance. TDY, however, behaves more as one might expect with improvement decreasing with distance. A strong negative correlation between distance from the monitor and improvement ratio implies that propagation fluctuations are dominant in the differential error. However, the verification and stability experiments have clearly shown that propagation fluctuations are much smaller than chain fluctuations and are on the order of receiver fluctuations. Since the Yankee signal path is the longest, one would expect propagation fluctuations to be more pronounced. Examination of the stability data also reveals that Yankee chain equipment fluctuations are somewhat smaller than for X-ray. This seems to explain both the decrease in improvement ratio with distance and the larger low-frequency spectral components observed for TDY.

Sears Point correcting Angel Island showed the best performance of the five pairs. The standard deviation of the corrected time differences was 0.2 ns for TDX, and 12.6 ns for TDY. A careful examination of the data reveals the following points: (1) the data sample for this pair was by far the largest, (2) portions of days 102 and/or 106 were missing at Point Molate, Hunters Point, and Treasure Island due to receiver simulator tests or receiver problems, and (3) these particular days showed significant chain fluctuations which were highly correlated at both Sears Point and Angel Island. These facts tend to make the improvement for Sears Point correcting Angel Island look much better than for the other pairs. Results from the Differential Loran-C Time Stability study show that 7 ns rms was the smallest DE standard deviation obtained (based on 1 week of data). Simulator tests performed on the receivers for comparable signal-to-noise ratios suggest that no further improvement is possible beyond this level.

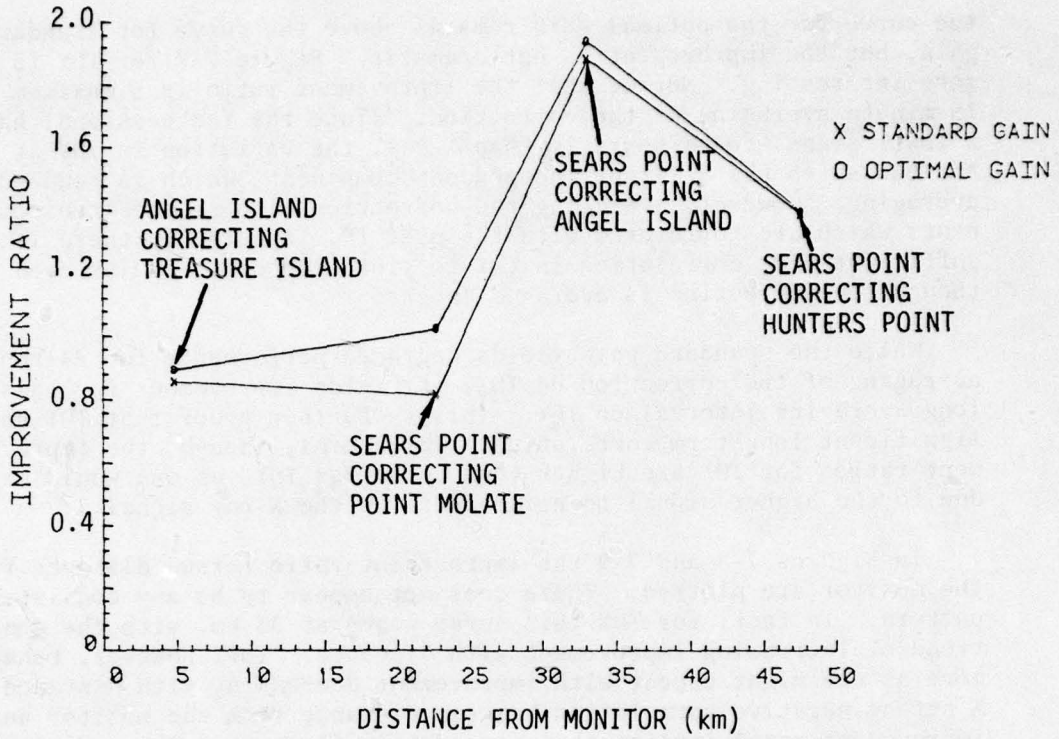

Figure 7-8. TDX improvement ratio versus distance from monitor.

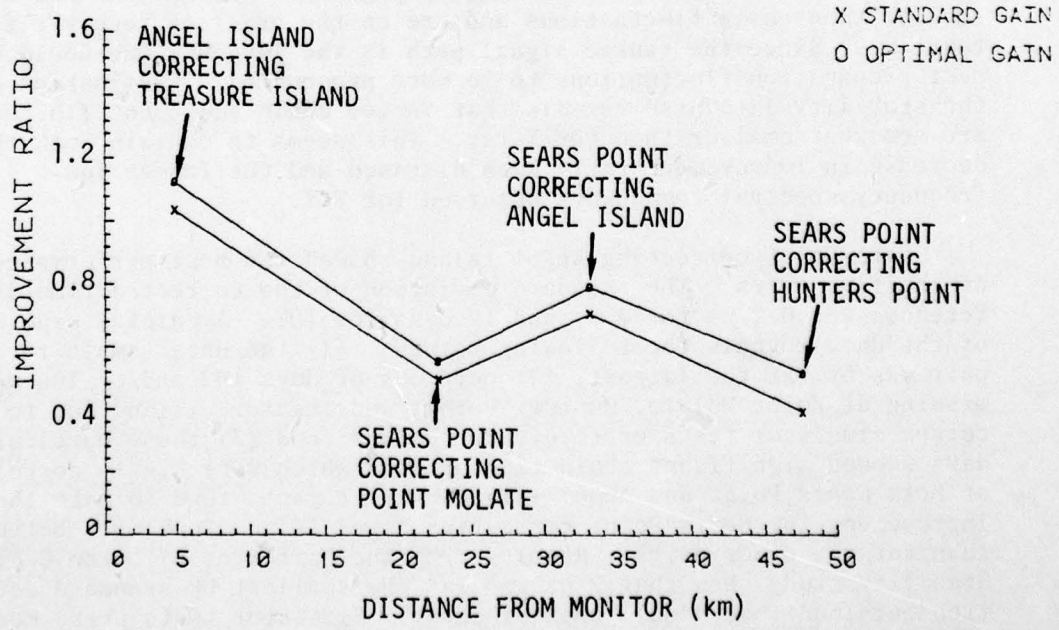

Figure 7-9. TDY improvement ratio versus distance from monitor.

The TDX data for most site pairs were highly correlated ($\rho > 0.85$). Thus, the improvement gained by using the optimal differential gain was only slight. The exception was Sears Point and Point Molate. The correlation between TDX at these locations was $\rho = 0.75$. The standard deviation of TDX was 18 ns at Point Molate and 21 ns at Sears Point. The standard deviation of the differential error for $K = 1$ was 14 ns and 12 ns for $K = 0.66$, about a 15 percent improvement. The improvement gained by using the optimal K was generally larger for TDY than TDX as expected, due to the lower signal-to-noise ratio on Yankee. The improvements due to the use of the optimal K are encouraging enough to warrant further investigation.

The optimal K derived here is based only on instantaneous signal fluctuations. We have already seen that there is significant time correlation in TDY. This suggests that the differential correction should be based on the output of a Kalman (or Weiner) filter which could exploit this time correlation in an optimal manner. Other extensions naturally handled by the Kalman filter structure would include multiple monitors.

Conclusions From Differential Loran-C Analysis

Since there is little or no correlation between differential improvement and distance from the monitor, we conclude that differential propagation fluctuations are not as significant as receiver and chain fluctuations. Furthermore, it appears that chain fluctuations are a significant error source in TDs measured in the San Francisco Bay area even though the System Area Monitor is nearby at Point Piños.

The encouraging results obtained by applying linear estimation theory to differential Loran-C indicates the possible gain from further work in that area. In particular, the results obtained here should be extended to take advantage of the sample-to-sample correlation which exists in the Loran-C signals and multiple monitors.

All of the results obtained show promise for differential Loran-C. Because of the predominance of chain and receiver fluctuations, it appears that one monitor could serve a very large service area.

VESSEL DATA

While measurements were being made at the fixed land sites, data were also being collected on board the research vessel Polaris in the harbor and harbor entrance. Figure 7-1 shows an outline of the area covered by the vessel. Both TOA and TD receivers collected data. The vessel position was measured quite accurately using the Trisponder radar system. The vessel position measurements should be an order of magnitude better than expected Loran-C errors to reasonably measure any errors in the Loran data. Summer data collected at Fort Cronkhite had suggested a 30-meter ($2D_{rms}$) Loran-C error, which dictates a

a requirement for a 3-meter ($2D_{rms}$) error in locating the vessel. It appears the Trisponder radar system (a master unit and track plotter on the vessel and four transponders on the shore) provided this accuracy. Vessel position was recorded every second. A total of 11 days of data were taken, 9 with 100-second averaging and sampling, and 2 with 10-second averaging and sampling of the Loran-C data.

The object of this phase of the experiment was to provide data for an assessment of absolute mode Loran-C in a typical harbor environment and to study grid anomalies produced by bridges. To assess the absolute mode, idealized grid parameters which were obtained by a least squares fit of land site data were used for conversion of time differences to latitude and longitude and visa versa.

Before comparison between the Trisponder position data and Loran-C data could be accomplished, a number of technical problems had to be addressed. These included: (1) correction of the Loran-C data to compensate for dynamic errors due to vessel motion and the long averaging times of the receivers, (2) the editing and filtering of the Trisponder data, and (3) proper handling of large data gaps in the Trisponder data. These are briefly discussed below.

To correct the Loran-C data for averaging errors, the Trisponder data were used to estimate vessel heading and speed. The receiver averaging was modeled and an expression was obtained for the error as a function of heading and speed. This expression was used along with the heading and speed data to estimate the error due to averaging for each TD. Finally, this estimate was subtracted from the Loran-C data.

The Trisponder data were found to have a relatively large number of bad data points and outliers. Much of this bad data was caused by signal scattering from large vessels which passed near the Polaris. A Kalman filter was used to edit these bad data. The Trisponder data were filtered in cartesian coordinates, and data editing was performed by comparing the data with its prediction from the filter. If the difference was too large, the data point was rejected and replaced by the prediction.

At other times the line-of-sight to the transponders was interrupted by large vessels. In this case data gaps up to 60 seconds occurred. To fill these gaps the predictions from the Kalman filter were used. However, if the filter covariance became too large, no comparison was made for that Loran-C sample and the Kalman filter was reinitialized.

To test the validity of the dynamic error removal algorithm, simulator tests were performed at EECEN. The LRTC-II simulator was programed to produce a series of TDs which simulated a vessel steaming at 6 knots. It was found that the dynamic error was corrected to within 10 ns.

Data Collection and Analysis

A block diagram of the processing system used to compare the Loran data to the Trisponder data is shown in Figure 7-10. An example vessel track is shown in Figure 7-11 along with the corresponding vessel position obtained from Loran-C. Figure 7-12 compares latitude and longitude as computed by the Trisponder (truth system) represented by the small dots and the Loran-C system as represented by the "fat" dots. Figure 7-13 shows time difference errors as arrows emanating from the "true" vessel position and pointing in the direction of time difference gradient. For TDX the arrows are at angles from the vertical of approximately 120° for positive errors and -30° for negative errors. TDY errors are represented by arrow points up (0°) for positive errors and down (180°) for negative errors.

The difference between true and measured position was generally low in the inner harbor, which follows from the fact that the placement of the land harbor sites used in the grid fitting is such that the grid is optimized for this area. Two areas exhibited systematic charting errors. They were near Angel Island and Alcatraz for both the X-ray and Yankee time differences. Pre-experiment analysis based on the land-sea interface phase recovery indicated that only X-ray would show large errors in these areas.

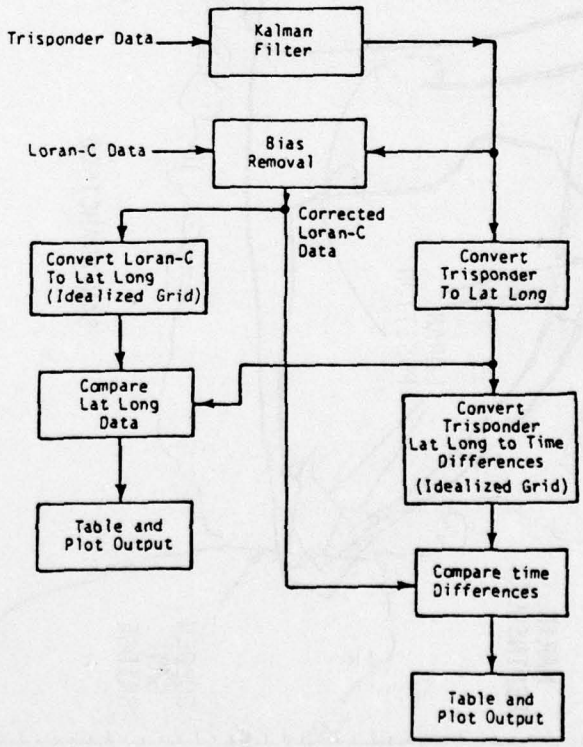

Figure 7-10. Block diagram of vessel data processing system.

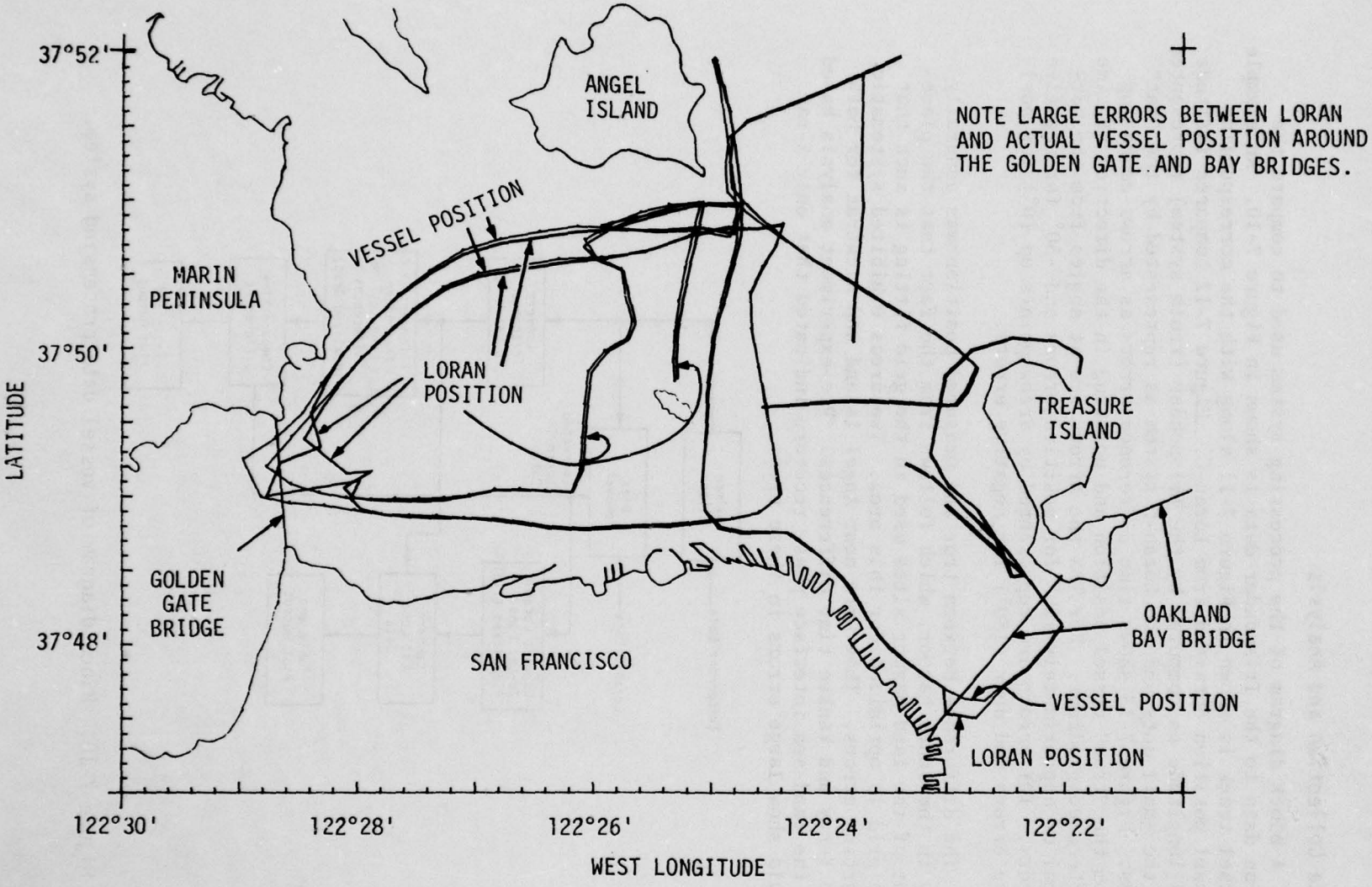

Figure 7-11. Vessel track from Trisponder and Loran-C data.

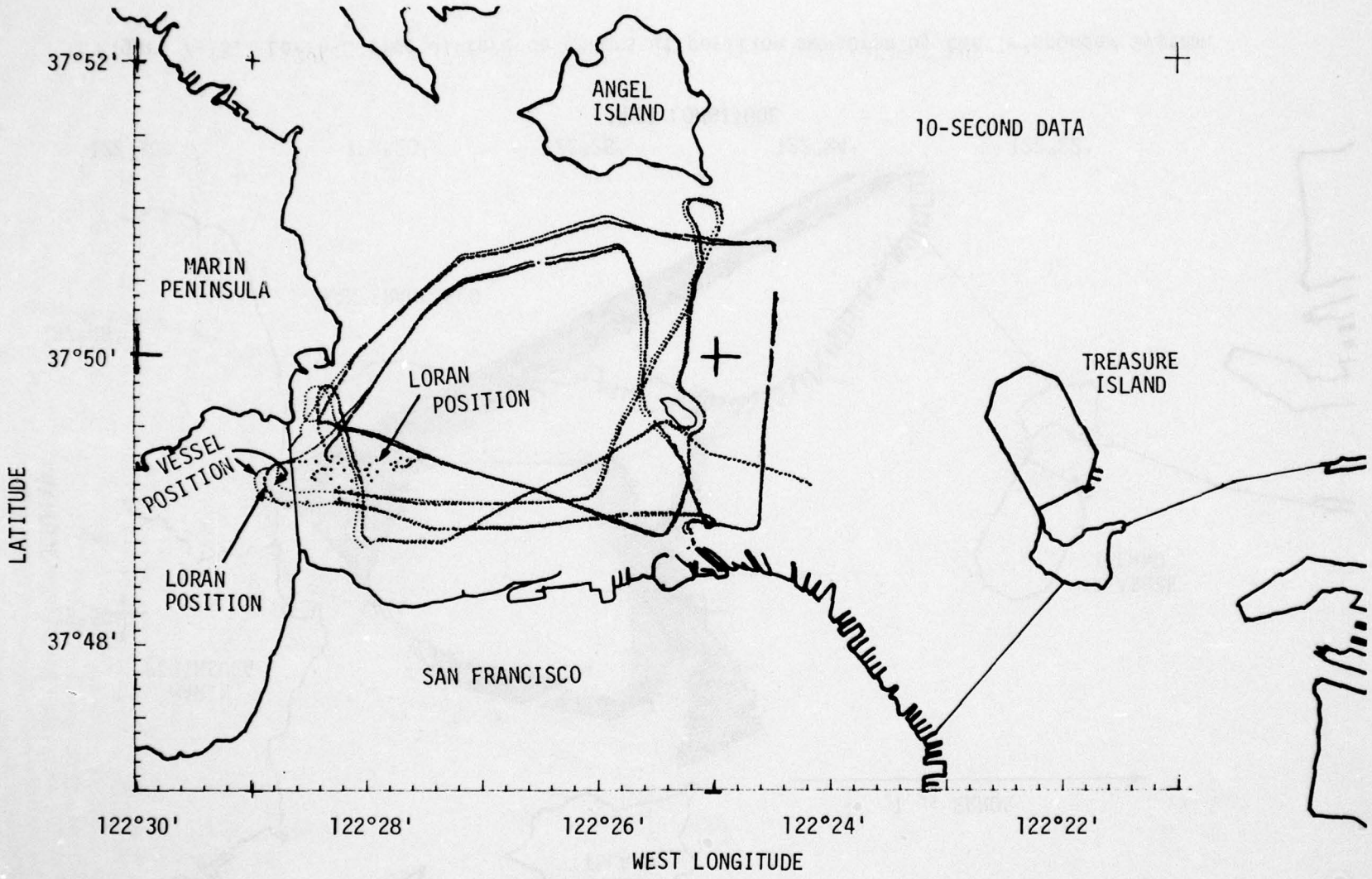

Figure 7-12. Detailed comparison of Trisponder and Loran-C measured vessel positions.

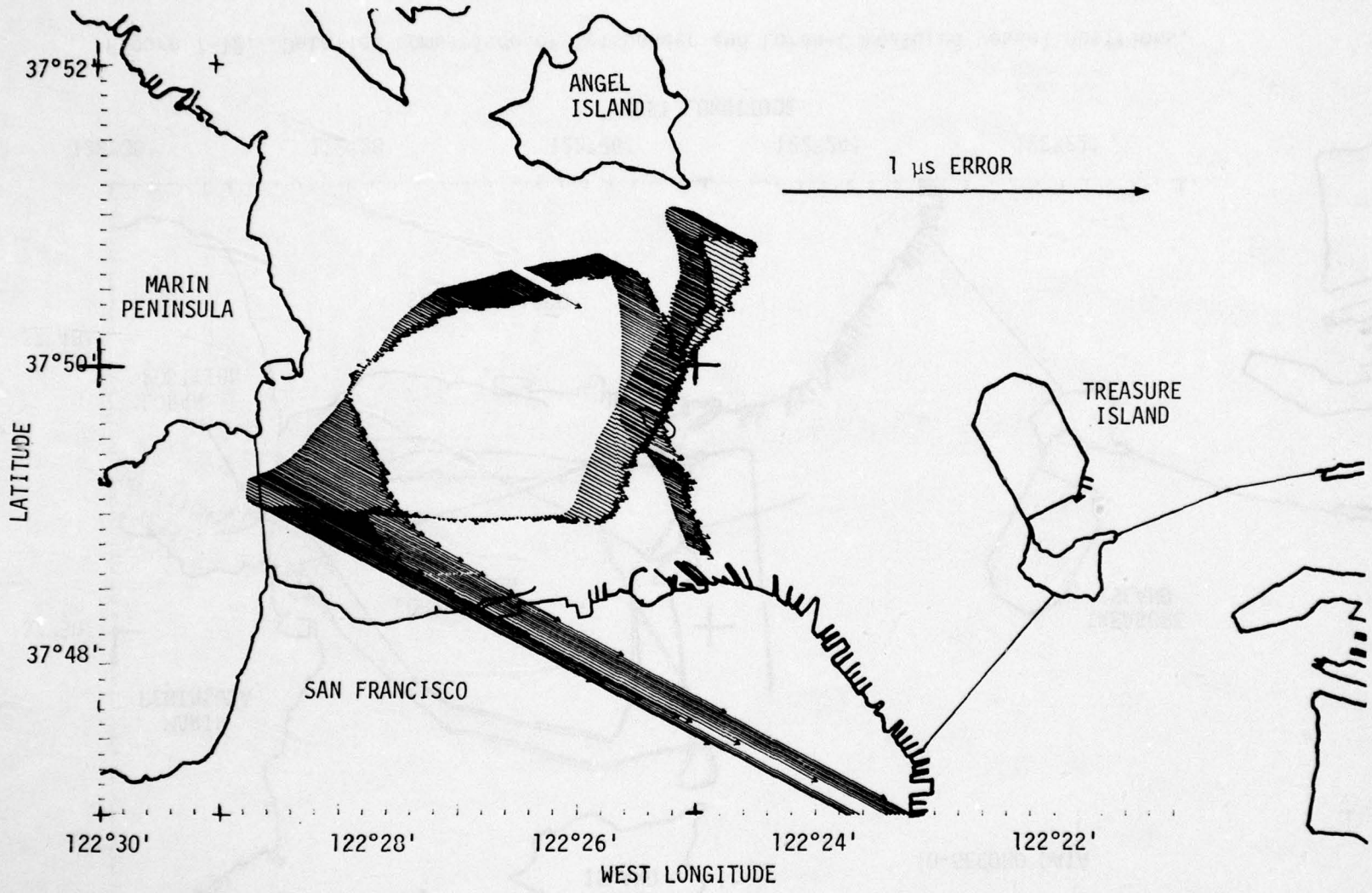

Figure 7-13. Loran-C time difference errors at position measured by the Trisponder System.

In an attempt to explain the systematic TD errors around Angel Island in both TDX and TDY, we considered prediction errors at Point Blunt and Alcatraz. For Point Blunt grid fit errors were 138 ns for TDX and -9 ns for TDY, while at Alcatraz we have -42.3 ns for TDX and 15 ns for TDY. The large error for TDX at Point Blunt seems to correlate well, and the errors in TDX for Alcatraz are in agreement for the area east of Alcatraz but not to the west. Furthermore, if we attempt to use the error contours from the planning phase, we again find good agreement for TDX. However, the large TDY errors around and to the west of Angel Island are predicted to be zero. Further analysis is needed to explain the behavior of TDY by considering other error sources. However, one cannot rule out the possibility that the error is really in the "truth" system and not Loran-C.

The errors around the three bridges follow the general pattern predicted by analysis in Reference 6-1. It was predicted that errors in TDX would be worst around the Golden Gate Bridge while errors in TDY would be worst around the Bay Bridge. The Richmond Bridge was not expected to produce severe errors in either TDX or TDY. The reasons for these predictions are as follows: (1) the Golden Gate has the largest cross section, (2) the X-ray signal passes almost parallel to the bridge while Master is almost perpendicular, (3) the reflection of Yankee from the Golden Gate would approximately cancel the effect of Master, and (4) the Richmond Bridge is too small to cause significant scattering. The TDY errors around the Golden Gate Bridge are somewhat larger than around the Bay Bridge but are smaller than the TDX errors around the Golden Gate. TDY errors around the Bay Bridge were larger than TDX errors, as expected.

One day of Loran-C data with 10-second averaging was collected in the Golden Gate Bridge area. The closer spaced samples gave a good picture of what happens as a vessel approaches the Golden Gate Bridge. An error buildup in TDX began about 1000 to 1200 meters from the bridge. This compares quite well with the start of the major lobe in Figure 7-5. The signal then became totally useless when the vessel approached within 400 to 600 meters of the bridge, in that the received signal became so unstable that it could not be used for navigation. The signal was again usable about 400 to 600 meters from the bridge on the seaward side.

Errors in position were higher in the San Pablo bay area and seaward from Golden Gate Bridge. These areas were not effectively sampled by the calibration sites, and thus the grid fit should be poor in these areas.

The means and standard deviations of the differences between grid predictions and measured data for the inner harbor (excluding the areas near the Golden Gate and Bay Bridges), are:

$$\overline{\tilde{TDX}} = 34.1 \text{ ns} \qquad \sigma_{\tilde{TDX}} = 65.1 \text{ ns rms}$$

$$\overline{\tilde{TDY}} = -0.6 \text{ ns} \qquad \sigma_{\tilde{TDY}} = 64.7 \text{ ns rms} \quad .$$

Note the mean offset in TDX could be corrected by changing the X-ray emission delay. In general the performance is quite good. If one considers that the standard deviations of the received signals are about 20 ns rms, then we see that approximately 60 ns rms is due to charting errors.

Conclusions from Vessel Data

The results of this experiment show that Loran-C can provide reliable and accurate navigation for use in piloting San Francisco Bay provided proper precautions are exercised near bridges and the proper equipment is used. The quality of the results is encouraging and shows that the software and techniques developed to process the vessel data form a solid basis for user equipment design and automated harbor calibration techniques.

Some general conclusions are also possible concerning the distortion caused by large bridges. Bridge height must be a significant fraction of a wavelength to produce significant signal distortion. This conclusion is based on a simplified analysis and the fact that the Richmond Bridge produces little or no distortion compared to the large Golden Gate and Bay Bridges. The simple scattering theory predicts fairly well the general behavior and spatial pattern of measured signal distortion.

SECTION 8

COMPARATIVE SYSTEM ANALYSIS

The purpose of this section is to compare the performance of Loran-C in San Francisco harbor in four modes of system operation: absolute mode, repeatable mode, differentially augmented absolute mode, and differentially augmented repeatable mode. Other augmentation techniques such as additional low-power secondaries will not be considered. Data presented in Sections 5 and 7 will be used to rank the four modes of system operation in terms of presently achieved accuracy as measured by error ellipses. Additionally, possible improvements in each of the modes of operation will be discussed as well as the feasibility of attaining improved accuracy and operational use of the modes.

ACCURACY REQUIREMENTS FOR HARBOR NAVIGATION

Although the signal analysis project was not tasked with the responsibility of determining accuracy requirements for harbor navigation, the following simple analysis is offered to assess the usefulness of the different modes of system operation.

San Francisco harbor is a large harbor. Due to its size, the accuracy requirements are not overly severe. For example, the narrowest point of the main shipping channel leading to the harbor entrance is 200 meters wide. The channel width under the Richmond-San Rafael Bridge is 200 meters, while the width of the inner Oakland harbor entrance channel is 150 meters. Thus we might choose an accuracy requirement of 50 meters $2D_{rms}$, giving a 50 percent safety margin.

PERFORMANCE OF THE ABSOLUTE MODE

Using the vessel data presented in Section 7, the $2D_{rms}$ for the absolute mode computed by standard techniques is 71.2 meters excluding data under the Golden Gate and Oakland Bay Bridges. This exclusion is not unreasonable because the prudent navigator would not rely on only one navigation aid. In times of poor visibility he would almost surely be using radar in addition to Loran-C. Hence he would know when he was approaching a large bridge and would not rely on Loran-C until he was clear of the bridge.

The data used to compute the $2D_{rms}$ error includes a 34 ns offset in TDX. If we assume that this offset can be measured and removed,

then the results becomes 60.8 meters $2D_{rms}$. However, the 71.2 meters $2D_{rms}$ represents approximately worst-case conditions.

REPEATABLE MODE PERFORMANCE

In the Loran-C repeatable mode, the user does not convert from Loran-C coordinates to geodetic coordinates. Rather he first establishes a set of way points to his destination during times of good visibility. Then during poor weather conditions he steers from way point to way point using his current TD and the next way point to establish his desired heading. For harbor navigation the heading information would be generated by the receiver. In fact, there is at least one receiver currently on the market which will compute heading information and cross track error.

To determine the accuracy in this case, we consider the TDs used to determine the way points to be statistically independent of the navigation TDs. Thus, we simply multiply the standard deviations of the TD's by the square root of two. The correlation coefficient remains unchanged. The average standard deviations of the harbor data were $\sigma_x = 21.2$, $\sigma_y = 22.5$. Thus for the repeatable mode we get standard deviations of $\sigma_x = 30.0$ ns and $\sigma_y = 31.8$ ns. This gives a $2D_{rms}$ of 38 meters.

PERFORMANCE OF DIFFERENTIALLY AUGMENTED ABSOLUTE MODE

The performance of the absolute mode previously presented was based on the vessel data. The standard deviations computed included both the effect of TD stability and charting errros. To estimate the performance of the absolute mode with differential augmentation requires an estimate of errors due to charting alone. The total standard deviations were $\sigma_x = 65.1$ ns and $\sigma_y = 64.7$ ns. Assuming that charting errors and temporal errors are uncorrelated, we obtain the following standard deviations due to charting:

$$\sigma_{xc} = (65.1^2 + 21.2^2)^{1/2} = 61.6 \text{ ns}$$

$$\sigma_{yc} = (64.7^2 + 22.5^2)^{1/2} = 60.7 \text{ ns}$$

If we use 14 ns as the average standard deviation of the corrected TDX and 15 ns for the corrected TDY, we obtain total standard deviations of

$$\sigma_{xT} = 63.2 \text{ ns}$$

$$\sigma_{yT} = 62.5 \text{ ns}$$

This yields a $2D_{rms}$ of 68.9 meters.

AD-A084 239 GENERAL ELECTRIC CO SANTA BARBARA CA TEMPO F/G 17/7
LORAN-C SIGNAL ANALYSIS.(U)
DEC 79 L W NELSON, B GAMBILL DOT-CG-64810A
UNCLASSIFIED GE79TMP-78 USCG -D-4-80 NL

2 OF 2
AD
A084239

END
DATE FILMED
6-80
DTIC

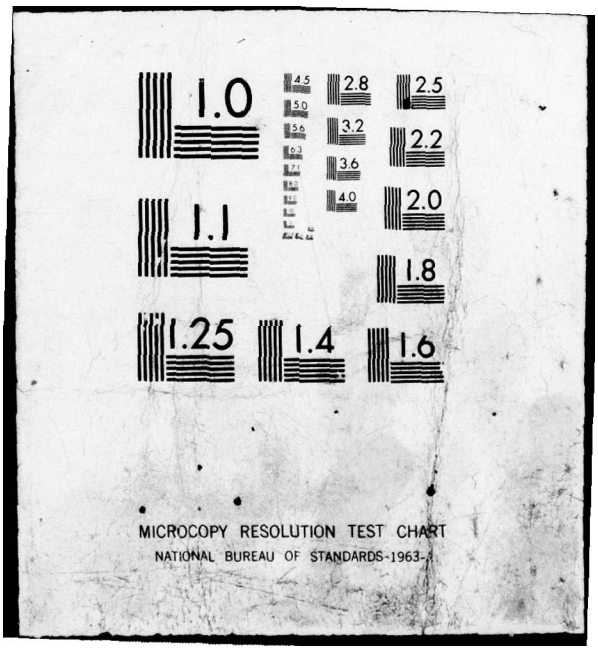
1.0
4.5
5.0
5.6
6.3
2.8
3.2
3.6
4.0
2.5
2.2
2.0
1.8
1.1
1.25
1.4
1.6
MICROCOPY RESOLUTION TEST CHART
NATIONAL BUREAU OF STANDARDS-1963-A

PERFORMANCE OF DIFFERENTIALLY AUGMENTED REPEATABLE MODE

In this mode of operation we assume that differential augmentation was used for both navigation and way point establishment. With this assumption and the previously stated standard deviations for corrected signals, we get a $2D_{rms}$ of 25.2 meters.

SYSTEM MODE RANKING

From the above mode performance estimates, it is clear that the differentially augmented repeatable mode is the best for navigation in San Francisco harbor. In fact the ranking conforms to what one would expect. Neither the absolute mode nor the differentially augmented absolute mode met the accuracy requirement of 50 meters $2D_{rms}$.

It is interesting to speculate about the reduction of charting errors that would be required for the absolute mode to meet the accuracy requirement. If the charting errors were reduced to 43 ns rms for both x and y, then the differentially augmented absolute mode would have a $2D_{rms}$ of 49.8 meters. A reduction to this level seems very feasible if one limits the area of an idealized grid. In other words, if several grids were used it is quite certain that this level could be attained.

FEASIBILITY AND USEFULNESS OF THE SYSTEM MODES

Although the repeatable mode (either augmented or unaugmented) has better performance than the absolute mode, it is generally not as useful as the absolute mode for area navigation. The reason is that the user is limited to a set of predetermined vessel tracks. For a user who repeatedly uses a particular harbor, such as a fisherman, the repeatable mode of operation adequately serves his needs, since he repeatedly follows a few well worn tracks. It is also well suited to very restricted waterways, where a vessel has no choice of direction but must remain in a narrow, tightly defined channel. However, for harbors such as San Francisco's, the repeatable mode is generally not as well suited as the absolute mode.

The implementation of the various system modes is feasible with present technology. However, for safe harbor and harbor entrance navigation, presently available displays of navigation information are in general inadequate. It is necessary to integrate current receivers with microprocessor and display technologies which will produce navigation information that can be quickly understood by the user. Some effort has been made to stimulate the development of such equipment. However, more is necessary if the use of Loran-C is to be extended into the harbor and harbor entrance environment.

CONCLUSIONS

It has been demonstrated that Loran-C can be used in the San Francisco harbor in the repeatable mode. Furthermore, the vessel data have shown that Loran-C can be used in most portions of San Francisco harbor for which an accuracy of 75 meters $2D_{rms}$ is sufficient. However, this is only achievable if the user has a Loran-C receiver with the performance capabilities of those used in these experiments. Furthermore, it is felt that coordinate conversion should be performed by microprocessors and navigation information be displayed on a CRT for truly feasible system use. Finally, it appears likely that charting errors can be reduced to levels that will allow use of the system in the absolute mode in San Francisco harbor if multiple grids are used.

SECTION 9
SYSTEM IMPROVEMENT

The equipment procured and maintained by the Coast Guard is under constant improvement. The new generation of solid-state transmitters installed in the new Gulf of Mexico chain offer extremely uniform pulses and are highly stable. System operational procedures are also being constantly improved. The CALOC control algorithm has led to better, more uniform chain control. Despite these and other system improvements, areas remain where further improvement can be achieved. This section will focus on chain control, which is one area where we believe additional research effort is needed.

The placement and number of system area monitors as well as the optimal use of SAM data for chain control need to be studied in the light of new and expanded roles for Loran-C such as harbor and river navigation and terrestrial uses. In fact, the lifetime of the Loran-C system may be shortened considerably unless its user community can be expanded by offering improved and expanded navigation capabilities. The answers to the following questions have been sought for some time:

- o How many System Area Monitors are needed for a given chain?
- o Where should System Area Monitors be placed?
- o How should the data from the System Area Monitors be utilized to best control the chain?

However, the need for answers is becoming more acute. Before a systematic treatment of these questions can be undertaken, a definition of the "prime service area" of a chain must be defined. Only then can the means be developed to provide the best possible navigation information to the user in this area. In other words, a cost function must be agreed upon which will allow us to judge the effectiveness of any particular control strategy.

Before the use of cesium standards at the transmitters, the secondary transmitters phase-locked their transmissions to the incoming master signal. Thus, the delay of each secondary signal was continuously being adjusted. The installation of cesium standards brought about a change in system operation. Since the emissions of the transmitters were now very stable, adjustments were not continuously required. The idea of using a System Area Monitor to collect data for

adjustment of the emission delays of the secondaries was conceived. Originally the SAM's were placed at the fringes of the coverage area but have now been moved into the prime coverage area. Current chain control policy can be stated as:

> The time difference of a particular master-secondary pair and its long-term average shall be maintained as close as as possible to a given reference value at the designated System Area Monitor.

The result of such a policy is that navigation signals in the vicinity of the SAM are very stable, while in the remainder of the coverage area the signals are uncontrolled. We have already seen that as a result of the close proximity to San Francisco of the Point Piños SAM, which controls both the X-ray and Yankee legs, the improvement offered by differential Loran-C in San Francisco harbor is smaller than that reported in Delaware Bay.

One of the shortcomings of such a control policy can be demonstrated by a simple example. Figure 9-1 shows the grid of a hypothetical master-secondary pair. The spacing in terms of time difference between the LOP's is constant. Consider a System Area Monitor located at the position marked SAM and a user at R. Figure 9-1 is for normal conditions

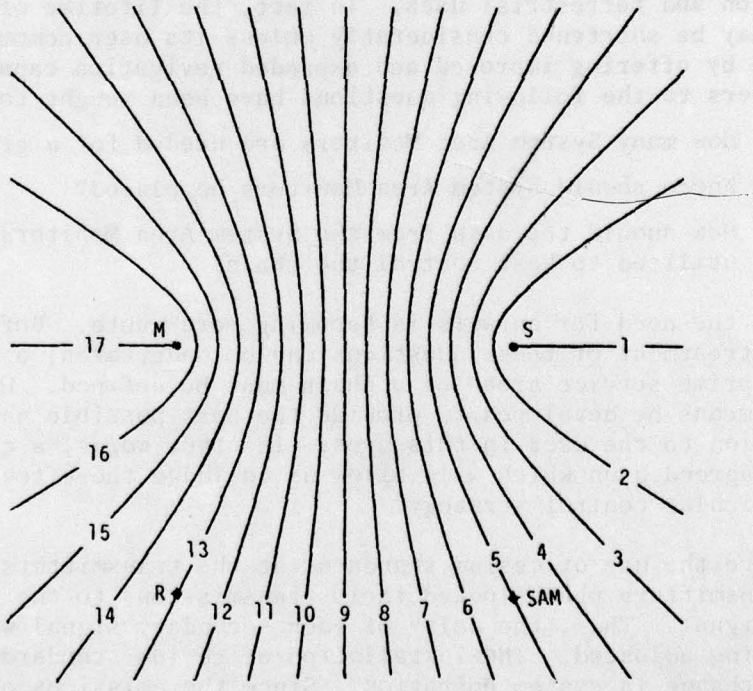

Figure 9-1. LOP's for a hypothetical grid with constant TD spacing under "normal conditions."

with TDs from 1 to 17. Now consider the effect of a uniform decrease in propagation velocity over the coverage area. This situaiton is shown in Figure 9-2, where the TD at SAM has changed from 5 to 4 while the user's TD has increased from 13 to 14. SAM detected a decrease in his TD and inserts an LPA of 1 to bring his TD back on the numbers. The effect of this LPA is seen in Figure 9-3. Now SAM's TD has returned to 5 but the user's TD has further increased to 15. Thus, errors due to a change in propagation velocity are well corrected in the vicinity of SAM but are actually magnified in the vicinity of the user at R.

If one is not interested in providing a stable signal at R, then the above policy is fine. However, consider the West Coast chain with Point Piños controlling X-ray and Yankee. In this configuration San Francisco harbor enjoys a very stable signal, while in Los Angeles and San Diego common mode propagation-induced fluctuations are exaggerated. If one is contemplating the use of Loran-C in all harbors of the West Coast USA, then a control policy should be determined to provide the best service to the most users.

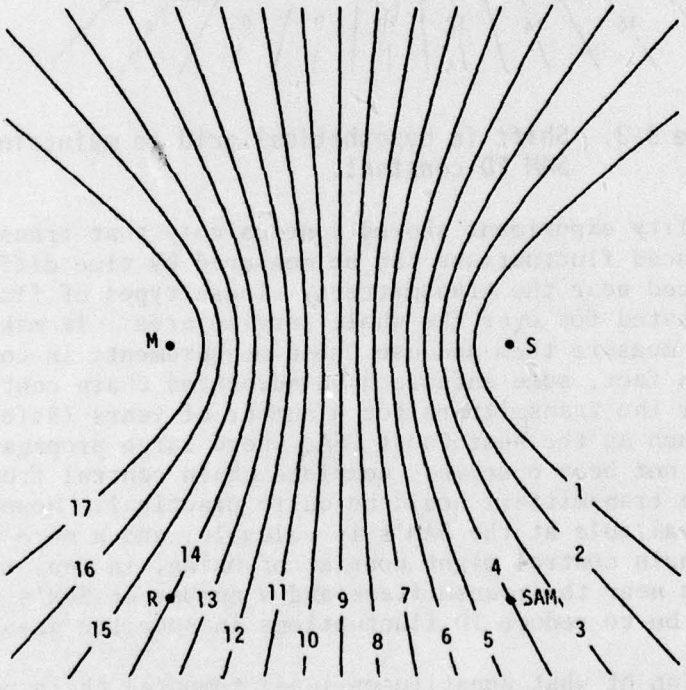

Figure 9-2. Change in hypothetical grid for uniform phase velocity decrease.

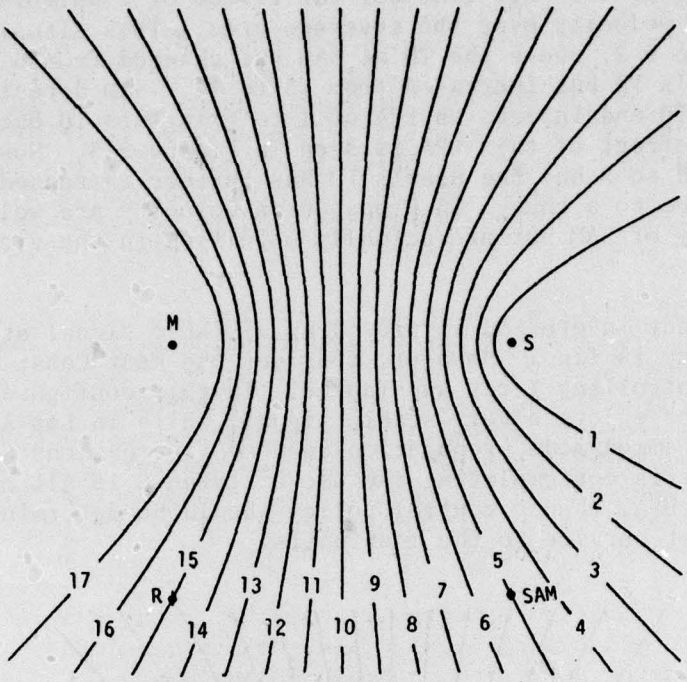

Figure 9-3. Shift in hypothetical grid to maintain SAM TD constant.

The stability experiment showed conclusively that transmitting equipment induced fluctuations can be measured by time difference receivers placed near the transmitters. These types of fluctuations can be compensated for over the whole service area. It make sense, therefore, to measure them and use these measurements in controlling the chain. In fact, some authors have advocated chain control from receivers near the transmitters for a number of years (Reference 9-1). For regions such as the West Coast USA, where large propagation fluctuations have not been observed, complete chain control from data taken near the transmitters would be quite practical. However, the information available at the SAM's is valuable, and a more prudent approach to chain control might consist of using, in real time, data from receivers near the transmitters and a number of SAM's whose purpose would be to reduce TD fluctuations in specific areas.

The question of what constitutes ideal temporal chain performance has been largely left unanswered. While a Loran-C chain services an area of the globe, current control is based on a point measurement.

9-1. Johler, J.R., et al, *Nanosecond Precision for Loran-C*, U.S. Department of Commerce, OT Tech. Memo 76-216, April 1976.

Obviously integrated area measurement of TDs is impossible, but is measurement at one point sufficient? Does one try to minimize temporal errors over the whole coverage area or only in a limited region? Should some areas of the coverage area such as harbors or inland waterways be given more weight than others? The answers to these questions are largely a function of policy which the Department of Transportation and the U.S. Coast Guard need to address. Once the policy is established, the performance index can be established and the optimal chain control methods derived.

One suggested policy might be to weight the importance of an area inversely in proportion to its Geometric Dilution of Precision (GDOP). Certain areas such as harbors or restricted waterways may have increased weighting. The objective of chain control might then be to minimize the weighted average temporal error over the service area. The rationale for this proposal is that the geometry of most chains is selected so that certain regions have a low GDOP. This in effect indicates a preference for these areas to have high accuracy. Thus, they should receive a higher weighting than areas of poor GDOP.

Once the cost function is established, the proper spatial sampling of temporal error can be established, ie, placement of the SAM's. An optimal algorithm for combining multiple measurements can then be developed.

APPENDIX

EXPERIMENT SITE LOCATIONS IN WGS 72 COORDINATES

A. Transmitter Locations

Site	North Latitude (deg, min, sec)			West Longitude (deg, min, sec)		
Master (Fallon, NV)	39	33	06.68	118	49	56.37
X-ray (Middletown, CA)	38	46	56.99	122	29	44.52
Yankee (Searchlight, NV)	35	19	18.18	114	48	17.43

B. Measurement Sites on the Propagation Path from Searchligh, NV to Fort Cronkhite, CA

Site	North Latitude** (deg, min, sec)			West Longitude** (deg, min, sec)			Distance From** Searchlight (Yankee) Transmitter (km)
Jean*	35	46	24.89	115	19	38.25	68.976
Tecopa**	35	49	05.58	116	11	05.02	136.678
Death Valley	36	03	32.45	116	50	19.47	201.449
Darwin	36	19	28.15	117	40	09.80	281.737
Delilah***	36	48	14.23	119	07	09.62	422.010
Frian†**	36	59	38.84	119	42	16.20	478.270
Merced**	37	11	19.51	120	21	08.31	539.778
Crows Landing**	37	25	30.67	121	06	18.81	611.493
Livermore**	37	37	26.00	121	46	03.10	674.053
Ft. Cronkhite	37	50	29.47	122	32	41.17	746.697

* Calibration site.
** Corrected for antenna offset from DMA markers - WGS 72 coordinates.
*** Inaccessible - no measurements.

C. Stability Experiment Sites

Site	North Latitude (deg, min, sec)			West Longitude (deg, min, sec)		
Arbuckle, CA	39	00	37.62	122	03	20.90
Silver Springs, NV	39	24	52.05	119	13	52.11
Jean, NV	35	46	24.90	115	19	38.25

D. Harbor Loran-C Experiment Sites

Alcatraz Island	37	49	33.58	122	25	19.79
Angel Island (Pt. Blunt)	37	51	11.13	122	25	10.31
Ballena Bay	37	45	54.67	122	17	11.91
Berkeley Marina	37	51	51.06	122	18	50.79
Collins Marine	37	47	07.73	122	23	15.46
Fort Mason	37	48	27.00	122	25	46.35
Fort Miley (VA Hospital)	37	46	57.99	122	30	17.63
Fort Point	37	48	22.38	122	27	58.11
Hunters Point	37	43	33.55	122	22	08.56
Point Bonita	37	49	19.18	122	31	39.85
Point Molate	37	56	47.50	122	25	37.87
Sears Point	38	09	03.33	122	26	46.45
Treasure Island	37	49	37.25	122	22	28.02

*U.S.GOVERNMENT PRINTING OFFICE : 1980 O-624-064/1576


ILMED
8